UNIVERSITÀ
DEGLI STUDI
DI PADOVA

TESI DI DOTTORATO

Sede Amministrativa: Università degli Studi di Padova

Facoltà di Scienze MM.FF.NN.

Dipartimento di Scienze Chimiche

SCUOLA DI DOTTORATO DI RICERCA IN SCIENZE MOLECOLARI

INDIRIZZO: SCIENZE CHIMICHE

CICLO XXIII

MODELLING OF SOLUTE PARTITIONING AND PERMEATION THROUGH LIPID MEMBRANES

Direttore della Scuola: Ch.mo Prof. Maurizio Casarin

Coordinatore d'indirizzo: Ch.mo Prof. Maurizio Casarin

Supervisore: Prof.ssa Alberta Ferrarini

Dottorando: Giulia Parisio

Index

Abstract

The interaction of molecular solutes with lipid bilayers, which includes water/bilayer partitioning and the process of passive non-mediated transport, is a fundamental topic in biological and pharmaceutical research, dealing with the role of the cell membrane in trafficking and signalling, with drug-design and drug-delivery. According to a simplified picture, a lipid bilayer is assimilated to an oil slab in water, so that logP is taken as a key quantity for the prediction of the membrane permeability of solutes. Actually, it has been recognized since a long time that a lipid bilayer is a structured environment, whose peculiar features have unexpected effects on the distribution and mobility of embedded solutes. In recent years, our knowledge in this field has significantly improved also due to the fundamental contribution of Molecular Dynamics techniques. However, atomistic simulations have a high computational cost, therefore, nowadays a great deal of effort is put into the development of so-called *coarse-grained models*, which combine the molecular representation of solute and environment with the definition of a smaller number of effective interaction sites.

In this thesis the problem has been addressed in a different way: the research has focused on the development of an *implicit membrane model*, wherein an atomic-level representation of the solute is used, while the lipid bilayer is described in terms of its collective properties. Models of this kind can be an important complement to atomistic simulations: besides having a reduced computational cost, which is essential for large scale screening of solutes, they can provide a clear insight into phenomena and their molecular determinant, since different contributions playing a role in a complex system can be disentangled, and molecular properties and interactions can be easily correlated with their effects. The challenge in this field is the introduction of a physically sound implicit description of the solute environment, which is especially difficult in the case of structured media.

Implict models are quite popular for solvation in isotropic and homogeneous solvents. The solvation process is usually represented as the switch on in succession of different solute-solvent interactions: 1) short range repulsions, which are involved in the formation of a solute-shaped cavity in the bilayer; 2) short range attractive (dispersion) interactions; 3) long range electrostatic interactions. The same solute-

solvent interactions take place in lipid bilayers where, however, they are modulated by the heterogeneity and order of this environment, which makes not straightforward the extension of implicit solvent models to these systems. In the development of implicit membrane models, the most effort was devoted to improving the description of the electrostatic contribution. This thesis focuses on nonpolar interactions and represents a first attempt to develop a consistent model, accounting for membrane heterogeneity and order. A generalized Born model is adopted for electrostatic solute-bilayer interactions. Short-range attractions and repulsions are introduced as distinct contributions: the free energy associated with dispersion interactions is expressed by a generalized London form, while the free energy change upon creation of a solute-shaped cavity is evaluated as the reversible volume work against the pressure exerted by the lipid bilayer. An additional contribution is introduced to account for the anisotropic interactions between the solute and the ordered lipid tails; to this purpose, a model originally developed for liquid crystals is used. The structural properties of the bilayer are represented trough the depth-dependent profiles of lipid density, lateral pressure and the acyl chain order parameter, which depend on the phase and chemical composition of the bilayer. The features of the solute enter the model in terms of atomic coordinates, charges, polarizabilities and molecular surface. Therefore this model can provide a detailed picture of the free energy landscape of a solute in a given bilayer, as a function of its position and orientation, which are intrinsically coupled by the structure of the environment. The availability of this free energy surface allows the calculation of orientational and positional distribution functions and average properties of the solute, which can be related to physical observables.

The solute affinity for the lipid bilayer environment underlies its permeation ability, which is another topic addressed by this thesis. Within the theoretical framework describing roto-translational diffusion as a stochastic process, we have derived a general expression for the flux of solutes across a lipid bilayer, taking into account the positional-orientational coupling, which was generally ignored by previous theories. Under suitable conditions, the main equation of the solubility-diffusion model was recovered, which relates the membrane permeability coefficient of a solute to its local partition and diffusion coefficients across the bilayer.

The theoretical models for solute partitioning and permeation developed in this thesis were implemented in a software package, which can be made available to the scientific community. Calculations can be performed at a very low computational cost: given the molecular structure of a medium-sized solute, its free energy surface as a function of its position and orientation in the bilayer is obtained in a few minutes on a desktop PC. Also the case of case of flexible solutes can be handled in an efficient way. The atomic coordinates of the solute can be obtained from experimental data of from quantum mechanical calculations. A preliminary parameterization of few bilayer properties is needed, which can be derived from experiments or from atomistic Molecular Dynamics simulations; in this thesis this was done for a liquid-crystalline DPPC (1,2-dipalmitoyl-sn-glycero-3-phosphocholine) bilayer. Some effort was also devoted to the definition of a consistent set of atomic transferable charges and polarizabilities, which were validated by comparing calculated and experimental solvation free energies for selected solutes in solvents of different polarity. Given the geometry of a solute, also its intrinsic membrane permeability coefficient is obtained, by combining the calculation of its water/membrane transfer free energy profile with the evaluation of its diffusion coefficient by a hydrodynamic model accounting for molecular shape.

The developed methodology was applied to a variety of solutes, differing for shape, size and polarity. Strongly nonuniform and anisotropic calculated distributions of solutes in the model lipid bilayer were found. In particular, dispersion interactions revealed to be determinant in confining solutes away from the middle of the bilayer, in the region below the hydrophobic/hydrophilic interface, where acyl chains reach their highest density. As expected, electrostatic interactions were found to favor the partitioning of polar compounds in the hydrophilic region of the bilayer. The order and cavity contributions to the solute-bilayer interaction, ignored by other implicit membrane models, were found to significantly affect the position and even more the orientation of solutes inside the bilayer. The comparison of our predictions with literature data, from experiments and Molecular Dynamics simulations, proved the capability of the developed methodology of capturing the important factors determining solute behaviour in the membrane environment.

The systems which were investigated include molecules of biological interest, like cholesterol, as well as drug-like solutes, fluorescent probes and fullerene C_{60}-

derivatives. For the latter system the theoretical predictions were combined with Electron Spin Resonance experiments in oriented bicelles. The integration of the methodology developed in this thesis with advanced quantum mechanical calculations of excited electronic states, which has started in collaboration with quantum chemists, appears promising to elucidate the relation between spectroscopic observables and the membrane distribution of fluorescent probes. Calculated permeability coefficients were found to be highly sensitive to solute molecular structure and mainly determined by solute partitioning; even for permeability properties, which represent a challenge for theoretical predictions, we got good agreement with experimental data reported in the literature.

Sommario

L'interazione di soluti molecolari con doppi strati lipidici, che include la loro distribuzione tra fase acquosa e membrana e il loro trasporto passivo non-mediato attraverso quest'ultima, è un tema fondamentale nella ricerca in campo biologico e farmaceutico che si occupa del ruolo delle membrane cellulari nei processi di trasporto di sostanze e trasmissione di segnali, della progettazione e veicolazione di farmaci.

Secondo una rappresentazione semplificata, un doppio strato lipidico è assimilato ad uno strato d'olio immerso in acqua, e il logP di un soluto è correlato alla sua capacità di attraversare la membrana. In realtà, da molto tempo è stato riconosciuto l'effetto che le proprietà strutturali peculiari di un doppio strato esercitano sulla distribuzione e sulla mobilità di soluti incorporati al suo interno. Negli ultimi anni il fondamentale contributo delle tecniche di Dinamica Molecolare ha favorito l'incremento delle conoscenze acquisite in questo campo. L'elevato costo computazionale delle simulazioni atomistiche ha poi promosso lo sviluppo di metodi *coarse-grained* che combinano una rappresentazione molecolare del soluto e dell'intorno con la definizione di un numero ridotto di siti effettivi di interazione.

In questa tesi il problema è stato affrontato con un approccio differente: l'attività di ricerca si è concentrata sullo sviluppo di un *modello implicito* per l'ambiente di membrana, in cui il soluto è rappresentato a livello atomistico, mentre il doppio strato lipidico è descritto in termini delle sue proprietà collettive. Modelli di questo tipo possono essere complementari alle simulazioni atomistiche: oltre ad avere un ridotto costo computazionale, essenziale per uno *screening* di soluti su larga scala, essi forniscono una chiara descrizione dei fenomeni di interesse e della loro origine a livello molecolare, scorporando diversi contributi e correlando proprietà e interazioni molecolari ai loro effetti. La sfida in quest'ambito sta nella difficoltà di fornire una descrizione implicita, fondata dal punto di vista fisico, dell'intorno del soluto, specialmente nel caso di mezzi strutturati.

Piuttosto diffusi sono i modelli impliciti per la solvatazione in mezzi omogenei e isotropi, di solito rappresentata come il risultato dell'instaurazione successiva di diverse interazioni soluto-solvente: 1) interazioni repulsive a corto raggio, associate al processo di formazione della cavità ospitante il soluto nel mezzo; 2) interazioni

attrattive a corto raggio (o di dispersione); 3) interazioni elettrostatiche a lungo raggio. Le stesse interazioni hanno luogo in ambiente di membrana dove tuttavia, esse sono modulate dalla struttura eterogenea e ordinata del doppio strato, il che rende non banale il problema dell'estensione dei modelli con solvente implicito a questi sistemi. Nello sviluppo di modelli per la rappresentazione implicita dell'ambiente di membrana, le risorse maggiori sono state impiegate per il miglioramento della descrizione del contributo elettrostatico alla solvatazione. In questa tesi l'attenzione è rivolta al contributo non polare, nel tentativo inedito di sviluppare un modello consistente che tenga conto della natura eterogenea e ordinata dell'ambiente di membrana. Un modello generalizzato di Born è stato adottato per la descrizione delle interazioni elettrostatiche tra soluto e doppio strato. Le interazioni attrattive e repulsive a corto raggio sono state introdotte sotto forma di contributi distinti: un'espressione di London generalizzata è utilizzata per l'energia libera associata alle interazioni di dispersione, mentre la variazione di energia libera associata al processo di creazione della cavità del soluto è data dal lavoro reversibile di volume compiuto contro la pressione esercitata dal doppio strato. Un contributo addizionale è introdotto per tener conto delle interazioni anisotrope tra il soluto e le code lipiche ordinate; a questo scopo è utilizzato un modello originariamente sviluppato per i cristalli liquidi. Le proprietà strutturali del doppio strato sono rappresentate attraverso i profili che decrivono la variazione di densità, pressione laterale, e parametro d'ordine delle catene aciliche, con la profondità, e che dipendono dalla fase e dalla composizione chimica del doppio strato. Le caratteristiche del soluto entrano nel modello in termini di coordinate, cariche e polarizzabilità atomiche, e superficie molecolare. Perciò questo modello è in grado di fornire una descrizione dettagliata della variazione di energia libera di un soluto in un determinato doppio strato, in funzione della sua posizione e orientazione che sono intrinsecamente accoppiate per effetto della struttura dell'intorno. La disponibilità di questa superficie di energia libera permette il calcolo di funzioni di distribuzione orientazionali e posizionali e proprietà medie del soluto che possono essere messe in relazione con osservabili fisiche.

L'affinità di un soluto per l'ambiente di membrana è alla base della sua capacità di permeazione attraverso il doppio strato, che costituisce un altro argomento di questa tesi. Nell'ambito della trattazione stocastica della diffusione roto-traslazionale,

abbiamo derivato un'espressione generale per il flusso di soluti attraverso un doppio strato che tiene conto dell'accoppiamento tra le variabili di orientazione e posizione, generalmente ignorato nelle teorie precedenti. Nelle condizioni appropriate, l'equazione principale del modello di solubilità e diffusione, che mette in relazione il coefficiente di permeabilità intrinseca in membrana di un soluto con i suoi coefficienti locali di partizione e diffusione attraverso il doppio strato, è stata riottenuta.

I modelli teorici sviluppati in questa tesi per la partizione e la permeazione di soluti in membrana sono stati implementati in un pacchetto software che potrà essere messo a disposizione della comunità scientifica. I calcoli richiedono un costo computazionale ridottissimo: data la struttura molecolare di un soluto di media grandezza, la sua superficie di energia libera in funzione della sua posizione e orientazione nel doppio strato si può ottenere in pochi minuti con un PC da tavolo. Anche il caso di soluti flessibili può essere affrontato in modo efficiente. Le coordinate atomiche del soluto si possono ottenere da dati sperimentali o calcoli quanto-meccanici. La necessaria parametrizzazione preliminare di alcune proprietà del doppio strato può essere derivata da esperimenti o simulazioni di Dinamica Molecolare: ciò è stato fatto in questa tesi per un doppio strato di DPPC (1,2-dipalmitoil-sn-glicero-3-fosfocolina) in fase liquido-cristallina. Parte del lavoro è stata anche dedicata alla definizione di un set consistente di cariche e polarizzabilità atomiche trasferibili, che è stato validato per confronto delle energie libere di solvatazione misurate e calcolate per alcuni soluti in solventi con diversa polarità. Data la geometria di un soluto, anche il suo coefficiente di permeabilità intrinseca in membrana può essere determinato combinando il calcolo del suo profilo di energia libera di trasferimento dall'acqua in membrana e del suo coefficiente di diffusione nei due mezzi tramite un modello idrodinamico che tenga conto della sua forma molecolare.

La metodologia sviluppata è stata applicata a vari soluti, differenti per forma, dimensioni e polarità. Le loro distribuzioni calcolate nel doppio strato modello sono risultate fortemente non uniformi e anisotrope. In particolare le interazioni di dispersione sono risultate determinanti nel confinare i soluti nella regione lontana dal centro del doppio strato, al di sotto dell'interfaccia tra le regioni idrofobica e idrofilica, dove la densità delle catene aciliche è massima. Come atteso, le interazioni

elettrostatiche sono risultate favorire la distribuzione di composti polari nella regione idrofilica del doppio strato. I contributi di ordine e cavità all'interazione tra soluto e doppio strato, ignorati in altri modelli impliciti sono risultati influenzare significativamente la posizione e ancor più l'orientazione dei soluti all'interno del doppio strato. Il confronto tra predizioni e dati di letteratura derivanti da esperimenti o simulazioni d Dinamica Molecolare ha dimostrato la capacità della metodologia sviluppata di individuare i fattori importanti nel determinare il comportamento di soluti in membrana.

I sistemi che sono stati investigati includono molecole di interesse biologico, come il colesterolo e molecole farmaco-simili, sonde fluorescenti e derivati fullerenici del C_{60}. In quest'ultimo caso le predizioni teoriche sono state combinate con esperimenti di Risonanza di Spin Elettronico in bicelle orientate. L'integrazione della metodologia sviluppata in questa tesi con calcoli quanto-meccanici di stati elettronici eccitati, frutto di una collaborazione agli inizi, sembra promettente allo scopo di chiarire la relazione tra osservabili spettroscopiche e distribuzione in membrana di sonde fluorescenti. I coefficienti di permeabilità calcolati sono risultati estremamente sensibili alla struttura molecolare dei soluti e determinati essenzialmente dalla loro distribuzione; anche in questo caso è stato riscontrato un buon accordo con i dati sperimentali riportati in letteratura.

Chapter 1
Introduction

1.1 Biological membranes and model lipid bilayers

The cell is the structural, functional and reproductive unit of all living organisms. Both in unicellular and multicellular organisms, cells live and evolve preserving their structural, functional and genetic identity, while interacting with their surrounding. The plasma membrane encloses the cell and regulates the exchange of substances and signals between the intra- and extra- cellular environments; in eukaryote cells internal process take place in subcellular organelles enclosed in membranes.

Lipids, proteins and, to a minor extent, carbohydrates constitute biological membranes, whose composition varies depending on membrane type, function and shape, cell type and species of the organism. The basic structure of all biological membranes is a hydrated lipid bilayer, composed of amphiphilic molecules. Electrostatic interactions and hydrogen bonds involve the hydrophilic lipid headgroups and hydrating water molecules near the bilayer surfaces, while dispersion interactions act between the hydrophobic lipid tails, in the bilayer core. Proteins can be found embedded in the lipid matrix as integral membrane proteins, or anchored to the bilayer through amphiphilic domains intercalated between lipid molecules, or interacting with the bilayer surface as peripheral membrane proteins. Oligosaccharides are covalently bound to the membrane in glycoproteins and glycolipids.

Membranes mediate the transport of molecules in and out of the cell and between intracellular compartments. Passive and active transport processes regulate the traffic of small molecules across biomembranes, down and against their concentration gradient, respectively, while macromolecules and large aggregates are internalized or extruded via endocytosis and exocytosis, which involve membrane budding and fusion. Membrane receptors play a fundamental role in signal transduction. The whole metabolic processes of photosynthesis and oxidative phosphorilation take place in membranes.

The properties of the lipid bilayer affect membrane processes, by modulating the interaction of the membrane with small solutes partitioning and diffusing in the lipid matrix, and with proteins whose mechanism of function usually involves structural changes.

The membranes of eukaryote cells contain up to 2000 lipid species, the most of which belong to three major classes, glycerophospholipids (40-60% of lipid amount in the plasma membrane of vertebrates), sphingophospholipids (10-20%) and sterols. Phosphatidylcholines (PC), phosphatidylethanolamines (PE), and phosphatidyl-serines (PS) are the most common glycerophospholipids; sphingomyelins (SM) are the most common sphingophospholipids (Figure 1). Phospholipid species are identified by their specific headgroup, which is zwitterionic in PC, PE and SM, and negatively charged in PS, and by the length and degree of unsaturation of their acyl chains. Cholesterol is the sterol of animal cell membranes (30-40% of lipid amount in the plasma membrane of vertebrates).

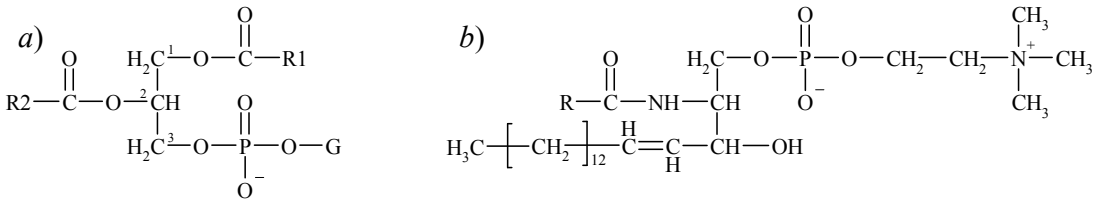

Figure 1: *a*) Molecular structure of glycerophospholipids. G indicates the lipid headgroup: $G=CH_2CH_2N(CH_3)_3^+$ in PC, $G=CH_2CH_2NH_3^+$ in PE, $G=CH_2CH(NH_3^+)COO^-$ in PS. R1 and R2 indicate the lipid tails. *b*) Molecular structure of SM. R indicates the variable lipid tail.

The distribution of lipid species across the bilayer and in the bilayer plane is non-homogeneous. Since the late '70s it has been known that, although containing almost the same number of lipids, the outer and inner leaflets of lipid bilayers have a different composition,[1] sphingolipids and PC being more abundant in the former, PS and PE in the latter; cholesterol, on the contrary, is equally distributed between the two leaflets. Transmembrane migration '*flip-flop*' events, which are extremely unlike for lipids with big polar headgroups, are frequent for cholesterol.[2] The hypothesis of a short- and long-range lateral organization of the lipids dates back to the late '90s,[3] but only recently the model has been defined unambiguously. "Membrane rafts are small (10–200 nm), heterogeneous, highly dynamic, sterol- and sphingolipid-enriched domains that compartmentalize cellular processes. Small rafts can sometimes be stabilized to form larger platforms through protein-protein and protein-lipid interactions."[4] *Rafts*, however, would represent only an intermediate level of organization in the complex hierarchy of structures formed by membrane lipids and proteins.[5] Nano- to micro-scaled domains may be transient or relatively stable, but

are all dynamic structures, their formation and disruption being regulated by lipid diffusion and lipid-protein interactions.[6]

The characterization of the interactions of lipid bilayers with incorporated solutes and associated proteins is of paramount interest when membrane permeability and protein activity are investigated. Studies, which would be hard in the complex environment of biological membranes, due to the presence of large amounts of proteins and a wide variety of lipid species, are usually carried out on model lipid bilayers composed only of few lipid species, usually up to three, characterized by a well defined phase behaviour.

Under the proper conditions, amphiphilic lipid molecules in water self-assemble into hydrated bilayers, with their hydrophilic heads exposed to water, and their hydrophobic tails extended towards the bilayer core, aligned, on average, with each other. A monocomponent phospholipid bilayer can be found in an ordered gel phase or in a fluid liquid crystalline phase, below and above its characteristic transition temperature respectively. Three-component lipid bilayers are usually mixtures of saturated and unsaturated phospholipids and cholesterol, with a characteristic ternary phase diagram comprising gel (solid-ordered), liquid crystalline (liquid-disordered) and intermediate liquid-ordered regions. In the liquid crystalline phase the lipid tails are oriented, on average, parallel to the bilayer normal (Figure 2).

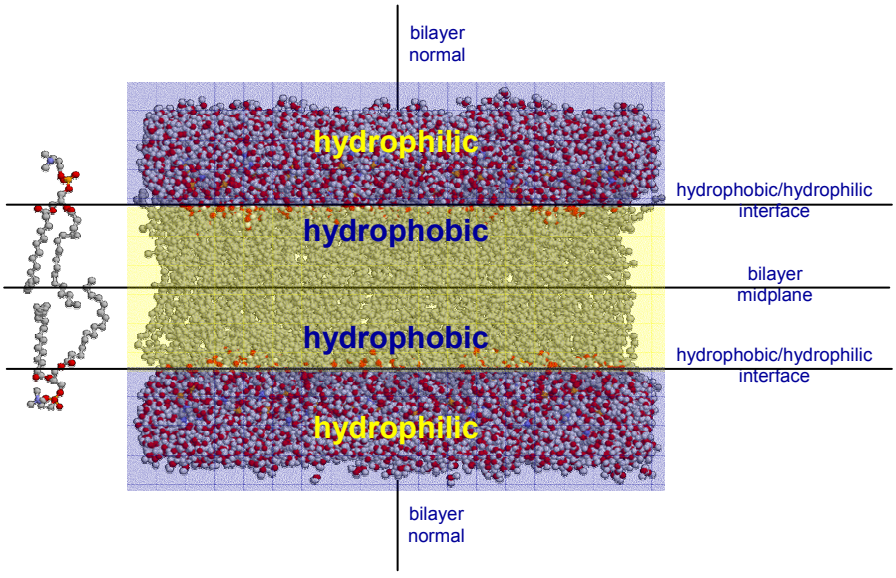

Figure 2: Representation of the structure of phospholipid molecules and of a hydrated lipid bilayer.

In fact, biological and model lipid bilayers show the same fundamental features: high heterogeneity along the bilayer normal, and axial order with respect to the bilayer normal in the hydrophobic region. The molecular structure of the constituting lipids determines the specific properties of bilayers. Thus, phospholipids differing in the size or charge of their headgroup, or in the length and unsaturation of their acyl tails, form bilayers with different hydration, surface area, thickness, curvature and degree of order.

1.2 Modelling solute partitioning and permeation across lipid bilayers

The structure and properties of the lipid bilayers of biomembranes affect the function of membrane proteins and the membrane binding and distribution of small molecules. The toxicity of a compound and/or its efficacy as a drug are related to its ability to cross the lipid bilayer of cell membranes. Drug permeability is also critical for optimal loading into and release from liposomal transport systems.[7] Bioinformatics and drug design represent thus the main field of application, promoting the investigation of the interactions of membranes with macromolecules and small solutes.

Heterogeneity and order, which in general distinguish interphases from bulk phases, introduce a dependence of the behaviour of a molecule on its localization within the lipid bilayer.[8] Detailed information on such effects, however, are experimentally hardly accessible, and suitable theoretical models are required to elucidate the mechanism of interactions of dispersed molecules with their micro-environment. Different approaches have been proposed for the modeling of solute partitioning and permeation across lipid bilayers, which are summarized in the following paragraphs.

1.2.1 Solute partitioning

All-atom Molecular Dynamics (MD) simulations provide the most detailed description of solute-solvent interactions. Their ability to characterize the behaviour of a solute in a lipid bilayer is however limited by the restricted size of the system which can be investigated, and the short time during which its evolution can be

followed. As a result the high computational effort required may be insufficient to guarantee an appropriate statistical sampling of slowly interconverting configurations. Coarse-grained simulations improve statistical sampling loosing atomistic detail, but force-field parametrization is not straightforward. Implicit solvent models are intended to maintain the atomistic representation of the solute, while disregarding the molecular discreteness of the environment and its configurational degrees of freedom. They require a theoretical rather than computational effort for the definition of a suitable mean field potential describing the average influence of the solvent on the solute behaviour. This task is especially challenging in the case of solutes in lipid bilayers, due to the complex organization of this environment with respect to bulk solvents.

Implicit solvent models are generally based on mean field potentials composed of a polar and a nonpolar contribution, arising from electrostatic and short-range solute-solvent interactions respectively.[9] The former contribution is usually expressed as the free energy of the solute charge distribution in the solvent dielectric as calculated according to a Generalized Born model; the latter contribution, comprising both the free energy associated with dispersion solute-solvent interactions and the work required for the creation of the solute cavity in the solvent medium, is usually represented by the solvent-accessible-surface-area (SASA) model.[10] However, while the dielectric constant of a solvent entering in the Born equation is a well defined property, the SASA model describes the solvent effect through an effective solvent-solute surface tension, i.e. a phenomenological solvation parameter which is fitted to experimental data to reproduce observed hydrophobicity or hydrophilicity.[11,12] While a good level of accuracy has been reached in the evaluation of the polar contribution to solvation by the development of improved GB models,[13] severe deficiencies have been recognized in the SASA approach, assuming a linear dependence of the nonpolar contribution on the solvent-accessible-surface-area of the solute, the proportionality constant being the solute-solvent effective surface tension. Scaled Particle Theory (SPT) provides an alternative approach for the evaluation of the nonpolar contribution to solvation, or, rather, of that part of the nonpolar contribution which can be traced back to the free energy cost of cavity creation.[14] However, although SPT-inspired arguments were brought to support the surface-area-dependence in the SASA expression, SPT actually predicts a crossover from volume-

dependence to surface-area-dependence of nonpolar solvation with increasing solute cavity size.[15,16,17] Such lengthscale dependence of hydrophobicity has been interpreted in terms of competing entropic and enthalpic contributions, dominating for small and large solute cavities respectively,[15,16,17] due to the persistence or disruption of the hydrogen-bonding network of water around the solute cavity[15,16,18]. Contextually, the linear surface-area-dependence of the free energy cost of cavity creation, in the limit of large cavities, has been described through the liquid-vapour surface tension of the solvent. However, attempts made in order to conciliate the solvent-cavity surface tension of SPT with the macroscopic property of the fluid have not been able to remove the discrepancies. [15,19-21] A coherent view of hydration and in general of the solvation process has emerged from the work by Graziano and collaborators.[22] According to this theory, the entropy change is related to the cavity contribution to hydrophobic solvation and is due to pure excluded volume effects, while the enthalphy change is related to the dispersion contribution and is due to solute-solvent attractive interactions. Graziano also pointed out that the processes of creation of a cavity in a liquid and creation of an interface between liquid and air are different, in that the entropy penalty associated with the former does not occur in the latter. The importance of decomposing the nonpolar interactions into repulsive (excluded volume) and attractive (dispersion) components was highlighted also by Levy and coworkers [23-25] and by Wagoner and Baker [26].

The simplest implicit membrane models adopted a GB model allowing the representation of the lipid bilayer as a low-dieletric slab embedded between two high-dielectric bulk water regions, and parameterize the SASA model to reproduce partitioning free energies between water and liquid hydrocarbons.[27] With their implicit membrane model, Tanizaki and Feig also followed the traditional approach from bulk solvent modeling but proposed a GB formalism allowing the representation of the lipid bilyer as a heterogeneous dielectric environment, and fitted the effective surface tension in the SASA model to the free energy profile of the apolar O_2 molecule across the lipid bilayer.[28]

In addition to the intrinsic inaccuracy of the SASA approximation, a fundamental limitation of implicit membrane GB/SASA approaches was recognized in that, besides hydrophobic thickness, specific structural properties of the bilayer environment are not taken into account. The effects of orientational order,

spontaneous curvature, area per chain, density and lateral pressure profiles on the behaviour of membrane permeants and proteins (and *vice versa*) are usually included in the so-called *membrane-focused* models, where, however, only a simplified representation of the solute is adopted.[29] Improved *solute-focused* approaches would combine a more accurate modeling of solute-membrane interactions with an adequate representation of the membrane structure.

1.2.2 Solute permeation

While active transport processes, making use of protein pumps, and protein carriers and channels, allow the mediated passive transport of ions, small solutes and drug-like molecules can cross cell membranes permeating through the lipid bilayer (non mediated passive transport), driven by a concentration gradient between the two aqueous regions at the membrane sides (Figure 3).

The membrane permeability coefficient P of a solute is defined from its flux per unit area J across the lipid bilayer and its concentration gradient $c''_w - c'_w$ between the aqueous solutions at the membrane sides (Figure 3), according to the relation:

$$J = -P\left(c''_w - c'_w\right). \tag{1}$$

A solubility-diffusion mechanism[30] has been proposed for passive transport, allowing the rationalization of the behaviour of solutes of different dimension, shape and chemical nature. According to this, solutes *i*) transfer from water to the membrane, *ii*) diffuse across the membrane, *iii*) transfer from the membrane to water. If transfer steps *i*) and *iii*) are assumed to be so fast that solute partitioning at the membrane/water interfaces is at equilibrium, the solute concentrations c'_m and c''_m, just inside the two leaflets of the bilayer, are related to the solute concentrations c'_w and c''_w, in the adjacent bulk water phases, (Figure 3) by the partition coefficient

$$K = \frac{c'_m}{c'_w} = \frac{c''_m}{c''_w}. \tag{2}$$

Then the first Fick's law relates the permeability coefficient P of the solute to its membrane/water partition coefficient K and its membrane diffusion coefficient D according to:

$$P = \frac{KD}{l} \tag{3}$$

where *l* is the membrane thickness.

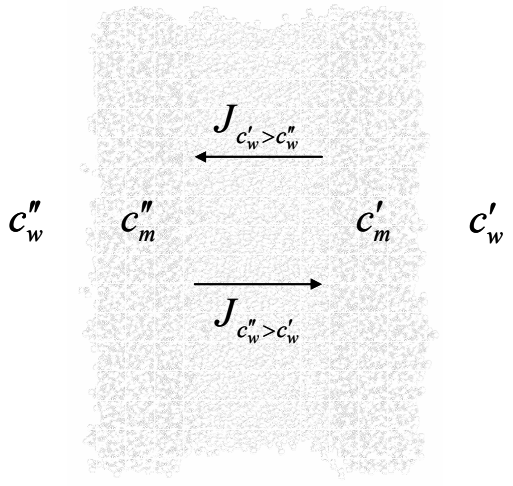

Figure 3: Non mediated passive transport of a solute across a lipid bilayer.

The correlation between the permeability of solutes and their oil/water partition coefficient was stated in the late 19th century by Ernest Overton in his famous rule,[31,32] and the *n*-octanol/water partition coefficient of a compound is still regarded as a good indicator of its membrane permeability[33]. A critical role of the molecular weight of solutes was also recognized, which was ascribed to the size-dependence of their diffusion coefficients.[34]. The selectivity of biological membranes and lipid bilayers for permeant size was found, however, to be similar to that of polymer membranes more than to that of bulk solvents.[35,36] Especially in the case of small molecules, such as water or urea, in fact, the size-dependence of membrane diffusion coefficients was found to be much steeper than that predicted by the Stokes-Einstein hydrodynamic model and found in most liquid hydrocarbons. According to the 'soft-polymer' theory, the solute diffusion in lipid bilayers, as well as in chain polymers, would proceed through adjacent transient cavities produced by molecular fluctuations in the membrane, and would be governed by the frequency of cavity formation and by the cavity size distribution. [35,36]

Eq.3 has the valuable feature of conjugating partition and diffusion properties, whose fundamental role, as determinants of solute permeability, has been widely recognized; this within a drastic approximation, that is, the description of the lipid bilayer as a homogeneous hydrocarbon layer where solute partition and diffusion coefficients are uniform.

In a more realistic representation of the structure of a hydrated lipid bilayer in the liquid crystalline phase, the bilayer environment is actually homogeneous in each section parallel to the bilayer plane, but highly heterogeneous along the bilayer normal. If position dependent partition and diffusion coefficients are introduced, eq.3 becomes

$$\frac{1}{P} = \int_0^l \frac{1}{K(Z)D(Z)}\,\mathrm{d}Z \tag{4}$$

where the integration variable Z is the solute position along the bilayer normal and the integral extends over the whole bilayer thickness. Eq.4 was derived in 1974 by Diamond, Szabo and Katz[37] who, however, could only draw the expected qualitative form of the $K(Z)$ and $D(Z)$ profiles of hydrophobic and hydrophilic nonelectrolytes. The integrand function represents the local resistance opposed by the membrane to solute permeation: high affinity for the bilayer environment and/or high diffusion rate yield low resistance and thus high solute permeability. Up to now both $K(Z)$ and $D(Z)$ have remained experimentally hardly accessible quantities, but in 1994 Marrink and Berendsen[38] proposed a computational method, which is now widespread, for their calculation from MD simulations[7,39-42].

According to a common procedure, in order to calculate partition and diffusion coefficients of a solute at n different positions along the bilayer normal, n different MD simulations are performed. During each simulation the solute molecule is constrained at a given position Z_n by an applied force equal and opposite to the resultant force F it experiences due to the interactions with the environment. The partition and diffusion coefficient, $K(Z_n)$ and $D(Z_n)$, are then calculated from the average value of the force in time $\langle F \rangle$,

$$\Delta G(Z_n) = -RT \ln K(Z_n) = -\int_0^{Z_n} \langle F(Z,t) \rangle \,\mathrm{d}Z\,, \tag{5}$$

and, according to the theory of Brownian motion, from the autocorrelation function of the random oscillation $\Delta F = F - \langle F \rangle$,

$$D(Z_n) = \frac{(RT)^2}{\int_0^{+\infty} \langle \Delta F(Z_n, t_0 + t)\, \Delta F(Z_n, t_0) \rangle \,\mathrm{d}t}\,. \tag{6}$$

The results of MD simulations provide evidence that, besides polar interactions favouring the partitioning or binding of hydrophilic solutes in the headgroup region

of the membrane, also the structural properties of the lipid bilayer, such as its packing density, lateral pressure and chain ordering, determine the membrane affinity of drug-like and small molecules, as well as the diffusion rate of small solutes.[7] This suggests that, for reliable prediction of the location of the barrier region to solute permeation, and of the selectivity of the membrane for permeant size, a proper model for solute-membrane interactions taking into account the effects of membrane structure is required.

It is worth noting that conformational and orientational changes take place, during the translocation of large drug-like molecules, on the nanosecond time-scale. Although neither conformational nor orientational degrees of freedom appear in eq.4, the constrained particle method provides, in fact, the conformational-orientational average of K and D, always compatibly with the possible limitations of MD approaches, which must combine sufficient statistical sampling with affordable computational cost.

1.3 PhD project and outline

The research project presented in this thesis had a twofold objective. The first is the development and implementation of an implicit membrane model overcoming the main limits of the existing approaches[29], which neglect the nonuniform and anisotropic nature of this environment. This model is intended to provide a detailed representation of the coupled positional-orientational distribution of solutes in membranes. The second objective is the re-examination of the heterogeneous solubility-diffusion model, with a proper account of the roto-translational couplings which characterize both the partition and diffusion properties of solutes in lipid bilayers.

Our implicit membrane model will be presented in Chapter 2, where the results obtained from the calculations performed on cholesterol will be reported as an illustrative example of the capabilities of the approach which has been developed.

A generalized formalism for the solubility-diffusion model including explicit orientational degrees of freedom will be proposed in Chapter 3, where an analytical expression for the permeability coefficient, analogous to eq.4, will be derived in the

limit of fast solute reorientation. Application to drug-like molecules, by integration of the implicit membrane model developed into the solubility-diffusion theory, is also presented in Chapter 3.

Further applications will be presented in Chapters 4-6, where the results will be discussed and compared with data available from literature.

Chapter 4 presents a joint theoretical and experimental investigation of the behaviour of pristine C_{60} and two N-substituted fulleropyrrolidines, one of which bearing a paramagnetic nitroxide group, in membrane; theoretical predictions are combined with Electron Paramagnetic Resonance (EPR) experiments in aligned bicelles.

In Chapter 5 we report the results obtained for a set of nonpolar compounds, which have been selected to highlight the effects of molecular size and shape on the preferred location and orientation of solutes in lipid bilayers.

Chapter 6 is dedicated to the fluorescent probes of membrane polarity Acdan, Prodan and Laurdan, whose spectroscopic behaviour in lipid bilayers presents controversial issues.

Conclusions on the predictive capability of the developed methodology will be drawn in Chapter 7, where we shall also discuss the limits of the approaches proposed in this thesis.

1.4 References

[1] Rothman, J.E.; Lenard, J. *Science* **1977**, *195*, 743-753.

[2] Lenard, J.; Rothman, J.E., *Proc. Natl. Acad. Sci. USA* **1976**, *73*, 391-395.

[3] Simons, K.; Ikonen, E. *Nature* **1997**, *387*, 569-572.

[4] Pike, L.J. *J. Lipid Res.* **2006**, *47*, 1597-1598.

[5] Anderson, R.G.W.; Jacobson, K. *Science* **2002**, *296*, 1821-1825.

[6] Almeida, P.F.F.; Pokorny, A.; Hinderliter, A. *Biochim. Biophys. Acta* **2005**, *1720*, 1-13.

[7] Xiang, T.-X.; Anderson, B.D. *Adv. Drug Deliv. Rev.* **2006**, 58, 1357-1378.

[8] De Young, L.R.; Dill, K.A. *Biochemistry* **1988**, *27*, 5281-5289. Marqusee, J.A.; Dill, K.A. *J. Chem. Phys.* **1986**, *85*, 434-444.

[9] Roux, B.; Simonson, T. *Biophys. Chem.* **1999**, *78*, 1-20.

[10] Still, W.C.; Tempczyk, A.; Hawley, R.C.; Hendrickson, T. *J. Am. Chem. Soc.* **1990**, *112*, 6127-6129.

[11] Feig, M.; Brooks, C.L. III *Curr. Opin. Struct. Biol.* **2004**, *14*, 217-224.

[12] Chen, J.; Brooks, C.L. III; Khandogin, J. *Curr. Opin. Struct. Biol.* **2008**, *18*, 140-148.

[13] Feig, M.; Im, W.; Brooks C. L. III *J. Chem. Phys*. **2004**, *120*, 903-911.

[14] Pierotti, R.A. *Chem. Rev.* **1976**, *6*, 717-726.

[15] Chandler, D. *Nature* **2005**, *437*, 640-647.

[16] Ashbaugh, H.S.; Pratt, L.R. *Rev. Mod. Phys.* **2006**, *78*, 159-178.

[17] Chen, J.; Brooks, C.L. III *J. Am. Chem. Soc.* **2007**, *129*, 2444-2445.

[18] Stillinger, F.H. *J. Solut. Chem.* **1973**, *2*, 141-158.

[19] Mayer, S.W. *J. Phys. Chem.* **1963**, *67*, 2160-2164.

[20] Reiss, H. *Adv. Chem. Phys.* **1966**, *9*, 1-84.

[21] Tanford, C. *Proc. Natl. Acad. Sci. USA* **1979**, *76*, 4175-4176.

[22] Graziano, G. *J. Chem. Soc. Faraday Trans.* **1998**, *94*, 3345-3352. Graziano, G. *Biophys. Chem.* **2003**, *104*, 393-405. Graziano, G. *Chem. Phys. Lett.* **2004**, *396*, 226-331. Graziano, G. *J. Phys. Chem. B* **2006**, *110*, 11421-11426. Graziano, G. *Chem. Phys. Lett.* **2007**, *442*, 307-310. Graziano, G. *J. Therm. Anal. Cal.* **2008**, *91*, 73-77.

[23] Gallicchio, E.; Kubo, M.M.; Levy, R.M. *J. Phys. Chem. B* **2000**, *104*, 6271-6285.

[24] Levy, R.M.; Zhang, L.Y.; Gallicchio, E.; Felts, A.K. *J. Am. Chem. Soc.* **2003**, *125*, 9523-9530.

[25] Gallicchio, E.; Levy, R.M. *J. Comput. Chem.* **2004**, *25*, 479-499.

[26] Wagoner, J.A.; Baker, N.A. *Proc. Natl. Acad. Sci. USA* **2006**, *103*, 8331-8336.

[27] Spassov, V.Z.; Yan, L.; Szalma, S. *J. Phys. Chem. B* **2002**, *106*, 8726-8738.

[28] Tanizaki, S.; Feig, M. *J. Chem. Phys*. **2005**, *122*, 124706.

[29] Grossfield, A. *Curr. Topics Membr.* **2008**, *60*, 131-157.

[30] Missner, A.; Pohl, P. *ChemPhysChem* **2009**, *10*, 1405-1414.

[31] Overton, C.E. *Vierteljahrsschr. Naturforsch. Ges. Zurich* **1899**, *44*, 88-135.

[32] Kleinzeller, A. *Curr. Top. Membr.* **1999**, *48*, 1-22.

[33] Lipinski, C.A. *Adv. Drug Del. Rev.* **1997**, *23*, 3-25.

[34] Finkelstein, A. *J. Gen. Physiol.* **1976**, *68*, 127-135.

[35] Lieb, W.R.; Stein, W.D. *Curr. Top. Membr. Transp.* **1971**, *2*, 1-39.

[36] Walter, A.; Gutknecht, J. *J. Membr. Biol.* **1986**, *90*, 201-217.

[37] Diamond, J.M.; Katz, Y. *J. Membr. Biol.* **1974**, *17*, 121-154; Diamond, J.M.; Szabo, G.; Katz, Y. *J. Membr. Biol.* **1974**, *17*, 148-152.

[38] Marrink, S.-J.; Berendsen, H.J.C. *J. Phys. Chem.* **1994**, *98*, 4155-4168.

[39] Marrink, S.-J.; Berendsen, H.J.C. *J. Phys. Chem.* **1996**, *100*, 16729-16738.

[40] Bemporad, D.; Essex, J.W.; Luttmann, C. *J. Phys. Chem. B* **2004**, *108*, 4875-4884.

[41] Berendsen, H.J.C. *Faraday Discuss.* **2010**, 144, 467-481.

[42] Orsi, M.; Essex, J.W. In Molecular simulations and biomembranes: from biophysics to function, Biggin, P.C.; Sansom, M.S.P. Eds., Royal Society of Chemistry 2010, pp. 77-91.

Chapter 2*

Solute partitioning into lipid bilayers: an implicit model for nonuniform and ordered environment

*This chapter is adapted from Parisio, G.; Ferrarini, A. *J. Chem. Theory Comput.* **2010**, *6*, 2267-2280. For Supporting Information (SI) see Appendix A.

2.1 Introduction

Partitioning of solutes into lipid bilayers has important implications: beside playing a role in cellular processes, it underlies the permeation of drugs across biomembranes. This has motivated along the years a steady effort to develop models able to catch the features of the membrane environment[1]. Traditionally, lipid bilayers have been approximated as slabs of apolar solvents in water and their high nonuniformity and orientational order have been neglected[2]. Actually, these are the most peculiar features of lipid bilayers, which are characterized by depth dependent anisotropic stresses and by enormous gradients of properties over a nanometer lengthscale. The profiles of density, lateral forces and order are strictly related to the lipid composition and the physical state of the bilayer: they depend on the acyl chain saturation and the head-group structure and exhibit significant differences between the liquid crystal and the gel phase. The importance of these aspects was early recognized by Dill and coworkers, who singled out the peculiar nature of partitioning when 'interfacial phases' are involved[3,4]. However, the structural features of lipid bilayers were generally ignored in subsequent studies, most of which focused on the effects of the dielectric discontinuity and tried to extend to its description the theoretical and computational methods developed for liquid solvents[5-7]. The introduction of bilayer properties into solvation theories is a difficult task: due to the inherent chemical and structural complexity, modeling of bilayers remains a challenge for statistical theories of liquids[8,9]. Only in a few exceptions the structural features of the bilayer were included in models for solute partitioning between water and lipid membranes. Xiang and Anderson evaluated the free energy change upon formation of a molecular cavity in the bilayer as the reversible work against the lateral pressure, including in this way the configurational entropy and the change in conformational energy of lipid chains[10]. They performed calculations for ellipsoidal solutes, with a lateral pressure profile obtained from coarse grained Molecular Dynamics simulations, and could predict the dependence of solute orientational order parameters on the molecular volume and on the ratio of the long to short molecular axis. Mitragotri and coworkers developed a model for the cavity work for ellipsoidal solutes in the ordered chain region[11]. It was based on a 2D form of scaled particle theory and related partition coefficients to solute size and bilayer properties, like

lipid density and lipid chain order parameters. Kessel and coworkers assumed a decomposition of the solute-bilayer interaction free energy in a set of contributions including, in addition to electrostatic and nonpolar terms, customary in solvation theories, two further terms accounting for elastic deformations of the bilayer and conformational restrictions of lipid chains induced by the solute[12]. The former contributions were described by continuum solvent models with atomistic representation of solute; for the latter the elastic continuum theory and a liquid crystal model, respectively, were used and, for simplicity, the solute was represented as a cylinder.

We present here a theoretical and computational method for modeling the free energy landscape of solutes in lipid bilayers, wherein the order and nonuniformity characteristics of this environment are consistently taken into account. The free energy of solutes is expressed as the superposition of the work required to form a molecular shaped cavity and other contributions associated with the switching on of solute-solvent interactions. The cavity work is evaluated on the basis of the lateral pressure profile[13]. A nonpolar and an electrostatic contribution are evaluated as a function of the density and permittivity gradients in the bilayer[14], respectively; a further term, explicitly accounting for the anisotropy of intermolecular interactions due to lipid chain order, is derived from liquid crystal theory[15]. The environment enters with its collective properties: dielectric permittivity, lateral pressure and density profile, in addition to acyl chain order parameters. Values appropriate for the physical state and composition of the bilayer can be obtained from Molecular Dynamics simulations or from experiments. An atomistic representation of the solute is used, comprising its geometry, charge distribution, polarizability and flexibility. Free energy maps are obtained as a function of molecular position and orientation, whose coupling is intrinsic to the bilayer structure.

In the next section the theoretical model is presented; first, the different contributions to the solute free energy are described, then suitable distribution functions and average values are introduced. In the third section computational details are reported. In the fourth section, cholesterol in liquid crystalline DPPC (1,2-dipalmitoyl-*sn*-glycero-3-phosphatidylcholine) is taken as an example to illustrate the features of the proposed methodology. The results are discussed in relation to experimental data and other theoretical-computational investigations. In the final section capabilities and

limits of the proposed approach are summarized and future developments are outlined.

2.2 Theory

The lipid organization in the bilayer defines an alignment axis, the so-called director (**n**), which in the liquid crystal phase is parallel to the bilayer normal (**N**). So, the degrees of freedom of a rigid solute within the lipid bilayer are: its position along the normal and its orientation with respect to it; the former is defined, in the bilayer frame, by the Z coordinate of the origin of the molecular frame, the latter by the Euler angles, $\Omega=(\alpha,\beta,\gamma)$, which specify the orientation of the molecular frame in the bilayer frame. (Actually, due to the axial symmetry of the environment, the X, Y coordinates of the origin of the molecular frame, as well as the Euler angle α, do not need to be specified). Reference frames and transformations are sketched in Figure 1. Our implicit model assumes that the solute positional and orientational distribution is determined by a mean field potential $U(\Omega,Z)$: this can be viewed as the energy of the 'solute microstate' (Ω,Z) in the solvent, under the implicit assumption that all degrees of freedom of the latter are averaged out, which gives $U(\Omega,Z)$ a free energy character. As customary in solvation models[16], we decompose the mean field potential experienced by a solute into a set of contributions:

$$U = U_{cav} + U_{el} + U_{disp} + U_{ord} \,. \tag{1}$$

The first term, U_{cav} , is related to the work required to form a molecular cavity in the medium, whereas the two next terms, U_{el} and U_{disp}, account for the switching on of electrostatic and dispersion interactions between solute and environment, respectively. In addition to these terms, which usually appear in solvation models, we have included a further contribution, U_{ord}, which can be traced back to the anisotropy of intermolecular interactions, due to acyl chain order, in the bilayer environment. In the following, the individual contributions to the mean field potential will be considered and the model adopted for each of them will be presented.

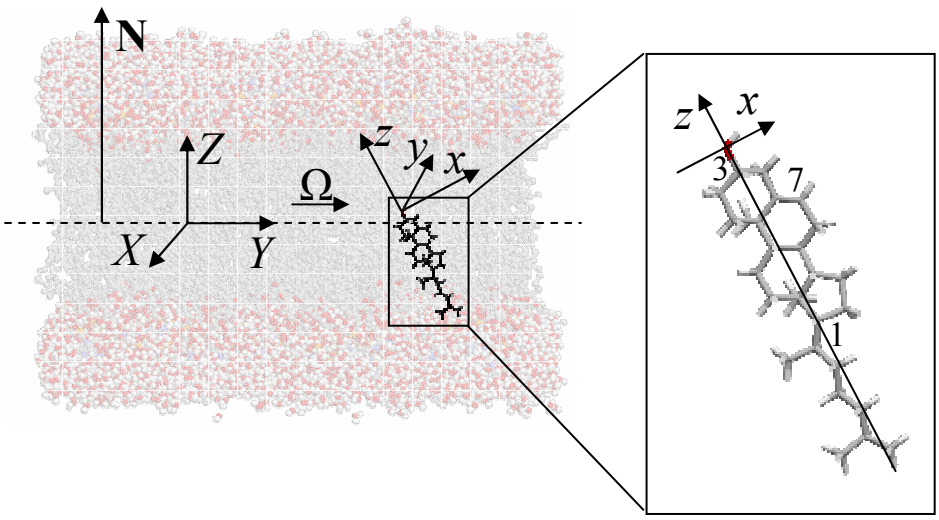

Figure 1: Cholesterol and DPPC bilayer, with the bilayer and the molecular reference frames, (*X,Y,Z*) and (*x,y,z*), respectively. The laboratory frame has its origin in the bilayer midplane and the *Z* axis parallel to the bilayer normal (**N**); the latter is directed from the midplane towards water. The molecular frame has its origin at the nuclear position of the oxygen atom and the *x, y,* and *z* axes anchored to the fused ring core, with the *z* axis parallel to the C_3-C_{17} segment and the *x* axis coplanar with C_7 (atom numbering as Figure S5). The Euler angles $\Omega=(\alpha,\beta,\gamma)$ specify the orientation of the molecular frame with respect to the laboratory frame.

2.2.1 Cavity work

The cavity contribution to the mean field potential is evaluated as the work against the external pressure to create a cavity containing the solute. As a consequence of the system organization, an axially symmetric pressure tensor can be defined in liquid crystalline bilayers; one of its components, the normal pressure P_N, is parallel to the normal and everywhere equal to the bulk water pressure, whereas the other component, the lateral pressure P_L, is a function of depth, due to the position dependence of forces in the interior of the bilayer. The difference $\pi(Z) = P_L(Z) - P_N$, generally denoted as lateral pressure profile, is identified with the opposite of a surface tension and describes the local tendency of the bilayer to contract, becoming thicker ($P_L - P_N < 0$), or to expand, becoming thinner ($P_L - P_N > 0$)[13,17-19]. Though not easily measurable, the lateral pressure profile across a lipid bilayer can be calculated. General forms can be derived by statistical-thermodynamics models[9], whereas more specific profiles can be obtained from atomistic simulations[20]. The lateral pressure should be intended as a force per unit area perpendicular to the bilayer plane, and varies dramatically with the position across the bilayer, ranging from very high positive to very low negative values within a few nanometres. Three

regions are generally identified: (1) the hydrophilic head group region, where $P_L>0$ due to electrostatic and steric interactions and hydration repulsion; (2) the membrane-water interface, where $P_L<0$ as a consequence of to the tendency to decrease the lipid-water interfacial area; (3) the bilayer interior, where again $P_L>0$, due to steric repulsions between hydrophobic chains. The stability of the bilayer is determined by the balance of these contributions. The lateral pressure profile is a specific property of the bilayer, which depends on its chemical composition and physical state[20,21]. The integral of the lateral pressure profile across a monolayer is equal to the opposite of its surface tension[22]. In a tensionless bilayer the surface tension vanishes: repulsion in hydrophobic and hydrophilic regions, mainly due to short range lipid-lipid interactions and headgroup hydration, is balanced by cohesion, ascribed to the hydrophobic effect, at the hydrophobic/hydrophilic interface. The first moment of the lateral pressure profile is related to the bending elastic modulus and the second moment to the saddle splay modulus[23-25].

The work required to create a molecular shaped cavity containing a solute at the position Z with orientation Ω is calculated as the integral[13]:

$$U_{cav}(\Omega,Z) = \int_{\substack{cavity\\length}} P_L(Z+z')\sigma(\Omega,Z+z')dz' \qquad (2)$$

where $\sigma(\Omega,Z+z')$ is the surface area of the section of the cavity at the coordinate $(Z+z')$ in the bilayer frame and the integral is over the length of the cavity, along the z' axis of a molecular frame parallel to the bilayer frame, with its origin in Z. $P_L(Z+z')$ is the lateral pressure at the same coordinate $(Z+z')$; in water it takes a constant value, equal to bulk pressure. Thus, changes in sign of the lateral pressure inside the bilayer correspond to regions where solute insertion is favorable ($P_L<0$, i.e. attractive interactions in the bilayer) and unfavorable ($P_L>0$, i.e. repulsive interactions in the bilayer).

2.2.2 Electrostatic interactions

The electrostatic contribution to the mean field potential is the work required to charge the solute in its environment. Within the continuum approximation, the molecule is treated as an assembly of charges in a low dielectric molecular cavity embedded in a dielectric medium and the electrostatic free energy is then evaluated

by solving the Poisson equation[26,27]. Approximate expressions for the electrostatic free energy are provided by the so called Generalized Born models[28,29]. They can account for the chemical structure of the solute at a low computational cost, which may be important when repeated calculations must be performed, as is our case, since several solute positions and orientations must be sampled. A difficulty in the case of bilayers derives from the nanoscale nonuniformity, which makes not obvious the definition of the dielectric permittivity[30]. Forms suitable for the membrane environment have been proposed[31-36]. In the approach developed by Tanizaki and Feig the phospholipid bilayer is modelled as a multilayer composed of a small number of dielectric slabs[14]. Describing the molecular charge distribution as a set of atomic charges located at the nuclear positions, the electrostatic free energy of the solute, in the Ω orientation at the *Z* position along the bilayer normal, is expressed as:

$$U_{el}(\Omega,Z) = -\frac{1}{2}\sum_{i=1}^{N}\sum_{j=1}^{N}\left(\frac{1}{\varepsilon_{in}} - \frac{1}{\frac{\varepsilon_{out}^{i}(Z_i)+\varepsilon_{out}^{j}(Z_j)}{2}}\right)\frac{q_i\, q_j}{\sqrt{r_{ij}^2 + R_i^B R_j^B e^{-\frac{r_{ij}^2}{FR_i^B R_j^B}}}} \qquad (3)$$

where summations are extended to all solute atoms (*N*), q_i is the atomic charge of the *i*th atom at the position Z_i, $\varepsilon_{out}^{i}(Z_i)$ is the local solvent (outer) dielectric constant defined on the basis of the *i*th atom van der Waals radius[14], ε_{in} is the solute (internal) dielectric constant, r_{ij} is the distance between the *i*th and the *j*th charges, *F* is an empirical parameter and and R_i^B is the effective Born radius of the *i*th atom. This is calculated as:

$$R_i^B = \frac{1}{C_0 A_{4\,i} + C_1\left(\frac{3\varepsilon_{out}(Z_i)}{3\varepsilon_{out}(Z_i)+2\varepsilon_{in}}\right)A_{7\,i}} + D + \frac{E}{\varepsilon_{out}(Z_i)+1} \qquad (4)$$

where C_0, C_1, *D*, *E* are empirical parameters and A_{4i}, A_{7i} are atom specific quantities defined as:

$$A_{n\,i} = \left(\frac{1}{(n-3)\left(R_i^{vdW}\right)^{n-3}} - \frac{1}{4\pi}\int\limits_{\substack{molecular\\ volume\\ r'>R_i^{vdW}}}\frac{1}{r'^{n}}d\mathbf{r}'\right)^{\frac{1}{n-3}} \qquad (5)$$

with R_i^{vdW} being the van der Waals radius of the *i*th atom.

2.2.3 Dispersion interactions

The dispersion contribution to the mean field potential is evaluated on the basis of the London expression, which for a pair of polarizable spherical particles, *i* and *j*, with volume polarizabilities α_i and α_j, reads: $U_{ij}^{disp} = -\frac{3}{4} I \frac{\alpha_i \alpha_j}{r_{ij}^6}$. Here r_{ij} is the distance between the centres of the spheres and *I* is the ionization potential, which is taken equal for the two particles. We represent solute and solvent molecules as assemblies of polarizable spheres and introduce the solvent nonuniformity through the position dependent density of its components; thus, the dispersion contribution to the solvation free energy of an arbitrary solute in the Ω orientation at the *Z* position along the bilayer normal, is calculated as:

$$U_{disp}(\Omega, Z) = -\frac{3}{4} I \sum_{i=1}^{N} \alpha_i \sum_{j=1}^{M} \alpha_j \int_{\substack{solvent \\ r' > R_i^d + R_j^{vdW}}} \frac{\rho_j (Z_i + z')}{r'^6} d\mathbf{r}' \qquad (6)$$

where *N* is the number of atoms in the solute and *M* is the number of polarizable units in the solvent. A coarse grained representation of this has been used, whose details are reported in Figure S2. The integral extends over the whole solvent volume outside a sphere centred on the *i*th solute atom, with radius equal to the sum of an effective radius (R_i^d) and the van der Waals radius of the *j*th solvent component (R_j^{vdW}); **r′**=(*x′*,*y′*,*z′*) is a vector position in a local frame, parallel to the bilayer frame, with its origin in the center of the *i*th atom, located at Z_i in the bilayer frame. In the integral, ρ_j is the number density of the *j*th polarizable unit of solvent, which is a function of the position along the bilayer normal, defined by the sum Z_i+*z′*. The atomic effective radius R_i^d is defined as[37]:

$$R_i^d = 1/\sqrt[3]{3} A_{6i} \qquad (7)$$

with A_{6i} calculated according to eq.5.

2.2.4 Anisotropic interactions with acyl chains

The contributions to the mean field potential considered so far retain the nonuniformity of the lipid bilayer, but neglect the presence of orientational order in the lipid chain region. In the liquid crystal phase chains are preferentially aligned along an axis (the director **n**), which coincides with the normal **N** and all properties

are axially symmetric with respect to this axis. The degree of alignment is quantified by the chain order parameters, S_{CD}^{i}, which take their name from the fact that they are obtained from NMR quadrupole splittings for deuteriated acyl chains[38]. They are defined as:

$$S_{CD}^{i} = \frac{3\left\langle \cos^2 \theta_i \right\rangle - 1}{2} \tag{8}$$

where θ_i is the angle between the C_iD bond and the bilayer normal (see Figure S1); the angular bracket denotes a statistical average. If acyl chains were perfectly aligned to the bilayer normal in the all-*trans* conformation, S_{CD}^{i} would be equal to -0.5 for any *i*; for randomly oriented chains (as in isotropic liquids), S_{CD}^{i} would vanish for any *i*. The S_{CD}^{i} order parameters are generally negative, since the C_iD bonds preferentially lie perpendicular to the bilayer normal. They exhibit typical profiles, which depend on the phospholipid structure and the physical state of the system; for saturated lipids, $\left|S_{CD}^{i}\right|$ decrease from relatively high values close to the headgroup, to small values on moving towards the chain end[38].

As a consequence of the chain order, anisotropic interactions are not totally washed out by the orientational average in the bilayer environment. It is important to realize that the interactions which we are considering here have axial symmetry, resulting from the partial alignment of chain segments, though they do not have the polar character originated by the presence of an interface. A related property is birefringence of lipid bilayers; the refractive index parallel to the bilayer normal (n_e) is higher than the perpendicular one (n_o)[39,40], which means that the average polarizability is higher perpendicular than parallel to the bilayer. To account for the anisotropy of the interactions of solutes with acyl chains, we have extended to bilayers a model which was originally proposed for thermotropic nematic liquid crystals[15]. This is a phenomenological molecular field model which has been proven to be able to capture the relation between molecular structure and orientational order in nematics, and has been successfully used to predict the dependence on molecular structure of diverse properties of nematic liquid crystals[41-43]. The model, which can be considered an extension of the Maier-Saupe theory[44] allowing for the account of the molecular shape, bases on the assumption that each element of the surface of a

molecule in the nematic phase (of symmetry $D_{\infty h}$) preferentially aligns to the director. The orienting potential, dU_{ord}, acting on each infinitesimal element dS of the molecular surface, is a function of the angle θ between its normal **s** and the director **n** and can be expanded on a basis of Legendre polynomials[45]. Given the symmetry of the system, the first non-vanishing term of this expansion is proportional to the second Legendre polynomial, thus:

$$dU_{ord} = k_B T \xi P_2(\cos\theta) dS \tag{9}$$

where k_B is the Boltzmann constant, T is temperature and ξ is a positive parameter, which quantifies the orienting strength of the environment; it depends on the degree of orientational order and vanishes in the isotropic phase. The overall orienting potential experienced by a molecule in the nematic phase is then obtained by integrating eq.9 over the molecular surface, S:

$$U_{ord}(\Omega) = k_B T \xi \int_S P_2(\cos\theta) dS . \tag{10}$$

It can be easily seen that, in the model case of a cylindrical particle with lateral area S_{cyl}, the Maier-Saupe form[44] is recovered, $U_{ord}(\beta) = -c_2 P_2(\cos\beta)$, where β is the angle between cylinder axis and nematic director and $c_2 = k_B T \xi S_{cyl}/2$:[46] the particle preferentially orients with its axis along the nematic director, with no distinction between parallel and antiparallel orientation. According to the molecular field theory, the orienting strength can be related to the order parameters of the nematic phase[47]; if mesogens are approximated as cylindrical particles, the relationship $\xi \propto \langle P_2 \rangle$ holds, where $\langle P_2 \rangle$ is the second rank order parameter, which specifies the degree of order of cylinders[15]. It may be worth remarking that the mean field potential, eq.10, is experienced by all molecules in the nematic system, both mesogens and solutes, if present. The specific form of this potential will depend on the molecular structure, through the molecular surface. On the contrary, the orienting strength ξ is a phase property; at low concentration of solutes it is nearly the same as for the pure nematic solvent, and is proportional to solvent order parameters.

Extension of the model to lipid bilayers requires the introduction of a position dependent orienting strength, $\xi = \xi(Z)$; so the orienting contribution to the mean field potential experienced by a solute in a lipid bilayer is expressed as:

$$U_{ord}\left(Z,\Omega\right)=k_BT\int_S\xi\left(Z+z'\right)P_2\left(\cos\theta\right)\mathrm{d}S \tag{11}$$

where z' is the position of the surface element dS along an axis parallel to the normal **N**, in a molecular frame parallel to the bilayer frame, with its origin in Z. The profile of the orienting strength, $\xi(Z)$ is a specific function of the bilayer, which depends on lipid composition and temperature. Extending to the bilayer the same considerations valid for nematics, we can assume a linear relationship between orienting strength ξ and S_{CD}^i order parameters: the orienting strength at the coordinate $\langle Z_i\rangle$, equal to the average position, along the bilayer normal, of the C_i atom, is expressed as: $\xi\left(\left\langle Z_i\right\rangle\right)=-\left(A/k_BT\right)S_{CD}^i$, where A is a positive constant. Given the S_{CD}^i order parameters, which are available from experiments or simulations, the values of A and $\langle Z_i\rangle$ can be determined as explained in the SI-1.

2.2.5 Density probability for solute position and orientation

For any molecular position along the bilayer normal and any molecular orientation in the bilayer frame of reference, the mean field potential $U(\Omega,Z)$ is calculated as the sum of the contributions expressed by eqs.2,3,6,11. Under the conditions of the canonical ensemble, the coupled positional-orientational distribution function can then be calculated as:

$$P\left(\Omega,Z\right)=\frac{e^{-\frac{U(\Omega,Z)}{k_BT}}}{Q} \tag{12}$$

with the partition function:

$$Q=\int_0^L dZ\int e^{-\frac{U(\Omega,Z)}{k_BT}}d\Omega \tag{13}$$

where T is the temperature, k_B is the Boltzmann constant and

$$\int\mathrm{d}\Omega=\int_0^{2\pi}\mathrm{d}\gamma\int_0^{\pi}\sin\beta\mathrm{d}\beta\ .$$

The normalization condition $\int_0^L dZ\int P\left(\Omega,Z\right)d\Omega=1$ holds. The integral over the Z variable is taken over the bilayer half-thickness, under the assumption that the midplane is a symmetry plane. The upper integration limit, L, depends on the system

under investigation. For the calculation of all those properties which only depend on the solute behaviour within the bilayer, but are unaffected by the relative amount of solute in water and bilayer, we can take as a reasonable choice for L a value large enough to ensure that for $Z=L$ the solute behaviour can be assumed to be the same as in bulk water.

We can then define the reduced probability distribution function:

$$P_{\Omega}(Z) = \frac{Q_{\Omega}(Z)}{Q} \tag{14}$$

where the orientational partition function is defined as:

$$Q_{\Omega}(Z) = \int e^{-\frac{U(\Omega,Z)}{k_B T}} d\Omega \tag{15}$$

so that the normalization condition $\int_0^L P_{\Omega}(Z)\,dZ = 1$ holds. The reduced distribution function $P_{\Omega}(Z)$ can be expressed in the Boltzmann form:

$$P_{\Omega}(Z) = \frac{e^{-\frac{u(Z)}{k_B T}}}{\int_0^L e^{-\frac{u(Z)}{k_B T}} dZ} \tag{16}$$

with

$$u(Z) = \text{const} - k_B T \ln Q_{\Omega}(Z), \tag{17}$$

which can be interpreted as the transfer free energy of the solute from water to the position Z in the bilayer, if the constant is taken equal to the value of $k_B T \ln Q_{\Omega}$ in bulk water.

Once the coupled positional-orientational distribution is known, the average value $\langle f \rangle$ of any arbitrary function $f(\Omega,Z)$ is defined as:

$$\langle f \rangle = \int_0^L dZ \int f(\Omega,Z) P(\Omega,Z)\, d\Omega\,. \tag{18}$$

Partially averaged functions may also be meaningful; for instance, the orientationally averaged value of the function $f(\Omega,Z)$ can be calculated as:

$$\langle f \rangle_{\Omega}(Z) = \frac{1}{P_{\Omega}(Z)} \int f(\Omega,Z) P(\Omega,Z)\, d\Omega\,. \tag{19}$$

2.2.6 Distribution functions for flexible solutes

The model can be easily extended to flexible solutes. Let us denote as $\boldsymbol{\chi}$ the torsional degrees of freedom of the solute; then, the mean field potential, eq.1, will become a function of the molecular conformation, $U(\Omega,Z,\boldsymbol{\chi})$. If $V(\boldsymbol{\chi})$ is the torsional potential of the molecule in vacuum, the coupled orientational-positional-torsional density probability of the solute is defined as:

$$P(\Omega,Z,\boldsymbol{\chi}) = \frac{e^{-\frac{V(\boldsymbol{\chi})}{k_B T}} e^{-\frac{U(\Omega,Z,\boldsymbol{\chi})}{k_B T}}}{Q} \tag{20}$$

with the partition function

$$Q = \int_0^L dZ \int d\Omega \int e^{-\frac{V(\boldsymbol{\chi})}{k_B T}} e^{-\frac{U(\Omega,Z,\boldsymbol{\chi})}{k_B T}} d\boldsymbol{\chi} \tag{21}$$

and the normalization condition $\int_0^L dZ \int d\Omega \int P(\Omega,Z,\boldsymbol{\chi}) d\boldsymbol{\chi} = 1$.

In analogy with what shown above, we can define a reduced position distribution function $P_{\Omega,\boldsymbol{\chi}}(Z)$:

$$P_{\Omega,\boldsymbol{\chi}}(Z) = \frac{Q_{\Omega,\boldsymbol{\chi}}(Z)}{Q} \tag{22}$$

with

$$Q_{\Omega,\boldsymbol{\chi}}(Z) = \int d\Omega \int e^{-\frac{V(\boldsymbol{\chi})}{k_B T}} e^{-\frac{U(\Omega,Z,\boldsymbol{\chi})}{k_B T}} d\boldsymbol{\chi} \tag{23}$$

and the normalization condition: $\int_0^L P_{\Omega,\boldsymbol{\chi}}(Z) dZ = 1$. In analogy with eq.17, we can define the free energy:

$$u(Z) = \text{const} - k_B T \ln Q_{\Omega,\boldsymbol{\chi}}(Z), \tag{24}$$

which includes entropic effects deriving from rotational and torsional restrictions in the bilayer environment.

The effect of the environment on the conformational distribution can be analysed in terms of the reduced conformational distribution functions, obtained by averaging over the orientational and positional degrees of freedom:

$$P_{\Omega,Z}(\boldsymbol{\chi}) = \frac{Q_{\Omega,Z}(\boldsymbol{\chi})}{Q} \tag{25}$$

with

$$Q_{\Omega,Z}(Z,\chi) = e^{-\frac{V(\chi)}{k_B T}} \int_0^L dZ \int e^{-\frac{U(\Omega,Z,\chi)}{k_B T}} d\Omega \tag{26}$$

and the normalization condition $\int P_{\Omega,Z}(\chi)\, d\chi = 1$. Eq.25 can also be expressed as:

$$P_{\Omega,Z}(\chi) = \frac{e^{-\frac{V'(\chi)}{k_B T}}}{\int e^{-\frac{V'(\chi)}{k_B T}} d\chi} \tag{27}$$

with

$$V'(\chi) = \text{const} - k_B T \ln Q_{\Omega,Z}(\chi). \tag{28}$$

If the constant is taken such that $V'(\chi) = V(\chi)$ for $U(\Omega,Z,\chi)=0$, eq.28 defines an effective torsional potential in the water/bilayer environment. Given the nonuniform character of this system, a more meaningful property should retain the position dependence. A depth dependent effective torsional potential $V'(Z,\chi)$ can be defined, from the reduced distribution function:

$$P_{\Omega}(Z,\chi) = \frac{Q_{\Omega}(Z,\chi)}{Q} \tag{29}$$

with

$$Q_{\Omega}(Z,\chi) = e^{-\frac{V(\chi)}{k_B T}} \int e^{-\frac{U(\Omega,Z,\chi)}{k_B T}} d\Omega \tag{30}$$

and the normalization condition $\int_0^L dZ \int P_{\Omega}(Z,\chi)\, d\chi = 1$. The effective torsional potential is then defined as:

$$V'(Z,\chi) = c(Z) - k_B T \ln Q_{\Omega}(Z,\chi) \tag{31}$$

With $c(Z)$ chosen in such a way that $V'(Z,\chi) = V(\chi)$ for $U(\Omega,Z,\chi)=0$.

The average value $\langle f \rangle$ of any arbitrary function $f(\Omega,Z,\chi)$ can be calculated as:

$$\langle f \rangle = \int_0^L dZ \int d\Omega \int f(\Omega,Z,\chi) P(\Omega,Z,\chi) d\chi; \tag{32}$$

partially averaged function can also be defined, in analogy with eq.19. In particular, the positional-orientational average for a given conformation can be calculated as:

$$\langle f \rangle_{\Omega,Z}(\boldsymbol{\chi}) = \frac{1}{P_{\Omega,Z}(\boldsymbol{\chi})} \int_0^L dZ \int f(\Omega,Z) P(\Omega,Z,\boldsymbol{\chi}) d\Omega ; \tag{33}$$

this is the property that would be calculated for the molecule frozen in the conformation specified by the $\boldsymbol{\chi}$ dihedrals. The full average, eq.32 can be obtained from partial averages, eq.33, as $\langle f \rangle = \int \langle f \rangle_{\Omega,Z}(\boldsymbol{\chi}) P_{\Omega,Z}(\boldsymbol{\chi}) d\boldsymbol{\chi}$.

If the torsional potential is characterized by localized minima, separated by barriers higher than few $k_B T$ units, the molecular flexibility can be described in terms of a finite number of conformers, corresponding to minima of the potential energy[48]. Then the single conformer orientational-positional distribution function

$$P_J(\Omega,Z) = \frac{e^{-\frac{V_J}{k_B T}} e^{-\frac{U_J(\Omega,Z)}{k_B T}}}{Q} \tag{34}$$

can be introduced, where the index J is used to indicate functions calculated for the Jth conformer ($\boldsymbol{\chi}=\boldsymbol{\chi}_J$), and integration over the $\boldsymbol{\chi}$ dihedrals can be replaced by summation over conformers; for instance, $Q = \sum_J \int_0^L dZ \int e^{-\frac{V_J}{k_B T}} e^{-\frac{U_J(\Omega,Z)}{k_B T}} d\Omega$.

2.3 Numerical Methods

Computation of each of the contributions to the mean field potential, eq.1, requires a definition of the solute molecular surface. The solvent-excluded surface[49], calculated as a triangulated surface according to the Sanner algorithm[50], is used. The expressions used to calculate eqs.2,5,6,11 are reported in the following. In these expressions N_f represents the number of triangular faces, $\boldsymbol{s}_J$, with components ($s_{J,X}$, $s_{J,Y}$, $s_{J,Z}$) in the bilayer frame, is the outwards pointing unit vector normal to the Jth face and S_J is the surface area of this face.

Eq.2. The volume integral in eq.2 is calculated as the sum over N_s slices of thickness $\Delta z'$ perpendicular to the bilayer normal:

$$\int_{\substack{molecular \\ length}} \pi(Z+z')\sigma(\Omega,Z+z')dz' = \sum_{i=1}^{N_s} \pi(Z+z'_i)\sigma(\Omega,Z+z'_i)\Delta z' \tag{35}$$

The section area, $\sigma(\Omega,Z+z'_i)$, is calculated from the perimeter of the λ-sided polygon, defined by the intersection of the triangulated surface with the ith plane, according to Surveyor's formula for non self-intersecting polygons[51]:

$$\sigma\left(Z+z'_i\right)=\left|\frac{1}{2}\sum_{\alpha=1}^{\lambda}\left(x'_\alpha y'_{\alpha+1}-x'_{\alpha+1}y'_\alpha\right)\right| \tag{36}$$

where $\left(x'_\alpha,y'_\alpha\right)$, with α=1,…,λ, are the coordinates of the polygon vertices, ordered according to consecutive sides, with the boundary condition $\left(x'_{\lambda+1},y'_{\lambda+1}\right)=\left(x'_1,y'_1\right)$.

Eq.5. The volume integrals A_{ni} , defined in eq.5, are conveniently rewritten in the form of surface integrals, using Gauss's theorem[52]:

$$A_{n\,i}=\left[\frac{1}{n-3}\left(\frac{1}{\left(R_i^{vdW}\right)^{n-3}}-\frac{1}{4\pi}\int\limits_{\substack{molecular\\volume\\r>R_i^{vdW}}}\left(-\nabla\cdot\frac{\mathbf{r}}{r^n}\right)d\mathbf{r}\right)\right]^{\frac{1}{n-3}}=\left[\frac{1}{4(n-3)\pi}\int_S\frac{\mathbf{r}}{r^n}\cdot\mathbf{s}\;dS\right]^{\frac{1}{n-3}} \tag{37}$$

The integral is then calculated as a sum over the triangular faces:

$$A_{n\,i}=\left(\frac{1}{4(n-3)\pi}\sum_{J=1}^{N_f}\frac{\mathbf{r}_{iJ}}{r_{iJ}^n}\cdot\mathbf{s}_J S_J\right)^{\frac{1}{n-3}} \tag{38}$$

where $\mathbf{r}_{iJ}$ is the vector from the centre of the ith atom to the centre of mass of the Jth face.

Eq.6. Due to the axial symmetry of the bilayer, the volume integral in eq.6 is conveniently calculated in cylindrical coordinates (z',q,ϕ):

$$\begin{aligned}\int\limits_{\substack{solvent\\r'>R_{ij}}}\frac{\rho_j\left(Z_i+z'\right)}{r'^6}\mathrm{d}\mathbf{r}'&=\left[\begin{array}{l}\displaystyle\int\limits_{R_{ij}}^{z'_{\max}}\rho_j\left(Z_i+z'\right)\mathrm{d}z'\int_0^\infty\frac{q}{\left(q^2+z'^2\right)^3}\mathrm{d}q\int_0^{2\pi}\mathrm{d}\phi+\\+\displaystyle\int\limits_{-R_{ij}}^{R_{ij}}\rho_j\left(Z_i+z'\right)\mathrm{d}z'\int\limits_{\sqrt{R_{ij}^2-z'^2}}^\infty\frac{q}{\left(q^2+z'^2\right)^3}\mathrm{d}q\int_0^{2\pi}\mathrm{d}\phi+\\+\displaystyle\int\limits_{-z'_{\max}}^{-R_{ij}}\rho_j\left(Z_i+z'\right)\mathrm{d}z'\int_0^\infty\frac{q}{\left(q^2+z'^2\right)^3}\mathrm{d}q\int_0^{2\pi}\mathrm{d}\phi\end{array}\right]\\&=\frac{\pi}{2}\left[\int\limits_{R_{ij}}^{z'_{\max}}\frac{\rho_j\left(Z_i+z'\right)}{z'^4}\mathrm{d}z'+\frac{1}{R_{ij}^4}\int\limits_{-R_{ij}}^{R_{ij}}\rho_j\left(Z_i+z'\right)\mathrm{d}z'+\int\limits_{-z'_{\max}}^{-R_{ij}}\frac{\rho_j\left(Z_i+z'\right)}{z'^4}\mathrm{d}z'\right]\end{aligned} \tag{39}$$

where $R_{ij} = R_i^d + R_j^{vdW}$. Under the assumption that the size of the sample is much larger than R_{ij}, the integrals over the q variable are calculated by extending to infinity the upper integration limit. In our calculations $z'_{\max} = 4R_{ij}$ was taken. The three integrals in the final expression are calculated with the composite midpoint formula[53].

Eq.11. The surface integral in eq.11 is simply calculated as the sum over all triangular faces:

$$\int_S \xi\left(Z+z'\right) P_2\left(\cos\theta\right) \mathrm{d}S = \sum_{J=1}^{N_f} \xi\left(Z+z'_J\right) \frac{3s_{J,Z}^2 - 1}{2} S_J \,, \tag{40}$$

where the position of the *J*th face is identified with that of its center of mass.

Free energy profiles and average quantities. Gauss-Legendre and Gauss-Chebyshev quadrature algorithms were used for numerical integration over the orientational variables β and γ, respectively[53]. Numerical integration over the position variable Z was simply performed according to the composite midpoint formula; calculations for cholesterol in DPPC were performed giving the upper integration limit the value *L*=45 Å. Convergence of numerical integrals was checked for free energy profiles and other average properties. A typical calculation, using 12 β, 24 γ and 91 Z points, takes a time of the order of hundreds of seconds of CPU time on a 2GHz desktop PC.

2.4 Cholesterol in DPPC

2.4.1 Bilayer parameterization Figure 2 shows the profiles of bilayer properties needed for the calculations. Lateral pressure[54], mass density[55] and S_{CD} order parameters[56] profiles were taken from Molecular Dynamics simulations of a DPPC bilayer in the liquid crystal phase at the temperature *T*=323 K. The definition of polarizable units and the corresponding mass density profiles, appearing in eq.6 are reported in Figure S2; the value $I=2\cdot10^{-18}$ J [57] was assumed in this equation. The outer dielectric constant profiles, used in eqs.3-4, were calculated on the basis of a three dielectric model, as proposed in ref.[14]. The empirical parameters appearing in eq.4 were determined by matching electrostatic free energies, calculated according to eq.3, to those calculated by finite difference solution of the Poisson equation, for a

test set of molecules (see SI-3). Part of the same molecules were used to check calculated water/*n*-octanol transfer free energies against experimental values (see SI-4). Given the S_{CD} order parameters, the profile of the orienting strength, $\xi(Z)$, entering eq.11, was obtained by nonlinear fitting of the values calculated at the average acyl chain carbon positions, $\xi(\langle Z_i \rangle)$ (see SI-1).

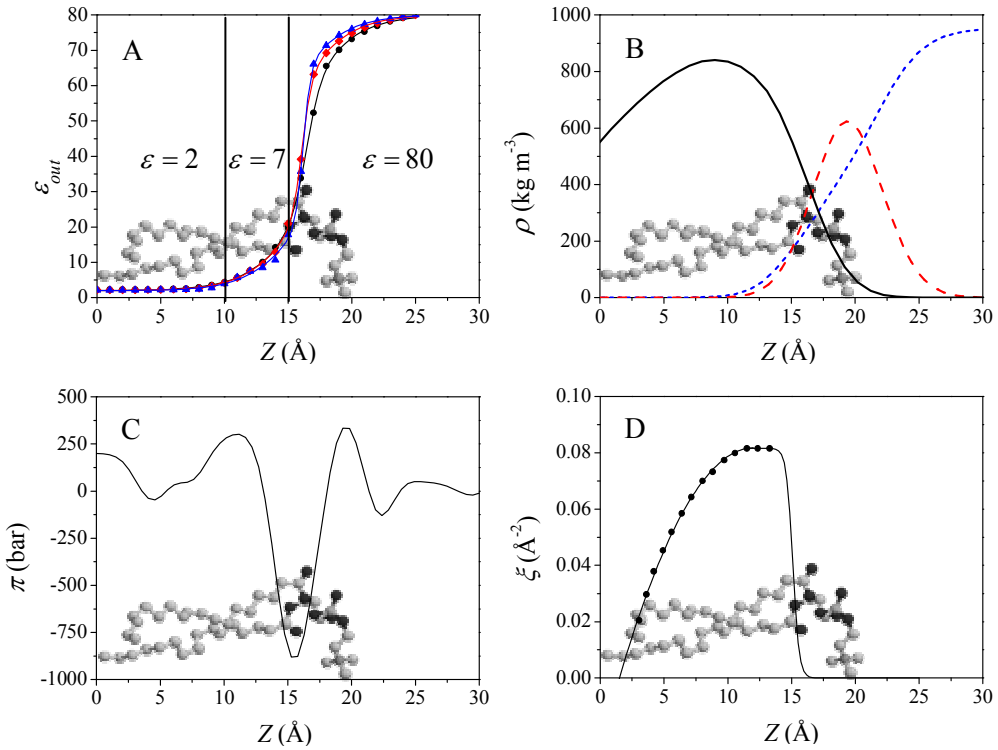

Figure 2: DPPC properties used in the calculations, shown as a function of the distance from bilayer midplane. A) Local dielectric constant profile calculated with a three dielectric model, as described in ref.[14], for ions of van der Waals radius equal to 1 Å (triangles), 1.85 Å (circles) and 1.5 Å (squares). B) Mass density profile for lipid tails (solid line), lipid headgroups (dashed line) and water (dotted line)[55]. C) Lateral pressure profile[54]. D) Orienting strength profile from S_{CD} order parameters for the *sn*1 acyl chain[56]. All the data refer to the temperature T=323 K. A phospholipid molecules is superimposed on each plot, to indicate different bilayer regions.

2.4.2 Solute structural data Nine conformers of cholesterol differing in the alkyl chain conformation, were taken for our calculations (see Figure S6). Conformer energy and geometry were obtained by DFT optimization in vacuum at the B3LYP/6-31g** level[58]. A common molecular frame was chosen for all conformers, with the origin at the nuclear position of the oxygen atom and the (x,y,z) axes fixed to the rigid core, as shown in Figure 1. Solute parameters used for calculations are summarized in Table 1.

Table 1: Parameters used in calculations for cholesterol.

van der Waals radii	H: 1.00Å; C: 1.85Å; O: 1.50Å[59]
Connolly surface	probe sphere radius = 3Å; vertex density = 13Å^{-2}
atomic charges	OPLS force field[60] (see Table S1)
atomic polarizabilities ($4\pi\varepsilon_0$ Å^3)	from bond polarizabilities[57] * H–C: 0.65; C–C: 0.57; C=C: 1.65; C–O: 0.64; O–H: 0.73
internal dielectric constant	$\varepsilon_{in} = 2$ [14]
Born empirical parameters	$F = 8$; $C_0 = 0.3028$; $C_1 = 1.009$; $D = 0.00$ Å^{-1}; $E = -0.16$ Å^{-1} **

* Half of a bond polarizability is assigned to each of the two connected atoms, hence the polarizability of an atom is obtained as half the sum of the polarizabilities of all the bonds in which it is involved.

** Obtained from optimization with respect to finite difference solution of the Poisson equation, for a test set of benzene derivatives (see SI-3), according to the procedure reported in ref.[61].

2.4.3 Results: free energy and distributions Figure 3 displays the transfer free energy profile and the corresponding position distribution function, calculated by averaging over all nine conformers of cholesterol. The transfer free energy profile exhibits a marked position dependence, not only near the water/bilayer interface, but also in the hydrocarbon region. The free energy minimum, which is about 13 kcal/mol lower than the free energy in bulk water, is reached when cholesterol is inserted in the bilayer, with the oxygen at a distance of about 18 Å from the midplane. The position distribution function $P_{\Omega\chi}$, shown in Figure 3, indicates that cholesterol, though confined with the oxygen atom near the hydrophobic/hydrophilic interface, may undergo wide-amplitude fluctuations parallel to the bilayer normal. Both the average position and the vertical distribution of cholesterol are in agreement with experimental data. By recent neutron scattering experiments, the center of mass of deuteriated sites of [2,2,3,4,4,6-$^2H_6$]-labeled cholesterol, in the liquid crystalline phase of different lipid bilayers, was found to be confined in a region a few Ångstroms wide, centered at approximately 16 Å from the midplane[62]. Vertical motions of cholesterol wider than 5 Å were also revealed by quasielestic neutron

scattering experiments in 40% cholesterol:DPPC bilayers in the liquid ordered phase[63].

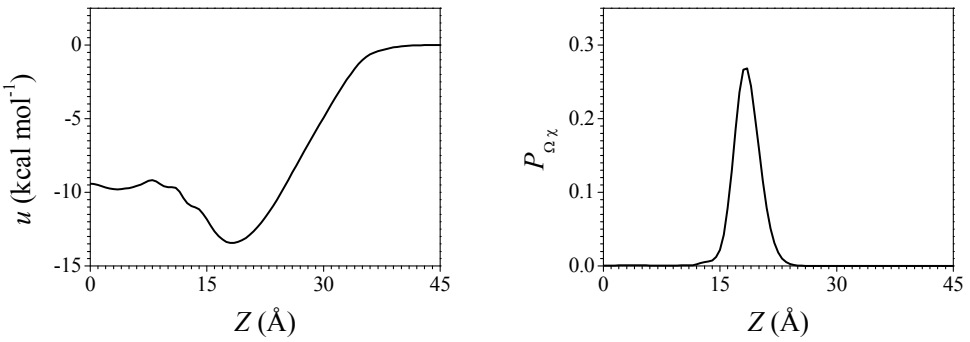

Figure 3: Transfer free energy (left) and position distribution (right) profiles of cholesterol as a function of distance of the oxygen atom from the bilayer midplane. The results shown here were obtained as averages over all conformers at the temperature *T*=323K.

The tail flexibility has negligible effects on the free energy profile of cholesterol (see Figure S7), which is not surprising, given the small size of the alkyl chain in comparison to the broad ring region and the reduced conformational space explored by the tail, due to steric constraints. For this reason in the following, until differently stated, we will simply refer to the results obtained for the B conformer of cholesterol (see Figure S6).

With the purpose of disentangling the role of the different contributions to the mean field potential, we show in Figure 4 the free energy profiles and the corresponding position distribution functions, obtained by excluding a single contribution at a time in eq.1. The figure clearly shows that dispersion interactions bear the main responsibility for the free energy decrease within the bilayer, in agreement with the simple picture of cholesterol brought into the bilayer by favorable interactions with lipid chains. Electrostatic interactions, which in the case of cholesterol mostly involve the OH group, have the effect of destabilizing upside down configurations, with this group located deep in the bilayer interior. The effects of the order and cavity contribution to the mean field potential will be clearer below, when the order parameters of cholesterol are discussed; however something can be anticipated in relation to the transfer free energy and the distribution profiles shown in Figure 4. The order contribution promotes alignment of the long axis of cholesterol to the director, i.e. the average orientation of acyl chains, which in the liquid crystalline

phase of DPPC coincides with the bilayer normal **N**. The small shift of the oxygen atom towards the lipid head-groups, which we can observe in Figure 4 upon inclusion of the order contribution in the mean field potential, can be explained by the fact that it allows a larger portion of the broad and thick core of cholesterol to lie in the most ordered lipid region (it may be useful to look at the molecular surface of cholesterol, which is shown in Figure S8). Given the strong orienting effect of the ordering term, the cavity contribution, which would bring about insertion of cholesterol flat at the hydrophobic/hydrophilic interface, where there is a deep well in the lateral pressure, seems to play a minor role.

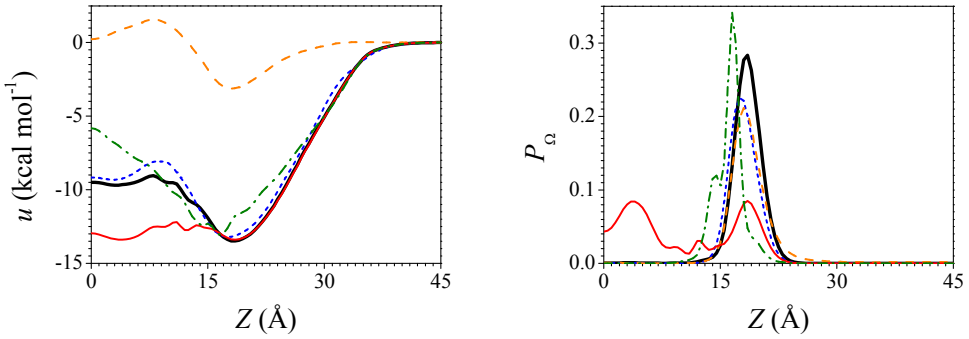

Figure 4: Transfer free energy (left) and position distribution (right) profiles calculated for cholesterol as a function of the distance of the oxygen atom from the bilayer midplane, using an incomplete form of the mean field potential $U(\Omega,Z)$. Profiles were obtained by excluding in turn the single cavity (thin dotted line), the electrostatic (thin solid line), the dispersion (thin dashed line), and the chain order (thin dash-dotted line) contribution in eq.1. The profiles from the complete form of the potential (thick solid line) are also shown for comparison. The results shown here were obtained for the B conformer, at the temperature T=323K.

The free energy profile shown in Figure 3 compares well with that reported in Figure 1b of ref.[64], which was obtained from long all-atom Molecular Dynamics simulations (3 μs long trajectories) of cholesterol in DPPC. Perhaps more interestingly, the relatively small differences between the free energy profiles obtained from all-atom simulations of cholesterol and its analog missing the hydroxyl group in DPPC, displayed in Figure S5 of the same reference[64], closely resemble the differences arising from removing electrostatic interactions in our model, as shown in Figure 4. There is however a scale factor: the transfer free energy calculated with our model is about 30% lower, in absolute value, than that obtained from simulations, which probably reflects a different parameterization of interactions. In fact, discrepancies of

this magnitude are not uncommon even between simulations using different force fields.

A major feature of our model is the inclusion of orientation-position coupling inside the lipid bilayer. Figure 5 shows the map of the mean field potential, calculated in correspondence of the maximum of the position distribution probability, as a function of the Euler angles (β,γ), defining the molecular orientation. The figure shows a strong dependence of the potential on the Euler angle β between the long axis of cholesterol and the bilayer normal (see Figure 1), with the energy increasing as cholesterol moves from parallel to antiparallel. The dependence of the mean field potential on the γ angle indicates that cholesterol has some preference to keep the molecular plane (i.e. the *xz* plane) parallel to the bilayer normal.

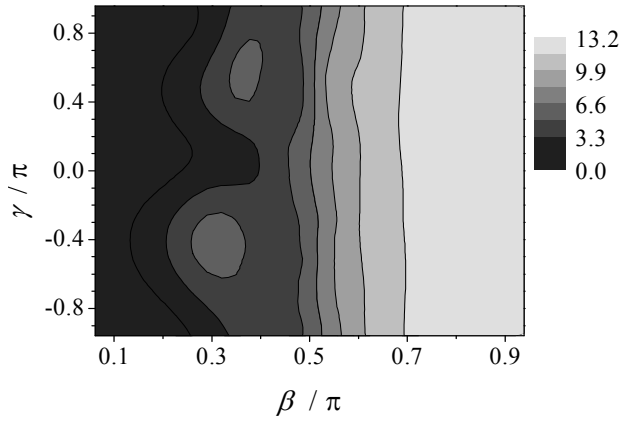

Figure 5: Contour plot of the mean field potential *U*, eq.1, as a function of the Euler angles (β, γ) defining the solute orientation in the bilayer frame (Figure 1), calculated in correspondence of the maximum of the position distribution. The results shown here were obtained for the B conformer of cholesterol at the temperature *T*=323K. Energies are expressed in kcal mol^{-1} and a value equal to zero is given to the minimum of the mean field potential in the plot.

A complete insight into the orientational behaviour of the solute is provided by orientational order parameters. The order parameter $\langle P_1 \rangle = \langle \cos\beta \rangle$ describes the polarity of the orientational distribution; it can take values ranging from -1 to 1, with the extremes corresponding to the molecular *z* axis antiparallel and parallel to the bilayer normal, respectively, going through 0 for an apolar distribution. The second rank order parameters $S_{ii} = (3\langle \cos^2\theta_{iZ} \rangle - 1)/2$, with θ_{iZ} denoting the angle between the *i*th molecular axis (*i*=*x,y,z*) and the bilayer normal, quantify the degree of alignment of molecular axes to the bilayer normal. Unlike $\langle P_1 \rangle$, the S_{ii} order parameters do not

distinguish between parallel and antiparallel orientations; they range between -0.5 (*i* axis perpendicular to the director) and 1 (*i* axis parallel to the director). Figure 6 shows the profile of the order parameters $\langle P_1 \rangle$ and S_{ii} calculated for the B conformer of cholesterol. Here, we can distinguish at least three zones: i) a first region where cholesterol is in upright orientations, well aligned to the bilayer normal **N** with its head in water or in the hydrophilic region, pointing towards water; ii) a second region where the oxygen atom is close to the midplane and the long axis is again aligned to **N**; iii) an intermediate region, where cholesterol lies inside the bilayer, with its long axis preferentially perpendicular to **N** and the molecular plane perpendicular to the bilayer plane.

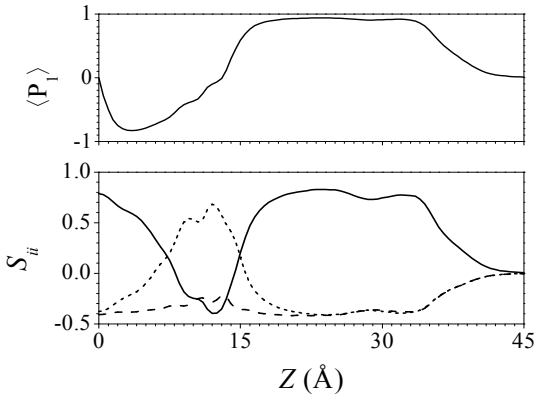

Figure 6: Local orientational order parameters calculated for cholesterol as a function of the distance of the oxygen atom from the bilayer midplane. The plot at the bottom shows the diagonal elements of the Saupe tensor, calculated in the molecular frame (Figure 1): S_{xx} (dotted line), S_{yy} (dashed line) and S_{zz} (solid line). The results shown here were obtained for the B conformer, at the temperature T=323K.

The result is a clear indication of the peculiar effects of the nanoscale organization of lipid bilayers. It must be remarked that the probability that cholesterol resides in the ii) or in the iii) regions is negligible, as shown in Figure 3. This is in agreement with the absence of experimental evidences for cholesterol lying flat inside DPPC bilayers. However we can speculate that such orientations may be favoured under different conditions, e.g. when the nature of phospholipids leads to a different balance of forces within the bilayer. Indeed, the existence of the horizontal orientation of cholesterol in poly-unsaturated phospholipids was recently demonstrated by neutron scattering investigations[62,65]. Some preference for orientations parallel to the bilayer plane was also found in atomistic simulations of

cholesterol, sitting in scarcely populated regions inside DPPC or other lipid bilayers[64].

With the help of Figure 7, which shows the order parameters calculated by excluding one contribution at a time, we can now distinguish the different contributions to the orientational order of cholesterol. From inspection of the plots in this figure we can draw the following picture.

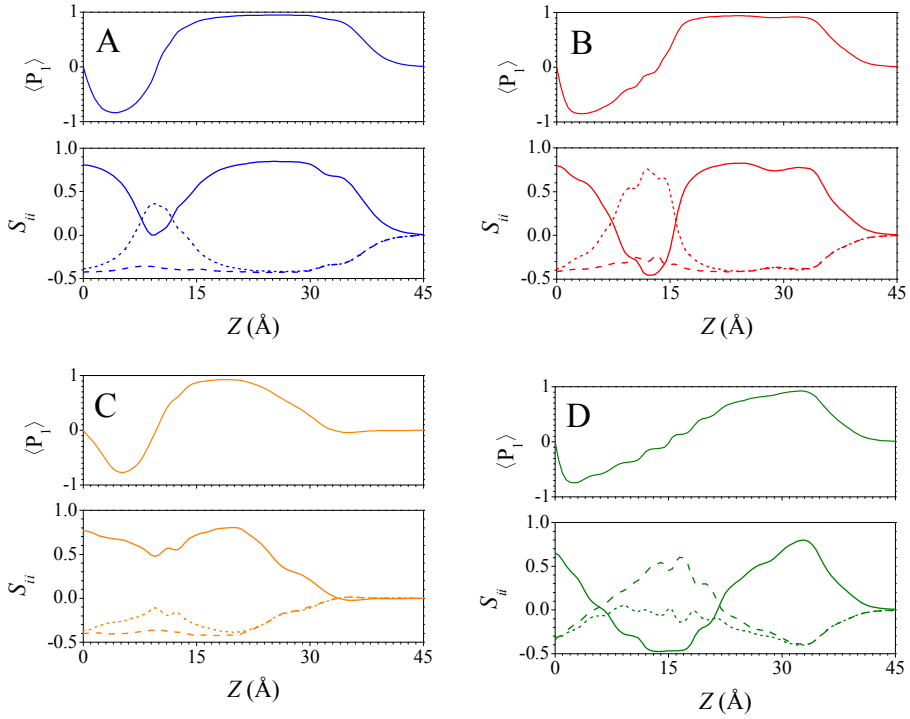

Figure 7: Local orientational order parameters calculated for cholesterol as a function of the distance of the oxygen atom from the bilayer midplane, using an incomplete form of the potential $U(\Omega,Z)$ in eq.1 of the main text. The results shown here were obtained by excluding in turn the cavity (A), the electrostatic (B), the dispersion (C) and the chain order (D) contribution in eq.1. For each case, the plot at the top displays the orientational average of the first Legendre polynomial, $\langle P_1 \rangle$, whereas that at the bottom shows the diagonal elements of the Saupe tensor, calculated in the molecular frame (Figure 1): S_{xx} (dotted line), S_{yy} (dashed line) and S_{zz} (solid line). The results shown here were obtained for the B conformer at the temperature T=323K.

The anisotropy of interactions of cholesterol with acyl chains bears the main, although not the only, responsibility for the orientational order of cholesterol across the bilayer. In its absence (Figure 7D) cholesterol would be significantly ordered in two zones, by virtue of dispersion and the cavity contributions. In the former region, part of cholesterol, comprising the oxygen atom, lies in water, and alignment of the long axis to the normal allows the molecule to insert as much as possible of its body

into the bilayer. In the latter region, the drop in lateral pressure at approximately 15 Å from the midplane and the optimization of dispersion interaction when a large portion of the solute resides in the region around 10 Å, promote horizontal orientation of the long molecular axis. Inclusion of the anisotropic interactions with acyl chains increases the degree of alignment of the long axis of cholesterol, when this is parallel to the bilayer normal, and differently stabilizes the orientations of the molecular plane, when the long axis lies perpendicular to the normal: orientations with this plane parallel are favoured over those with the plane perpendicular to lipid chains. Electrostatic interactions, which have the main responsibility for keeping the polar group of cholesterol in the hydrophilic region, are not very important for the orientational order of this molecule.

Accurate information on orientational order is obtained from quadrupole splittings in NMR spectra of specifically deuteriated samples. We have calculated the order parameters for the C_3H bond and the tail CH bonds (see Figure S5), defined as in eq.8, which can be directly compared with experimental data. The value S_{CD}=-0.33 was obtained for the C_3H bond after averaging over all the nine conformers; the negative sign indicates the tendency of this bond to lie perpendicular to the bilayer normal. Figure 8 shows the position dependence of the $|S_{CD}|$ order parameters calculated for the alkyl chain CH bonds of cholesterol. In addition to the order parameters obtained as averages over all nine conformers, those calculated for the single conformers are shown; the former and the latter would correspond to experimental data for fast and slow conformational motions (on the NMR timescale), respectively. We can see that, for bonds between C_{22} and C_{24}, significantly different order parameters are predicted for the nine conformers, due to their different chain geometry. We can also see that, even after the conformational average, different order parameters are obtained for the pairs of deuterons at C_{22}, C_{23} and C_{24}; this means that deuterons linked to the same carbon atom have a different average orientation in the bilayer. Quadrupole spectra of cholesterol specifically deuteriated at C_{24} were reported for a wide range of temperatures in the liquid crystal phase of 3:7 (molar ratio) cholesterol-DMPC mixtures[67]. From the quadrupole splittings, 33.2 and 42 kHz, measured at about 10°C above the melting temperature, $|S_{CD}|$ values equal to 0.26 and 0.33, respectively, can be estimated, assuming a deuterium quadrupole coupling constant equal to 170 kHz[68]. The average order parameters

calculated for the two C_{24}-D bonds, S_{CD}=-0.24 and S_{CD}=-0.34, are in line with experiment. As for the C□H bond, the quadrupole splitting Δν~84 kHz was reported in ref.[66] for 5 mol % cholesterol in DPPC at the temperature T=47°C, from which the value $|S_{CD}|$~0.33 is derived assuming again a deuterium quadrupole coupling constant equal to 170 kHz. The agreement between predicted and experimental order parameters for different sites is a good check for the ability of our model to predict the orientational behaviour of cholesterol in the bilayer environment.

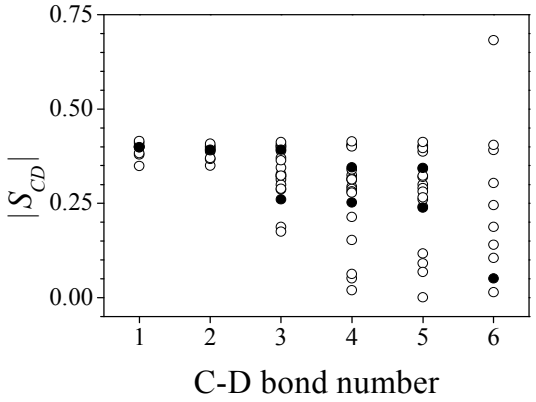

Figure 8: $|S_{CD}|$ order parameters, calculated for the alkyl chain of cholesterol at the temperature T=323K. Full symbols: averages over conformers. Open symbols: individual conformers. Bonds are numbered as follows: 1 for C_{17}-D, 2 for C_{20}-D, 3 for C_{22}-D, 4 for C_{23}-D, 5 for C_{24}-D, 6 for C_{25}-D (atom numbering as in Figure S5).

Finally, we report in Table 2 a list of properties calculated for cholesterol by averaging over all degrees of freedom (translational, orientational and conformational), according to eq.32. Such averages make sense in the case of cholesterol, which is predicted to be mostly confined in a region with uniform orientational behaviour within the bilayer. The properties reported in Table 2 are close to those calculated for the single A or B conformers (see Figure S6); these are very similar to each other and are predicted to be significantly more probable than the other conformers. In fact, not only A and B are, according to DFT calculations, the most stable in vacuum, but they are further stabilized by the bilayer environment, as shown by the values of the difference $\Delta V_J = V'_J - V_J$, calculated according to eq.28 and reported in Figure S6. The very high $\langle P_1 \rangle$ value, close to 1, indicates the strong preference of cholesterol for orientations parallel to the bilayer normal with the hydroxyl group pointing towards water, over antiparallel orientations. The preference for parallel over perpendicular orientation of the long molecular axis is quantified by

the $S_{z'z'}$ value. The principal axis system of the Saupe matrix (x',y',z'), shown in Figure S9, does not exactly coincide with the molecular frame (x,y,z); in particular, the major alignment axis (z') is tilted by about 14° with respect to the molecular z axis (shown in Figure 1). Of the two other principal alignment axes, y', nearly perpendicular to the molecular plane, is predicted to have higher tendency to lie perpendicular to the bilayer normal than x'.

Table 2: Average properties calculated for cholesterol in DPPC bilayer at the temperature T=323K. $\langle Z \rangle$ is the average distance of the oxygen atom from the midplane, $\langle P_1 \rangle$ is the average value of the cosine of the angle between the bilayer normal and the z molecular axis (Figure 1) and $S_{i'i'}$ (i=x,y,z) are the principal values of the Saupe matrix.

$\langle Z \rangle$	$\langle P_1 \rangle$	$S_{x'x'}$	$S_{y'y'}$	$S_{z'z'}$
18.5 Å	0.86	-0.31	-0.45	0.76

2.5 Conclusions

In a recent review, the need of new implicit models of membranes, combining an atomistic solute representation with better account of bilayer structure, was stressed[2]. The present work is an effort in this direction; the main new features, which are generally ignored by the existing models, are summarized in the following.

The anisotropy and non-uniformity of the bilayer environment are included, in a way that allows for a realistic account of the chemical composition and physical state of the phospholipid system; they are introduced through the profiles of lateral pressure, density, order parameters and dielectric permittivity. Appropriate values of these for a given membrane can be derived from experiments or from atomistic simulations. The elastic response of the bilayer is, at least in part, implicitly contained in the cavity contribution to the mean field potential.

The full solute distribution function, accounting for the coupling between molecular position, orientation and conformation, is calculated. Detailed information is provided, not only on the preferred configurations, but also on fluctuations about them. This is important to get a realistic description of the behavior in the fluid

bilayer environment where solutes, though confined, may undergo wide displacements and reorientations, which are likely to be essential for their biophysical role.

In its present form, the model ignores the membrane perturbation induced by the solute; therefore it is not suitable at high solute concentration. However the theoretical framework presented here allows the inclusion of the bilayer response and future effort in this direction is planned.

To illustrate the capability of our model, we have presented the case study of cholesterol in DPPC. We have calculated a variety of properties, showing that the method proposed here is suitable for a general description of solutes in the bilayer environment. The use of the model allows us to disentangle the different contributions to solute properties in the bilayer and to shed light on the often unexpected effects of the anisotropy and nonuniformity of this environment. Small conformational effects are found for cholesterol, which is not surprising, in view of the small size of the flexible tail, if compared with the broad rigid core. Comparison of our results with experiment and simulations is very encouraging. The free energy profile calculated for cholesterol across the bilayer exhibits the same features as the profile obtained from all-atom Molecular Dynamics simulations[63]. Strong position/orientation couplings emerge: cholesterol is predicted to be mostly buried in the bilayer, with its head in the hydrophilic region and its long axis nearly perpendicular to the surface. When embedded deeper in the bilayer, cholesterol is predicted to change its average orientation and to preferentially keep its long axis parallel to the surface. According to our calculations, the latter configurations should have very low probability for cholesterol in liquid crystalline DPPC; however they may become more significant in other lipid systems. Interestingly, cholesterol lying flat, close to the bilayer centre was recently revealed by neutron scattering studies in unsaturated lipids[64,65].

The method proposed here is computationally cheap; a detailed insight into the properties of a given solute/bilayer pair can be reached at very low cost, so we think that it could be usefully exploited to different purposes. It can provide the free energy landscapes needed to model solute permeability through membranes. Moreover, it may be suitable to mimic the bilayer environment in Monte Carlo and Molecular

Dynamics simulations and to be integrated with quantum mechanical calculations of spectroscopic observables in lipid membranes[69].

Abbreviations

DPPC:1,2-DiPalmitoyl-sn-glycero-3-PhosphatidylCholine

DMPC: 1,2-DiMyristoyl-sn-glycero-3-PhosphatidylCholine

DFT: Density Functional Theory

Supporting Information Available. Supporting Information contains: derivation of the relationship between orienting strength ξ and S_{CD} order parameters; definition of polarizable units in DPPC and corresponding mass density profiles; list of molecules used to parameterize the electrostatic contribution to the mean field potential; calculated and experimental water/*n*-octanol transfer free energies; atom labels and OPLS charges for cholesterol; list of cholesterol conformers considered in calculations with their torsional energy; representation of the molecular surface of cholesterol and of the principal axis system of its Saupe ordering tensor; plot of transfer free energy calculated for nine conformers of cholesterol in DPPC. This information is available free of charge via the Internet at http://pubs.acs.org/.

2.6 References

[1] White, S.H.; Wimpley, W.C. Membrane protein folding and stability: physical principles. *Ann. Rev. Biophys. Biomol. Struct.* **1999**, *28*, 319-365.

[2] Grossfield A. Implicit modeling of membranes. *Curr. Top. Membr.* **2008**, *60*, 131-157.

[3] De Young, L.R.; Dill, K.A. Solute partitioning into lipid bilayer membranes. *Biochemistry* **1988**, *27*, 5281-5289.

[4] Marqusee, J.A.; Dill, K.A. Solute partitioning into chain molecule interphases: monolayers, bilayer membranes, and micelles. *J. Chem. Phys.* **1986**, *85*, 434-444.

[5] Tobias, D.J. Electrostatic calculations: recent methodological advances and applications to membranes. *Curr. Opin. Struct. Biol.* **2001**, *11*, 253-261.

[6] Feig, M.; Brooks, C.L. Recent advances in the development and application of implicit solvent models in biomolecule simulations. *Curr. Opin. Struct. Biol.* **2004**, *14*, 217-224.

[7] Chen, J.; Brooks, C.L.; Khandogin, J. Recent advances in implicit solvent-based methods for biomolecular simulations. *Curr. Opin. Struct. Biol.* **2008**, *18*, 140-148.

[8] Fattal, D.R.; Ben-Shaul, A. A molecular model for lipid-protein interactions in membranes: the role of hydrophobic mismatch. *Biophys. J.* **1993**, *65*, 1795-1809.

[9] Fattal, D.R.; Ben-Shaul, A. Mean-field calculations of chain packing and conformational statistics in lipid bilayers: comparison with experiments and molecular dynamics studies. *Biophys. J.* **1994**, *67*, 983-995.

[10] Xiang, T.; Anderson, B. Molecular distributions in interphases: statistical mechanical theory combined with Molecular Dynamics simulation of a model lipid bilayer. *Biophys. J.* **1994**, *66*, 561-572.

[11] Mitragotri, S.; Johnson, M.E.; Blankschtein, D.; Langer, R. An analysis of the size selectivity of solute partitioning, diffusion, and permeation across lipid bilayers. *Biophys. J.* **1999**, *77*, 1268-1283.

[12] Kessel, A.; Ben-Tal, N.; May, S. Interactions of cholesterol with lipid bilayers: the preferred configuration and fluctuations. *Biophys. J.* **2001**, *81*, 643-658.

[13] Cantor, R.S. Lateral pressures in cell membranes: a mechanism for modulation of protein function. *J. Phys. Chem.* **1997**, *101*, 1723-1725.

[14] Tanizaki, S.; Feig, M. A generalized Born formalism for heterogeneous dielectric environments: application to the implicit modeling of biological membranes. *J. Chem. Phys*. **2005**, *122*, 124706:1-13.

[15] Ferrarini, A.; Moro, G.J.; Nordio, P.L.; Luckhurst, G.R. A shape model for molecular ordering in nematics. *Mol. Phys.* **1992**, *77*, 1-15.

[16] Mennucci, B.; Cammi, R.; Eds. Continuum Solvation Models in Chemical Physics; Wiley: Chichester, 2007.

[17] Cantor, R.S. Lipid composition and the lateral pressure profile in bilayers. *Biophys. J.* **1999**, *76*, 2625-2639.

[18] Cantor, R.S. The influence of membrane lateral pressures on simple geometric models of protein conformational equilibria. *Chem. Phys. Lipids* **1999**, *101*, 45-56.

[19] Marsh, D. Lateral pressure in membranes. *Biochim. Biophys. Acta* **1996**, *1286*, 183-223.

[20] Patra, M. Lateral pressure profiles in cholesterol-DPPC bilayers. *Eur. Biophys. J*. **2005**, *35*, 79-88.

[21] Baoukina, S.; Marrink, S.J.; Tieleman, D.P. Lateral pressure profiles in lipid monolayers. *Faraday Disc.* **2010**, *144*, 393-409.

[22] Rowlinson, J.S.; Widom, B. Molecular Theory of Capillarity; Clarendon: Oxford, 1982.

[23] Helfrich, W. In Physics of Defects; Balian, R.; Kleman, M.; Poirier, J.P., Eds.; North-Holland Publishing: Amsterdam, 1981; pp 716-755.

[24] Szleifer, I.; Kramer, D.; Ben-Shaul, A.; Gelbart, W.M.; Safran, S.A. Molecular theory of curvature elasticity in surfactant films. *J. Chem. Phys.*, **1990**, *92*, 6800-6817.

[25] Kozlov, M.M. In Soft Condensed Matter Physics in Molecular and Cell Biology; Poon, W.C.H.; Andelman, D. Eds.; Taylor&Francis: Boca Raton, 2006; pp 79-96.

[26] Honig, B.; Sharp, K.; Yang, A.-S. Macroscopic models of aqueous solutions: biological and chemical applications. *J. Phys. Chem.* **1993**, *97*, 1101-1109.

[27] Baker, N.A. Poisson-Boltzmann methods for biomolecular electrostatics. *Methods Enzymol.* **2004**, *383*, 94-118.

[28] Still, W.C.; Tempczyk, A.; Hawley, R.C.; Hendrickson, T. Semianalytical treatment of solvation for molecular mechanics and dynamics. *J. Am. Chem. Soc.*, **1990**, *112*, 6127-6129.

[29] Bashford, D.; Case, D.A. Generalized Born models of macromolecular solvation effects. *Annu. Rev. Phys. Chem.* **2000**, *51*, 129-152.

[30] Stern, H.A.; Feller, S.E. Calculation of the dielectric permittivity profile for a nonuniform system: application to a lipid bilayer simulation. *J. Chem. Phys*. **2003**, *118*, 3401-3412.

[31] Spassov, V.Z.; Yan, L.; Szalma, S. Introducing an implicit membrane in Generalized Born/Solvent Accessibility continuum solvent models. *J. Phys. Chem. B* **2002**, *106*, 8726-8738.

[32] Lazaridis, T. Effective energy function for proteins in lipid membranes. *Proteins* **2003**, *52*, 176-192.

[33] Im, W.; Feig, M.; Brooks, C.L. An implicit membrane generalized born theory for the study of structure, stability, and interactions of membrane proteins. *Biophys. J.* **2003**, *85*, 2900-2918.

[34] Sigalov, G.; Scheffel, P.; Onufriev, A. Incorporating variable dielectric environments into the generalized Born model. *J. Chem. Phys.* **2005**, *122*, 094511:1-15.

[35] Ulmschneider, M.B.; Ulmschneider, J.P.; Sansom, M.S.P.; Di Nola, A. A generalized Born implicit membrane representation compared to experimental insertion free energies. *Biophys. J.* **2007**, *92*, 2338-2349.

[36] Sengupta, D.; Smith, J.C.; Ullmann, G. Partitioning of side-chain analogues in a five-slab membrane model. *Biochim. Biophys. Acta* **2008**, *1778*, 2234-2243.

[37] Gallicchio, E.; Levy, R.M. AGBNP: an analytic implicit solvent model suitable for Molecular Dynamics simulations and high-resolution modeling. *J. Comp. Chem.* **2003**, *25*, 479-499.

[38] Seelig, J. Deuterium magnetic resonance: theory and application to lipid membranes. *Q. Rev. Biophys.* **1977**, *10*, 353-418.

[39] Mishima, K. In Advances in Planar Lipid Bilayers and Liposomes; Liu Leitmannova, A.; Tien, H.T.; Eds.; Academic Press: London, 2006; Vol. 3, pp 55-84.

[40] Ramsden, J.J. Molecular orientation in lipid bilayers. *Phil. Mag. B* **1999**, *79*, 381–386.

[41] Ferrarini, A.; Moro, G.J.; Nordio, P.L. Simple molecular model for induced cholesteric phases. *Phys. Rev. E* **1996**, *53*, 681-688.

[42] Ferrarini A. Shape model for the molecular interpretation of the flexoelectric effect. *Phys. Rev. E* **2001**, *64*, 021710:1-11.

[43] Cestari, M.; Bosco, A.; Ferrarini, A. Molecular field theory with atomistic modeling for the curvature elasticity of nematic liquid crystals. *J. Chem. Phys.* **2009**, *131*, 054104:1-16.

[44] Maier, W.; Saupe, A. A simple molecular-statistics theory of the nematic liquid-crystalline phase. Part I. *Z. Naturforsch. A* **1959**, *14A*, 882-900; A simple molecular-statistics theory of the nematic liquid-crystalline phase. Part II. *ibidem* **1960**, *15A*, 287-292.

[45] Abramowitz, M.; Stegun, I.A. Handbook of Mathematical Functions; Dover: New York, 1972.

[46] Ferrarini, A.; Luckhurst, G.R.; Nordio, P.L.; Roskilly, S.J. Prediction of the transitional properties of liquid crystal dimers. A molecular field calculation based on the surface tensor parametrization. *J. Chem. Phys.* **1994**, *100*, 1460-1469.

[47] Luckhurst, G.R. In The Molecular Physics of Liquid Crystals; Luckhurst, G.R.; Gray, G.W.; Eds.; Academic: London, 1979; pp 85-119.

[48] Flory, P.J. Statistical Mechanics of Chain Molecules; Interscience: New York, 1969.

[49] Richards, F.M. Areas, volumes, packing and protein structure. *Annu. Rev. Biophys. Bioeng.* **1977**, *6*, 151-176.

[50] Sanner, M.F.; Olson, A.; Spehner, J.-C. Reduced surface: an efficient way to compute molecular surfaces. *Biopolymers* **1996**, *38*, 305-320.

[51] Stewart, J. Calculus, 4th Edn.; Brooks/Cole Publishing Company: Pacific Grove, 1999.

[52] Arfken, G.B.; Weber, H.J. Mathematical Methods for Physicist 4th Edn.; Elsevier: Boston, 2005.

[53] Quarteroni, A.; Sacco, R.; Saleri, F. Numerical Mathematics; Springer: New York, 2000.

[54] Ollila, O.H.S.; Róg, T.; Karttunen, M.; Vattulainen, I. Role of sterol type on lateral pressure profiles of lipid membranes affecting membrane protein functionality: comparison between cholesterol, desmosterol, 7-dehydrocholesterol and ketosterol. *J. Struct. Biol.* **2007**, *159*, 311-323.

[55] Kupiainen, M.; Falck, E.; Ollila, S.; Niemelä, P.; Gurtovenko, A.A. Free volume properties of sphingomyelin, DMPC, DPPC, and PLPC bilayers. *J. Comp. Theor. Nano*, **2005**, *2*, 401-413.

[56] Falk, E.; Patra, M.; Karttunen, M.; Hyvönen, M.T.; Vattulainen, I. Lessons of slicing membranes: interplay of packing, free area, and lateral diffusion in phospholipid/cholesterol bilayers. *Biophys. J.* **2004**, *87*, 1076-1091.

[57] CRC Handbook of Chemistry and Physics 85th Edn.; Lide, D.R.; Ed.; CRC: Boca Raton, 2004.

[58] Frisch, M.J. *et al.*, Gaussian03, Revision C.02 (Gaussian, Inc., Wallingford CT, 2004).

[59] Bondi, A. Van der Waals volumes and radii. *J. Phys. Chem.* **1964**, *68*, 441-451.

[60] Jorgensen, W.L.; Maxwell, D.S.; Tirado-Rives, J. Development and testing of the OPLS all-atom force field on conformational energetics and properties of organic liquids. *J. Am. Chem. Soc.* **1996**, *118*, 11225-11236.

[61] Feig, M.; Im, W.; Brooks, C.L. Implicit solvation based on generalized Born theory in different dielectric environments. *J. Chem. Phys*. **2004**, *120*, 903-911.

[62] Harroun, T.A.; Katsaras, J.; Wassall, S.R. Cholesterol hydroxyl group is found to reside in the center of a polyunsaturated lipid membrane. *Biochemistry* **2006**, *45*, 1227-1233.

[63] Gliss, C.; Randel, O.; Casalta, H.; Sackmann, E.; Zorn, R.; Bayerl, T. Anisotropic motion of cholesterol in oriented DPPC bilayers studied by quasielastic neutron scattering: the liquid-ordered phase. *Biophys. J.* **1999**, *77*, 331-340.

[64] Bennett, W.F.D.; MacCallum, J.L.; Hinner, M.J.; Marrink, S.J.; Tieleman, D.P. Molecular view of cholesterol flip-flop and chemical potential in different membrane environments. *J. Am. Chem. Soc.* **2009**, *131*, 12714-12720.

[65] Kučerka, N.; Marquardt, D.; Harroun, T.A.; Nieh, M.-P.; Wassall, S.R.; Katsaras, J. The functional significance of lipid diversity: orientation of cholesterol in bilayers is determined by lipid species. *J. Am. Chem. Soc.* **2009**, *131*, 16358-16359.

[66] Guo, W.; Kurze, V.; Huber, T.; Afdhal, N.H.; Beyer, K.; Hamilton, J.A. A solid-state NMR study of phospholipid-cholesterol interactions: sphingomyelin-cholesterol binary system. *Biophys. J.* **2002**, *83*, 1465-1478.

[67] Dufourc, E. J.; Parish, E. J.; Chitrakorn, S.; Smith, I.C.P. Structural and dynamical details of the cholesterol-lipid interaction as revealed by deuterium NMR. *Biochemistry* **1984**, *23*, 6062-6071.

[68] In the experiments reported in ref.[67] the magnetic field was perpendicular to the bilayer normal.

[69] Pavanello, M.; Mennucci, B.; Ferrarini, A. Quantum-mechanical studies of NMR properties of solutes in liquid crystals: a new strategy to determine orientational order parameters. *J. Chem. Phys.* **2005**, *122*, 064906:1-9.

Chapter 3

Solute permeation across lipid bilayers: a generalized inhomogeneous solubility-diffusion model

3.1 Introduction

Theoretical and computational methods for the prediction of the membrane permeability of molecular solutes may be very useful for drug design. A high sensitivity to the atomic-scale details must be a feature of models intended to this purpose, since the presence or the absence of functional groups, as well as the molecular size, are widely recognized to affect the ability of drug-like solutes to diffuse across the lipid bilayer of cell membranes or liposomes[1].

A common approach to evaluate the membrane permeability of solutes across lipid bilayers is represented by heterogeneous solubility-diffusion model which was derived in 1974 by Diamond *et al.*[2]. They addressed the problem of membrane permeability from the thermodynamic point of view of the Nernst-Planck equation for the description of the diffusion process.[2] The permeability coefficient P of a solute is expressed as

$$\frac{1}{P} = \int_{\substack{bilayer \\ thickness}} \frac{1}{K(Z)D(Z)} \mathrm{d}Z \,, \tag{1}$$

where K and D are the local partition and diffusion coefficient, respectively, which depend on the solute position Z along the bilayer normal.[2,3] Actually, due to the nonuniformity and orientational order of the bilayer environment, the effects of solute-membrane interactions on membrane permeability should be more adequately represented by position- and orientation- dependent partition and diffusion coefficients.

A result analogous to eq.1 had already been obtained in 1940 by Kramers, who had applied the stochastic equations describing Brownian motion, in the large friction limit, to the calculation of the rate of chemical reactions.[4] Kramers used the expression he derived to calculate the flux of particles escaping from a potential hole over a potential barrier.[4] Just in the same way the permeability coefficient given by the solubility-diffusion equation is related to the flux of solute molecules crossing the barrier region within the bilayer opposing the highest resistance to solute permeation.[2]

Eq.1 is also at the basis of the method which is used to evaluate permeability coefficients from MD simulations, since the possibility of directly studying the mechanism of the process at the molecular level is still out of reach, due to its prohibitive computational cost. Therefore atomistic or coarse-grained MD simulations are usually performed on solute particles constrained at different positions Z across a lipid bilayer[3], in order to obtain the $K(Z)$ and $D(Z)$ profiles in eq.1. Constrained particles explore different orientations during the simulation, and hence, provided that an efficient statistical sampling is performed, orientational effects on K and D are averaged out.

We derive here a general expression for the flux of a solute across a lipid bilayer, taking into account not only the dependence of solute properties on the position Z within the bilayer, but also that on the orientation Ω (see Figure 1 in Chapter 2), which was generally ignored by previous theories. The implicit membrane model we have developed provides direct access to the coupled positional-orientational distribution of solutes in lipid bilayers, and is suitable for integration into the generalized solubility-diffusion theory we are proposing. In two limiting cases we will be able to obtain an analytical expression for the permeability coefficient P, defined as the proportionality constant between the flux of solute across the membrane and the difference in solute concentration between the two aqueous compartments separated by the membrane. Within the theoretical framework describing roto-translational diffusion as a stochastic process, an expression analogous to eq.1, relating the permeability coefficient of the solute with its position-dependent partition and diffusion coefficients, will be derived in the limit of fast solute reorientation, the orientational dependence of K and D being averaged out by fast rotational motions between successive translational displacements. Under this assumption, the equilibrium distribution function of the solute, $P_{\Omega}(Z)$, or, equivalently, its water-bilayer transfer free energy profile, $u(Z)$, defined in ref.[5] (Chapter 2), will be used to calculate the permeability coefficients of selected molecules in a liquid-crystalline DPPC bilayer.

The theoretical derivation proposed will be reported in the following, and the results obtained from application of the methodology to drug-like solutes will be shown and discussed.

3.2 Theory

A symmetrical lipid bilayer will be considered where the position Z and orientation Ω of a solute are defined with respect to the bilayer (laboratory) and molecular reference frames as in Figure 1 of Chapter 2. At equilibrium the coupled orientational-positional distribution of the solute in the bilayer is only determined by solute-membrane interactions and hence is symmetrical with respect to the bilayer midplane. The concentration gradient driving the diffusion of the solute across the membrane induces a non-equilibrium distribution of the solute, and hence an imbalance in solute concentration between the two leaflets of the bilayer. The roto-translational motion of solute particles governs the evolution of the non-equilibrium distribution towards equilibrium and originates the permeating flux.

3.2.1 The stochastic description of roto-translational diffusion

The Fokker-Planck-Smoluchowski equation[6]

$$\frac{\partial}{\partial t} p(\Omega, Z, t) = \Gamma(\Omega, Z)\, p(\Omega, Z, t) \tag{2}$$

describes the time evolution of the non-equilibrium distribution function $p(\Omega,Z,t)$ in terms of the roto-translational diffusion operator Γ, defined as:

$$\Gamma(\Omega, Z) = \vec{\nabla}^T \mathbf{D}(\Omega, Z)\, p_{eq}(\Omega, Z) \vec{\nabla} p_{eq}^{-1}(\Omega, Z). \tag{3}$$

The equilibrium distribution function $p_{eq}(\Omega,Z)$ represents the stationary limit of the evolution of $p(\Omega,Z,t)$:

$$\lim_{t \to +\infty} p(\Omega, Z, t) = p_{eq}(\Omega, Z) \tag{4}$$

and both $p(\Omega,Z,t)$ and $p_{eq}(\Omega,Z)$ are defined so that the normalization conditions

$$\int_{-L}^{L} \mathrm{d}Z \int p(\Omega, Z, t)\, \mathrm{d}\Omega = \int_{-L}^{L} \mathrm{d}Z \int p_{eq}(\Omega, Z)\, \mathrm{d}\Omega = 1 \tag{5}$$

hold. The limits ($\pm L$) of the integrals over the Z variable in eq.5 are taken to represent the bilayer thickness; a definition of this will be given below. Both the $\vec{\nabla}$ operator (the superscript ^{T} indicates the transpose) and the diffusion tensor **D** in eq.3 have translational and rotational components which are expressed in terms of positional and orientational variables, respectively. The explicit form of $\vec{\nabla}$ is given by

$$\vec{\nabla} = \begin{pmatrix} \vec{\nabla}_{transl} \\ \vec{\nabla}_{rot} \end{pmatrix}; \quad \vec{\nabla}_{transl} = \begin{pmatrix} \frac{\partial}{\partial X} \\ \frac{\partial}{\partial Y} \\ \frac{\partial}{\partial Z} \end{pmatrix} \quad \vec{\nabla}_{rot} = \begin{pmatrix} \frac{\partial}{\partial \alpha} \\ \frac{\partial}{\partial \beta} \\ \frac{\partial}{\partial \gamma} \end{pmatrix} \tag{6}$$

where X, Y and Z are the Cartesian coordinates in the laboratory frame (*LF*), and the Euler angles α, β, and γ define the rotation from the laboratory to the molecular (*MF*) frame ($\Omega = \alpha,\beta,\gamma$). In the absence of roto-translational coupling, the diffusion tensor **D** expressed in the *LF* has the form:[7]

$$\mathbf{D}(\Omega, Z) = \begin{pmatrix} \mathbf{D}_{transl}(\Omega, Z) & 0 \\ 0 & \mathbf{D}_{rot}(\Omega, Z) \end{pmatrix}$$

$$\mathbf{D}_{transl} = \begin{pmatrix} D_{XX} & D_{XY} & D_{XZ} \\ D_{YX} & D_{YY} & D_{YZ} \\ D_{ZX} & D_{ZY} & D_{ZZ} \end{pmatrix} \quad \mathbf{D}_{rot} = \begin{pmatrix} D_{\alpha\alpha} & D_{\alpha\beta} & D_{\alpha\gamma} \\ D_{\beta\alpha} & D_{\beta\beta} & D_{\beta\gamma} \\ D_{\gamma\alpha} & D_{\gamma\beta} & D_{\gamma\gamma} \end{pmatrix}. \tag{7}$$

The **D** tensor is block-diagonal for highly symmetrical particles, but in most cases the roto-translational coupling is in fact negligible. The transformations relating the diffusion tensors in eq.7 to the Cartesian tensors $\mathbf{D}^{MF}_{transl}$ and $\mathbf{D}^{MF}_{rot}$ defined in the *MF*, are given by:[7]

$$\mathbf{D}^{LF}_{transl}(\Omega, Z) = \mathbf{R}^{T}(\Omega)\mathbf{D}^{MF}_{transl}(\Omega, Z)\mathbf{R}(\Omega) \tag{8}$$

$$\mathbf{D}_{transl}(\Omega, Z) = \mathbf{D}^{LF}_{transl}(\Omega, Z) \tag{9}$$

$$\mathbf{R}(\Omega) = \begin{pmatrix} \cos\beta\cos\gamma & \sin\gamma & -\sin\beta\cos\gamma \\ -\cos\beta\sin\gamma & \cos\gamma & \sin\beta\sin\gamma \\ \sin\beta & 0 & \cos\beta \end{pmatrix} \tag{10}$$

$$\mathbf{D}^{LF}_{rot}(\Omega, Z) = \mathbf{R}^{T}(\Omega)\mathbf{D}^{MF}_{rot}(\Omega, Z)\mathbf{R}(\Omega) \tag{11}$$

$$\mathbf{D}_{rot}(\Omega, Z) = \mathbf{M}(\Omega)\mathbf{D}^{LF}_{rot}(\Omega, Z)\mathbf{M}^{T}(\Omega) \tag{12}$$

$$\mathbf{M}(\Omega) = \begin{pmatrix} -\cos\gamma/\sin\beta & \sin\gamma/\sin\beta & 0 \\ \sin\gamma & \cos\gamma & 0 \\ \cos\beta\cos\gamma/\sin\beta & -\cos\beta\sin\gamma/\sin\beta & 1 \end{pmatrix}. \tag{13}$$

Under the assumption of negligible roto-translational coupling, the diffusion operator Γ can be written as

$$\Gamma(\Omega,Z)=\Gamma_{transl}(\Omega,Z)+\Gamma_{rot}(\Omega,Z), \tag{14}$$

and the evolution of the non-equilibrium distribution $p(\Omega,Z,t)$ is described by the two independent operators:

$$\Gamma_{transl}(\Omega,Z)=\vec{\nabla}^{T}_{transl}\mathbf{D}_{transl}(\Omega,Z)\,p_{eq}(\Omega,Z)\vec{\nabla}_{transl}\,p^{-1}_{eq}(\Omega,Z) \tag{15}$$

$$\Gamma_{rot}(\Omega,Z)=\vec{\nabla}^{T}_{rot}\mathbf{D}_{rot}(\Omega,Z)\,p_{eq}(\Omega,Z)\vec{\nabla}_{rot}\,p^{-1}_{eq}(\Omega,Z). \tag{16}$$

Since the permeability coefficient P is defined by the relation

$$J=-P\Delta C \tag{17}$$

between the flux J and the concentration difference ΔC between the two aqueous solutions in contact with the membrane, it is convenient to switch from a distribution-based description to a concentration-based description of the diffusion process. If the concentration difference at the two bilayer/water interfaces $\Delta C=C(L)-C(-L)$ is considered in eq.17, P coincides with the intrinsic permeability coefficient, which is exclusively determined by solute diffusion within the membrane environment. This is obtained experimentally after correction of the apparent permeability coefficient directly accessible from measurements.[8]

The equilibrium and non-equilibrium probability distributions, $p_{eq}(\Omega,Z)$ and $p(\Omega,Z,t)$, can be related to the concentration fields, $C_{eq}(\Omega,Z)$ and $C(\Omega,Z,t)$, by

$$C_{eq}(\Omega,Z)=\frac{N}{N_A V}\,p_{eq}(\Omega,Z) \tag{18}$$

$$C(\Omega,Z,t)=\frac{N}{N_A V}\,p(\Omega,Z,t), \tag{19}$$

where N is the total number of solute molecules, N_A is Avogadro's number and V is the volume element where the concentration is evaluated. The time evolution of $C(\Omega,Z,t)$ is governed by the diffusion equation

$$\frac{\partial}{\partial t}C(\Omega,Z,t)=\Gamma(\Omega,Z)C(\Omega,Z,t). \tag{20}$$

Through the identity

$$\Gamma(\Omega,Z)C(\Omega,Z,t)=-\vec{\nabla}^{T}\vec{J}(\Omega,Z,t) \tag{21}$$

the diffusion operator in eq.20 is related to the flux vector $\vec{J}(\Omega,Z,t)$, whose translational and rotational components

$$\vec{J}(\Omega,Z,t)=\begin{pmatrix}\vec{J}_{transl}(\Omega,Z,t)\\ \vec{J}_{rot}(\Omega,Z,t)\end{pmatrix} \tag{22}$$

are independent under the assumption of negligible roto-translational coupling, and given by

$$\vec{J}_{transl}=\begin{pmatrix}J_X\\ J_Y\\ J_Z\end{pmatrix}\quad \vec{J}_{rot}=\begin{pmatrix}J_\alpha\\ J_\beta\\ J_\gamma\end{pmatrix}. \tag{23}$$

Since the permeability coefficient in eq.17 is related only to the component of the flux along the bilayer normal, *Z*:

$$J_Z(\Omega,Z,t)=-D_{ZZ}(\Omega,Z)\,p_{eq}(\Omega,Z)\frac{\partial}{\partial Z}p_{eq}^{-1}(\Omega,Z)C(\Omega,Z,t), \tag{24}$$

eq.20 is conveniently rewritten in the form

$$\frac{\partial}{\partial t}C(\Omega,Z,t)=-\frac{\partial}{\partial Z}J_Z(\Omega,Z,t)+\ldots, \tag{25}$$

where the dots stand for terms which do not contribute to the permeating flux (eq.17) and will not be shown explicitly.

All possible solute orientations contribute to the permeating flux. With the aim of isolating the orientational dependence in eq.25, the non-equilibrium probability distribution is rewritten as the product

$$p(\Omega,Z,t)=p_\Omega(Z,t)\,p(\Omega,t;Z) \tag{26}$$

between the conditional probability $p(\Omega,t;Z)$, that a solute particle in Z is found in the orientation Ω, and the orientationally-averaged positional distribution

$$p_\Omega(Z,t)=\int p(\Omega,Z,t)\,\mathrm{d}\Omega \tag{27}$$

which are defined so that the normalization conditions

$$\int_{-L}^{L}p_\Omega(Z,t)\,\mathrm{d}Z=\int p(\Omega,t;Z)\,\mathrm{d}\Omega=1$$

hold. The corresponding concentration field $C_\Omega(Z,t)$ averaged over orientations is defined as

$$C_\Omega(Z,t)=\frac{N}{N_A V}p_\Omega(Z,t) \tag{28}$$

so that the non-equilibrium concentration field can be expressed as

$$C(\Omega,Z,t)=C_{\Omega}(Z,t)\,p(\Omega,t;Z)\,. \tag{29}$$

Integrating eq.25 over the orientational variables we obtain

$$\int\frac{\partial}{\partial t}C(\Omega,Z,t)\,\mathrm{d}\Omega=-\int\frac{\partial}{\partial Z}J_{Z}(\Omega,Z,t)\,\mathrm{d}\Omega+\int\ldots\,\mathrm{d}\Omega\,; \tag{30}$$

making use of eq.29, the lhs member becomes

$$\int\frac{\partial}{\partial t}C(\Omega,Z,t)\,\mathrm{d}\Omega=\frac{\partial}{\partial t}C_{\Omega}(Z,t) \tag{31}$$

and eq.30 is written as

$$\frac{\partial}{\partial t}C_{\Omega}(Z,t)=-\frac{\partial}{\partial Z}J_{Z_{\Omega}}(Z,t)+\ldots \tag{32}$$

having defined the integrated flux $J_{Z_{\Omega}}(Z,t)$ as

$$\int J_{Z}(\Omega,Z,t)\,\mathrm{d}\Omega=J_{Z_{\Omega}}(Z,t)\,. \tag{33}$$

For eq.17 to hold, the permeation process must have reached a steady-state regime where

$$\frac{\partial}{\partial t}C_{\Omega}(Z,t)=0\,; \tag{34}$$

and then, since the explicit term in eq.32 is independent of the others:

$$J_{Z_{\Omega}}(Z,t)=J_{Z} \tag{35}$$

Once the time-dependence is dropped from eq.24, the permeating flux is given by the general expression

$$J_{Z}=-\int D_{ZZ}(\Omega,Z)\,p_{eq}(\Omega,Z)\frac{\partial}{\partial Z}p_{eq}^{-1}(\Omega,Z)\,C(\Omega,Z)\,\mathrm{d}\Omega\,, \tag{36}$$

where the non-equilibrium concentration field is now given by

$$C(\Omega,Z)=C_{\Omega}(Z)\,p(\Omega;Z)\,. \tag{37}$$

3.2.2 Limiting cases

To extract the expression for the permeability coefficient *P*, eq.36 should now be reduced in the form of eq.17. Here we consider two limiting cases in which eq.36 can be easily handled:

1. if reorientational motion is much faster than translation, the orientational distribution at any position can be assumed to be at equilibrium, then

$$C(\Omega,Z) = C_{\Omega}(Z)\, p_{eq}(\Omega;Z), \tag{38}$$

where $p_{eq}(\Omega;Z)$ is defined so that

$$p_{eq}(\Omega,Z) = p_{eq\,\Omega}(Z)\, p_{eq}(\Omega;Z) \tag{39}$$

with (40)

$$p_{eq\,\Omega}(Z) = \int p_{eq}(\Omega,Z)\,\mathrm{d}\Omega;$$

2. if reorientational motion is much slower than translation, molecules can be assumed to diffuse without changing their orientation with stationary flux

$$J_Z(\Omega) = -D_{ZZ}(\Omega,Z)\, p_{eq}(\Omega,Z)\frac{\partial}{\partial Z} p_{eq}^{-1}(\Omega,Z) C(\Omega,Z); \tag{41}$$

under this assumption the orientational distribution at any position is isotropic as in bulk water.

Case 1. Substituting eq.38 into eq.36 and rearranging gives

$$\frac{J_Z}{p_{eq\,\Omega}(Z)\int D_{ZZ}(\Omega,Z)\, p_{eq}(\Omega;Z)\,\mathrm{d}\Omega} = -\frac{\partial}{\partial Z}\left[p_{eq\,\Omega}^{-1}(Z) C_{\Omega}(Z)\right]. \tag{42}$$

If the orientationally averaged diffusion coefficient $D_{ZZ_{\Omega}}(Z)$ is defined by

$$\int D_{ZZ}(\Omega,Z)\, p_{eq}(\Omega;Z)\,\mathrm{d}\Omega = D_{ZZ_{\Omega}}(Z), \tag{43}$$

the integration on Z over the bilayer thickness of eq.42 gives the expression

$$J_Z \int_{-L}^{L} \frac{1}{p_{eq\,\Omega}(Z) D_{ZZ_{\Omega}}(Z)}\,\mathrm{d}Z = p_{eq\,\Omega}^{-1}(|L|)\left[C_{\Omega}(L) - C_{\Omega}(-L)\right] \tag{44}$$

where the concentration difference is

$$\left[C_{\Omega}(L) - C_{\Omega}(-L)\right] = \Delta C\,. \tag{45}$$

If the orientationally-averaged partition coefficient $K_{\Omega}(Z)$ is defined as

$$K_{\Omega}(Z) = p_{eq\,\Omega}(Z)\, p_{eq\,\Omega}^{-1}(|L|), \tag{46}$$

by comparison between eq.44 and eq.17 the permeability coefficient can be identified with:

$$P = \left[\int_{-L}^{L} \frac{1}{K_{\Omega}(Z) D_{ZZ_{\Omega}}(Z)}\,\mathrm{d}Z \right]^{-1}. \tag{47}$$

The main equation of the heterogeneous solubility-diffusion model, eq.1, is

recovered if the position-dependent partition and diffusion coefficients *K* and *D* are identified with the corresponding quantities K_Ω and D_{ZZ_Ω}, defined as orientational averages, in eq.47.

Case 2. Integration on *Z* over the bilayer thickness of eq.41 gives

$$J_Z(\Omega)\int_{-L}^{L}\frac{1}{D_{ZZ}(\Omega,Z)\,p_{eq}(\Omega,Z)}\mathrm{d}Z=-p_{eq}^{-1}(\Omega,|L|)\left[C(\Omega,L)-C(\Omega,-L)\right], \tag{48}$$

where the orientation-dependent concentration difference is

$$\left[C(\Omega,L)-C(\Omega,-L)\right]=\Delta C(\Omega)=\frac{\Delta C}{4\pi}. \tag{49}$$

The last equality holds since all orientations are equally probable in water.

If the orientation-dependent partition coefficient $K(\Omega,Z)$ is defined by

$$K(\Omega,Z)=p_{eq}(\Omega,Z)\,p_{eq}^{-1}(\Omega,|L|), \tag{50}$$

the orientation-dependent permeability coefficient is given by

$$P(\Omega)=\left[\int_{-L}^{L}\frac{1}{K(\Omega,Z)\,D_{ZZ}(\Omega,Z)}\mathrm{d}Z\right]^{-1}. \tag{51}$$

Molecules in different orientations can be treated as if they were solutes of different species, all contributing to the total flux

$$J_Z=\int J_Z(\Omega)\mathrm{d}\Omega=-\frac{\Delta C}{4\pi}\int P(\Omega)\mathrm{d}\Omega\,; \tag{52}$$

and the solute permeability coefficient turns out to be

$$P=\frac{1}{4\pi}\int P(\Omega)\mathrm{d}\Omega\,. \tag{53}$$

Some insight into the relative timescales of translational and rotational motions of small and drug-like solutes in lipid bilayers was provided by Stouch and coworkers.[9,10]Among the first MD studies of solute diffusion in lipid membranes, they presented the results of their simulations of benzene[9] and of the nifedipine analogue, 1,4-dihydropyridine[10], in DMPC bilayers. They performed unconstrained MD simulations on solute molecules placed, at the beginning of the simulations, at different depth in the bilayer, and then allowed to move freely. During the simulation time of 2 ns, the nifedipine analogue was found to explore a range of positions of

about 6Å along the bilayer normal and a more or less wide range of orientations, depending on its initial position, at the bilayer centre or near the hydrophobic/hydrophilic interface, while only few interconversions took place between different conformational states. A timescale of the order of nanoseconds was estimated for the reorientational motions of this molecule. Wider displacements and free rotation were observed for benzene during 1 ns-long simulations. A reorientational correlation time of 25 ps was calculated for this small molecule. In the light of these results the approximation made in *Case 1* seems reasonable both for small- and medium-sized compounds. The approximation made in *Case 2*, is expected to hold for larger nano-scaled solutes, with hindered reorientational motions.

In refs.[9,10] Stouch and coworkers also reported the diffusion coefficients of benzene and 1,4-dihydropyridine at different depths in the lipid bilayer, calculated from the time evolution of the mean squared displacement of the molecules during the simulations. The solute size effect observed on the variation of the calculated diffusion coefficients with solute position was regarded by the authors as their most important results. While benzene was found to diffuse three times faster near the bilayer centre than in the interfacial region, the larger nifedipine analogue everywhere diffused with the same rate. This was intended to confirm the 'soft-polymer' hypothesis, according to which the jump-like diffusion of the small benzene molecule would be enhanced by the size distribution of the cavities in the lipid matrix, while the formation of large cavities fitting drug-like molecules would be unlikely. The Stokes-Einstein hydrodynamic model would then apply to drug-like solutes, large enough to allow the representation of the membrane environment as a continuum with an almost uniform viscosity. On the contrary, microscopic effects would determine the different diffusion properties of small molecules like benzene in different micro-environments within the membrane. The 'soft-polymer' model explains this behaviour with the depth-dependence of the frequency of formation and the size distribution of cavities produced by the motion of lipids. However this size effect might be explained by the simple fact that smaller solutes can probe the membrane micro-heterogeneity with higher resolution than larger molecules. The larger nifedipine analogue occupies, with its body, a cavity extending through different regions within the bilayer, and may experience an average viscosity which

varies only little across the bilayer. On the contrary, benzene fills a cavity of reduced dimension, and might be able to sense the local viscosity of its surroundings. Then, while the 'soft-polymer' hypothesis was invoked to account for the behaviour of very small molecules (MW<50),[11] a hydrodynamic model with a heterogeneous bilayer viscosity may be suitable for medium- as well as large-sized solutes. It might be worth noting that the force autocorrelation function method as well as the mean squared displacement method, commonly used for the calculation of diffusion coefficients from MD simulations, rely on the validity of the Einstein's hydrodynamic description of the system under investigation.

3.2.3 Integration of the implicit membrane model presented in Chapter 2 into the generalized solubility-diffusion theory

Our implicit membrane model for solute partitioning[5] (Chapter 2) can be integrated into the expressions derived in the previous section to calculate the intrinsic permeability coefficients *P*.

If the orientational distribution of the solute is assumed to equilibrate rapidly between subsequent diffusive steps, the partition coefficient K_Ω in eq.46 can be calculated from the water-bilayer transfer free energy *u*, introduced in eq.17 of Chapter 2, as

$$K_\Omega(Z) = e^{-\frac{u(Z)}{k_B T}}; \tag{54}$$

this can then be introduced into eq.47 for the calculation of the permeability coefficient *P*.

It is worth noting that the location of the bilayer/water interface is usually not defined unambiguously, and when the local resistance to permeation $\left(K_\Omega(Z) D_{ZZ_\Omega}(Z)\right)^{-1}$ in water is not much smaller than in the bilayer, the choice of the integration limits in eq.47 may have dramatic effects.[12] As a reasonable choice we have taken for *L* the lowest value ensuring that for $Z \geq L$ the local resistance is the same as in bulk water.

3.3 Case studies

3.3.1 Compounds under investigation

With the aim of exploring the effect of different substituent and assessing the independence of their contributions to the permeability of drug-like molecules, Xiang and Anderson reported the permeability coefficients of some derivatives of *p*-toluic acid and *p*-methylhippuric acid, measured in transport experiment on the two sets of solutes across egg lecithin planar bilayers and large unilamellar vescicles respectively.[13,14] Their analysis of the data collected at different pH led them to conclude that over the pH range between 5 and 10 the measured apparent permeability coefficients arose from the diffusion of the acids in their undissociated form across the membranes. The intrinsic permeability coefficients determined by Xiang and Anderson for the neutral species of the substituted acids span a range of five orders of magnitude both in the *p*-toluic and in the *p*-methylhippuric series,[13,14] which seem to represent good test sets for the sensitivity of predictive methods.

We calculated the intrinsic permeability coefficients *P* of four of the substituted *p*-toluic acids in ref.[13] (Figure 1) in a liquid-crystalline lipid bilayer. Their intrinsic permeability coefficients determined by Xiang and Anderson[13] are reported in Table 1.

1: R=H
2: R=OCH_3
3: R=OH
4: R=$C(O)NH_2$

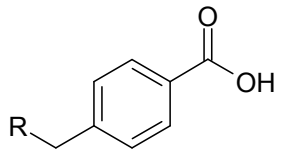

Figure 1: Structures of α-substituted *p*-toluic acids.

Table 1: Intrinsic permeability coefficients of *p*-toluic acids in Figure 1.[13]

	R	*P* (cm s^{-1})
1	-H	1.1
2	$-OCH_3$	$3.5 \cdot 10^{-1}$
3	-OH	$1.6 \cdot 10^{-3}$
4	$C(O)NH_2$	$4.1 \cdot 10^{-5}$

The choice of solutes of similar size and shape allowed us to focus on the effects of different functional groups on permeability. Polar substituents are generally introduced to enhance the water solubility of compounds selected for drug development. This inevitably reduces the affinity of these solutes for the membrane environment, i.e. their lipophilicity, and can have dramatic effects on their membrane permeability. Benzene represents a suitable term of comparison for the evaluation of

the effects of the chemical modifications introduced in compounds 1-4, and was expected to exhibit quite different partition properties due to its hydrophobic nature. Essex and coworkers determined the permeability coefficient of this solute in liquid-crystalline DPPC and DMPC bilayer either from atomic-level or multiscale MD studies. [15,16] An atomistic representation of the solute was adopted in both cases, a constrained particle method was applied, and the permeability coefficient of benzene was calculated according to the inhomogeneous solubility-diffusion model.[15,16] Similar values were obtained from the two approaches, although a different description of the lipid bilayer was adopted, by the use of atomic-level and coarse-grained force fields, respectively.[15,16]

3.3.2 Results and Discussion

3.3.2.1 Drug-like molecules

Free energy and distribution profiles were calculated for solutes 1-4, with local order parameters describing solute average orientation with respect to the bilayer normal at any depth in the bilyer. Calculations were performed starting from molecular properties of the solutes and phase properties of a DPPC bilayer at a temperature T=323K which were parameterized as in ref.[5] (Chapter 2). A common molecular frame was chosen which is shown in Figure 2. All calculated profiles are reported in Figures 3-4, where the location of the hydrophobic/hydrophilic interface, which can be identified with the average position of acyl chain carbonyl groups, as well as the average position of phosphate groups, are also shown.

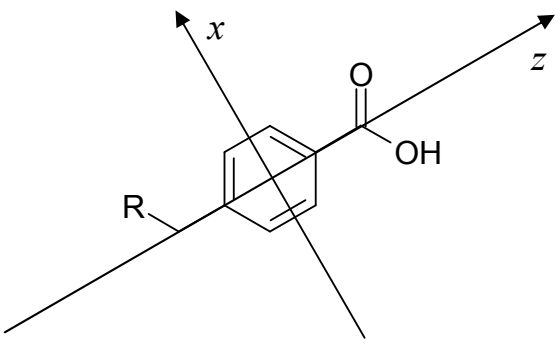

Figure 2: The molecular frame defined for solutes 1-4 has its origin in the centre of the benzene ring; the *z* axis connects the two *para*-substituents, the *x* axis is coplanar with the aromatic system and the *y* axis points upward out of the ring plane.

The transfer free energy profiles and the positional distributions in Figure 3 show similar features for all the investigated compound. The free energy minima (Figure 3 left) are located in the carbonyl region at the hydrophobic/hydrophilic interface, and are reflected by peaked distributions around Z=14Å for compounds 1 and 2 and around Z=17Å for compounds 3 and 4 (Figure 3 right). The presence of the polar carboxylic group restrains molecules from residing deeper in the apolar chain region, and is responsible for the rise in transfer free energy near the bilayer midplane; this effect is amplified in compounds 3 and 4 by the presence of the oxydrilic and amidic group respectively. For these solutes the distribution is narrower and shifted towards the polar headgroup region, while their location in the bilayer centre becomes even less favourable than for compounds 1 and 2.

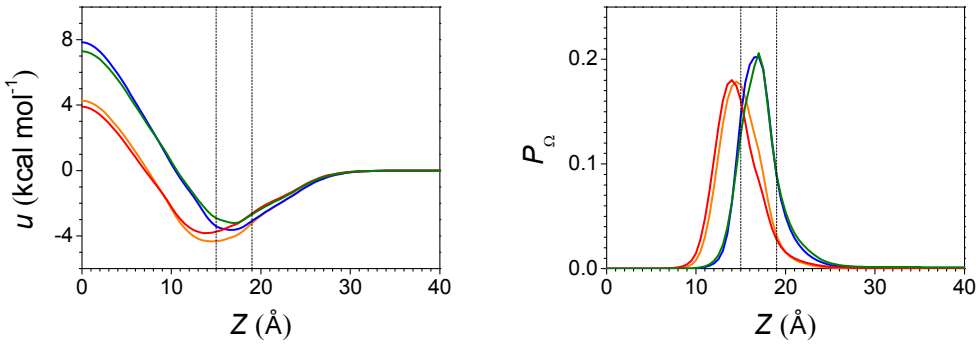

Figure 3: Transfer free energy $u(Z)$ (left) and position distribution function $P_\Omega(Z)$ (right) calculated for solutes 1 (red line), 2 (orange line), 3 (green line), and 4 (blue line) as a function of the distance of the ring centre from the bilayer midplane. The coordinate Z=0 corresponds to the bilayer midplane. The vertical lines indicate the average position of carbonyl and phosphate groups. Given the symmetry of the system, only one half of the bilayer is shown.

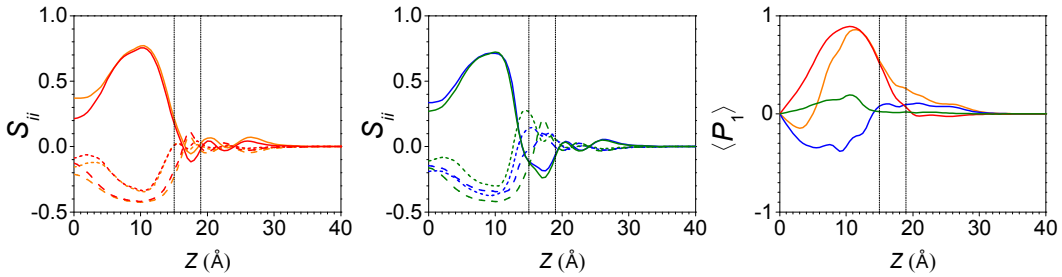

Figure 4: Orientational order parameters S_{ii} (left and centre: S_{xx} dotted, S_{yy} dashed and S_{zz} solid) and $\langle P_1 \rangle$ (right) calculated for solutes 1 (red line), 2 (orange line), 3 (green line), and 4 (blue line) in the molecular frame (Figure 2) as a function of the distance of the ring centre from the bilayer midplane. The coordinate Z=0 corresponds to the bilayer midplane. The vertical lines indicate the average position of carbonyl and phosphate groups. Given the symmetry of the system, only one half of the bilayer is shown.

The orientational behaviour of the solutes is conveniently characterized by the orientational order parameters $S_{ii} = \langle(3\cos^2\theta_i - 1)/2\rangle$ and $\langle P_1\rangle = \langle\cos\theta_z\rangle$, where θ_i is the angle between the ith molecular axis and the bilayer normal. The order parameter profiles across the bilayer are shown in Figure 4. We can see that substituent polarity also affects the orientation of solutes at their preferred positions: compounds 1 and 2 preferentially align their long axis to the bilayer normal ($S_{zz}>0$ near Z=14Å) pointing their carboxylic group towards water ($\langle P_1\rangle>0$ near Z=14Å), while their molecular plane is preferentially kept perpendicular to the bilayer plane ($S_{yy}<<0$ near Z=14Å); as a result of the presence of two polar substituents on the opposite sides of their benzene ring, compounds 3 and 4 lie with their long axis parallel to the bilayer plane ($S_{zz}<0$ and $\langle P_1\rangle\approx 0$ near Z=17Å) with no preferred orientation for their molecular plane ($S_{xx}\approx S_{yy}$ near Z=17Å).

While static properties of solutes in a lipid bilayer reflect the equilibrium positional and orientational distribution and mainly represent the behaviour of solute molecules in the free energy minimum, transport properties are determined by the whole pattern of the free energy profile across the bilayer. In fact, given the form of the solubility-diffusion equation, solute partitioning in the most unfavoured regions of the bilayer represents the main barrier to solute permeation: the exponential dependence of the partition coefficient K_Ω on the transfer free energy (eq.54) amplifies free energy differences, so that while transfer free energies in Figure 4 vary between –4 and +4/+8 kcal mol^{-1}, K_Ω spans a range of 5/8 orders of magnitude. Compared with this, variations in the solute diffusion coefficient across the bilayer are expected to be negligible; moreover the results of the MD study by Alper and Stouch[10] support the assumption of a uniform diffusion coefficient D of drug-like molecules across the whole bilayer thickness. With this in mind, and given the symmetry of the lipid bilayer we are considering, the solubility-diffusion equation (eq.47) can be simplified, and the intrinsic permeability coefficient P can be calculated as

$$P = \frac{D}{2\int_0^L \exp\left(u(Z)/k_B T\right) \mathrm{d}Z}. \tag{55}$$

We chose D=2·10^{-6}cm^{2}s^{-1} as a reasonable estimate of the diffusion coefficient of solutes 1-4, slightly larger than D=1.3·10^{-6}cm^{2}s^{-1} reported in ref.[10] for the larger drug analogue 1,4-dihydropyridine. The integrand function in eq.55 calculated for solutes

1-4 is plotted in Figure 5. Intrinsic permeability coefficients calculated for 1-4 are reported in Table 2 with the integrated area in Figure 5; experimental intrinsic permeability coefficients in Table 1 are also reported for comparison. As can be seen, calculated *P* values are in good agreement with experimental data from ref.[13].

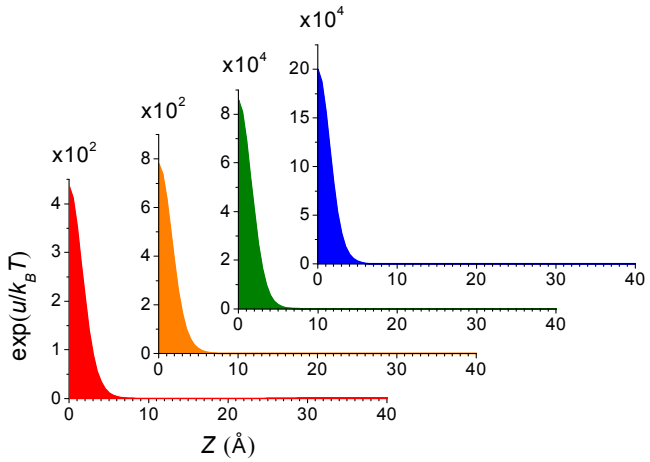

Figure 5: Integrated area in eq.55 calculated for solutes 1 (red), 2 (orange), 3 (green), and 4 (blue). Given the symmetry of the system, only one half of the bilayer is shown.

	R	Area (cm) (Fig.5)	P_{calc} (cm s^{-1})	P_{exp} (cm s^{-1})[13]
1	-H	$9.3 \cdot 10^{-6}$	$1.1 \cdot 10^{-1}$	1.1
2	$-OCH_3$	$1.7 \cdot 10^{-5}$	$6.1 \cdot 10^{-2}$	$3.5 \cdot 10^{-1}$
3	-OH	$1.8 \cdot 10^{-3}$	$5.7 \cdot 10^{-4}$	$1.6 \cdot 10^{-3}$
4	$C(O)NH_2$	$3.9 \cdot 10^{-3}$	$2.6 \cdot 10^{-4}$	$4.1 \cdot 10^{-5}$

The experimental trend in Table 2 was rationalized relating the permeability decrease from solute 1 to solute 4 with the increased hydrogen-bonding ability, which would reduce solute partitioning in the apolar region of the bilayer.[14] Among different bulk hydrocarbon solvents, 1,9-decadiene was found to better mimic the microenvironment of a barrier region within the egg lecithin bilayer, which, alone, would determine the whole membrane resistance to solute permeation. This rate-limiting region was hence recognized in the ordered region where the unsaturations along egg lecithin alkyl chains concentrate.[13,14]

As Figure 5 shows, only a confined region within the model DPPC bilayer significantly contributes to the integral in eq.55: it is the most internal region of the bilayer and extends for less than 5 Å on both sides of the bilayer midplane. According to this result the disordered hydrophobic core of a DPPC bilayer would represent the barrier region opposing to the permeation of compounds in Figure 1.

Saturated DPPC chains in this region should be reasonably well mimicked by a hydrocarbon bulk solvent like *n*-hexadecane, hence a correlation between the permeability coefficients of solutes 1-4 in DPPC and their hexadecane/water partition coefficient could be expected. On the other hand, the pattern of the exponential function in Figure 5 justifies *a posteriori* the assumption of a uniform diffusion coefficient, as it is at least in the region of interest. As a first approximation, *n*-hexadecane could be taken to represent not only the hydrophobicity but also the disordered structure of the bilayer core,[17] and the isotropic translational diffusion coefficient of 1-4 in this bulk solvent could be used in eq.55. We calculated it by the molecular-surface-based method for the computation of hydrodynamic transport properties of arbitrarily shaped molecules implemented in the BEST software package[18]. Taking for *n*-hexadecane a viscosity of $3.3 \cdot 10^{-3}$ Pa·s,[19] from the trace of the translational diffusion tensors, we obtained for all the compounds in Figure 1 an average diffusion coefficient $D \sim 1.9 \cdot 10^{-6} cm^2 s^{-1}$, in close agreement with our previous estimate.

Despite their different interpretation, experimental and calculated data in Table 2 show the same trend and orders of magnitude. The discrepancy between calculated and experimental permeability coefficients observed for 1-3 would probably be removed by a more accurate evaluation of their diffusion coefficient, while the overestimation of the permeability coefficient of 4 may reflect the major role played in this case by hydrogen bonding with water and lipids, which is actually ignored in our implicit membrane model.

This is a valuable and encouraging result, especially considering that MD simulations employed for the prediction of the permeability coefficients of molecules across lipid bilayers, have not reached better outcomes[20]. It should be mentioned however that the most common experimental procedures for the determination of the permeability coefficients of drug-like molecules make use of membrane systems which are far different from simple lipid bilayers. Caco-2 [8,21] and PAMPA[22] permeability assays are carried out respectively on cell monolayers and mixed lipid/solvent artificial membranes of unknown phase; the permeability coefficients they provide correlate with drug absorption *in vivo* but are usually hardly reproduced by calculations. MD simulations carried out to this purpose have been able to provide relative permeabilities of common drugs with similar structures, yet

overestimating absolute coefficients of orders of magnitude.[20] The application of our implicit membrane model to the calculation of the partition properties of these solutes and of their intrinsic permeability coefficients would be a good test of its predictive capability.

3.3.2.2 Benzene

The location of the minimum of the transfer free energy profile calculated for benzene (Figure 6 left) is the same found for solutes 1 and 2, bearing the most hydrophobic substituents among the *p*-toluic acid derivatives in Figure 1. Although the well is slightly deeper for larger solutes than for benzene, an overall stronger affinity for the membrane environment is predicted for the latter, whose partitioning near the bilayer centre is not so dramatically unfavoured, with respect to bulk water, as it is for 1 and 2. Correspondingly, the distribution profile calculated for benzene (Figure 6 right), shows that, although, like 1 and 2, this solute is mainly distributed at distances between 11Å and 19Å from the bilayer midplane, a nonzero probability exists of finding it more deeply buried in the hydrophobic region of the bilayer. Hence, as expected, the presence of the highly polar carboxylic substituent, is found to hinder the partitioning of 1 and 2 in the tail region of the lipid bilayer, with respect to the hydrophobic benzene molecule. However, significant variations between the free energy profiles in Figure 6 produce only minor changes in the corresponding distribution profiles.

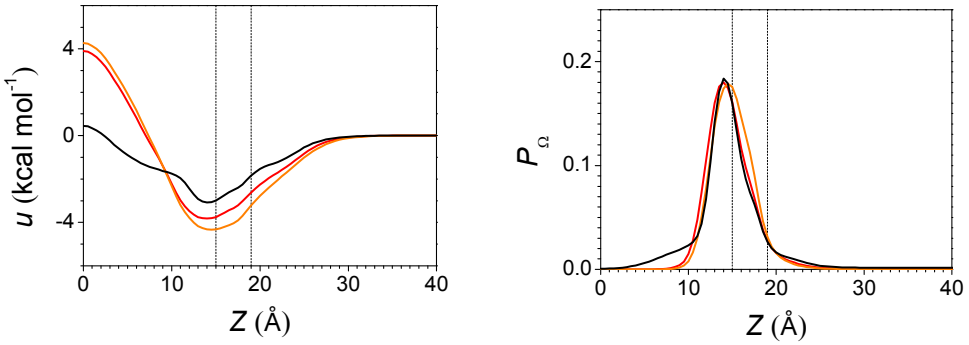

Figure 6: Transfer free energy $u(Z)$ (left) and position distribution function $P_\Omega(Z)$ (right) calculated for benzene (black line) as a function of the distance of the molecular centre of mass from the bilayer midplane. The profiles calculated for 1 and 2 shown in Figure 3 are reported here for comparison. The coordinate Z=0 corresponds to the bilayer midplane. The vertical lines indicate the average position of carbonyl and phosphate groups. Given the symmetry of the system, only one half of the bilayer is shown.

A more striking effect is seen from the comparison of the exponential functions plotted in Figure 7. The stabilization of benzene in the hydrophobic region of the bilayer, with respect to 1 and 2, is reflected by a huge reduction of the energy barrier at the bilayer centre, which was found to determine the permeation rate of the hydrophilic compounds. Partitioning in the outer regions of the bilayer, entering and exiting the membrane (region II in Figure 7), which did not significantly contribute to the integrated area in Figure 5, influences the permeation process in the case of benzene, as also the crossing of the membrane core does (region I in Figure 7) to a comparable extent.

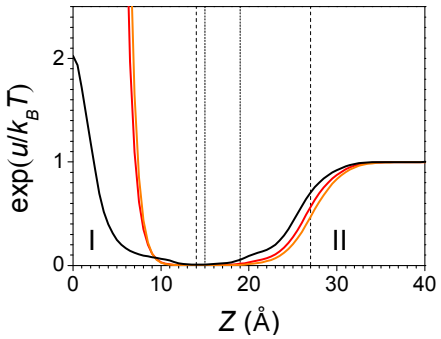

Figure 7: Integrand partition function calculated for benzene (black line). The profiles calculated for 1 and 2 shown in Figure 5 are reported here for comparison. The vertical dotted lines indicate the average position of carbonyl and phosphate groups. The vertical dashed lines indicate the boundary chosen between regions I and II, and the hydrated-bilayer/bulk-water interface according to refs.[3,17]. Given the symmetry of the system, only one half of the bilayer is shown.

As demonstrated by the MD analysis in ref.[9], the diffusion properties of benzene are non-uniform across a lipid bilayer. However, although this prevented us from applying eq.55 to the case of benzene, the shape of the profile reported in Figure 7, allowed a different simplification of the solubility-diffusion equation (eq.47). In fact, the pattern of the exponential function allows the breaking of the integral in eq.47 into two parts, corresponding to the two distinct regions I and II in Figure 7. These can be represented, respectively, by the low density tail region and the low density headgroup region of the lipid bilayer, as defined by Marrink and Berendsen in their 'four-region' model[3]. According to the thicknesses and locations reported for the regions of a liquid-crystalline DPPC bilayer[3,17], region I in Figure 7 nearly coincides with the disordered region of the terminal methyl groups, extending for 6Å from the midplane in each leaflet of the bilayer, while region II actually comprises both the hydrated surface region of the bilayer, extending in the range 20Å<Z<27Å, and the

adjacent water layer extending towards the bulk of the aqueous environment. If hexadecane and bulk water are taken to represent the transport properties of regions I and II, respectively [17], the isotropic diffusion coefficient of benzene in these two bulk solvents, D_h and D_w, can be introduced, and the permeability coefficient calculated as

$$P = \left(\frac{2}{D_h} \int_{\mathrm{I}} \exp\left(u(Z)/k_B T\right) \mathrm{d}Z + \frac{2}{D_w} \int_{\mathrm{II}} \exp\left(u(Z)/k_B T\right) \mathrm{d}Z \right)^{-1} . \qquad (56)$$

We used the BEST software package to calculate both D_h and D_w and, taking $3.3 \cdot 10^{-3}$ Pa·s and $1.0 \cdot 10^{-3}$ Pa·s for the viscosities of hexadecane and water, respectively,[19] we obtained $D_h = 2.5 \cdot 10^{-6} \mathrm{cm^2 s^{-1}}$ and $D_w = 8.4 \cdot 10^{-6} \mathrm{cm^2 s^{-1}}$. Concerning the integration of the exponential function in Figure 7, we chose Z=14Å as the boundary between regions I and II, so that the first integral in eq.56 was taken over the range 0Å<Z<14Å, while the second extended from 14Å to the upper integration limit L. The problem arose of a reasonable choice of L, since in the situation depicted in Figure 7, it was shown to be a critical parameter. In fact the definition of the bilayer thickness or of the location of the bilayer/water interface is somehow ambiguous. According to the 'four-region' model proposed by Marrink and Berendsen[3], Z=27Å represents the upper boundary of the perturbed water layer in the proximity of the surface of a liquid-crystalline DPPC bilayer, where the organization of water molecules differs from that typical of bulk water. However, as can be seen from the profile in Figure 7, the behaviour of benzene is affected by the presence of the lipid bilayer even quite far beyond this border, and, since the intrinsic permeability is defined in order to account for the effect of the membrane on solute diffusion, the integral in the solubility-diffusion equation has to be extended over the whole region where the solute deviates from its behaviour in bulk water. Figure 8 shows how the integral over region II in eq.56 calculated for benzene varies while L is moved from Z=27Å, corresponding to the interface between the hydrated bilayer and bulk water, to Z=45Å, where the profile in Figure 7 has undoubtedly reached the constant value $\exp(u/k_B T)$=1 defined for solutes in bulk water. When the integral is extended in the bulk water region its increase becomes linearly dependent with the increase in L. Thus the calculated curve progressively approximates the line of unitary slope, also shown in Figure 8, as L approximates the limit of the bulk water region.

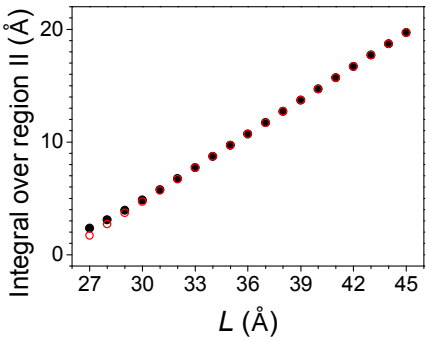

Figure 8: Dependence of the integral over region II in eq.56, calculated for benzene, on the upper integration limit *L* (black filled circles). A unitary slope curve would be observed (red empty circles) if bulk water would extend over the whole investigated *L* range.

We chose *L*=35Å, where the deviation from the linear behaviour is about the 0.1% of the integrated area, as a good level of approximation, and obtained for benzene a calculated permeability coefficient *P*=(14.3±0.5)cm/s.[23] Despite discrepancies in the estimate of the diffusion coefficient of benzene in different regions of the bilayer, our calculations and the MD simulations in refs.[15,16] yield similar permeability coefficients. *P*=(7.8±2.6)cm/s and *P*=(10±1)cm/s were obtained by Essex and coworkers from atomic-level and multiscale simulations respectively, although quite different free energy and local resistance profiles were provided by the two different approaches for benzene. The free energy profile we determined closely resembles that reported from the multiscale study in ref.[16]. In particular, the presence of a free energy minimum in the region of the lipid carbonyl groups and the free energy barrier in the centre of the bilayer are predicted by both the coarse-grained description of the lipid bilayer adopted by Orsi *et al.*[16] and our implicit membrane model. On the contrary, an almost flat free energy profile of benzene in the hydrophobic core of the lipid bilayer was reported from atomic-level MD simulations in ref.[15], where the barrier to solute permeation was individuated in correspondence of a free energy maximum in the headgroup region of the bilayer.

The inclusion, in our implicit membrane model, of favourable excluded volume effects in the low density tail region, may lead to higher partitioning of benzene in the hydrophobic core of the lipid bilayer and hence higher solute permeability. However, in absence of experimental data on the membrane permeability coefficient of benzene, we are not able to assess if this truly represents a deficiency of our

approach, or if, even in the case of small molecules, the model we have developed captures the most important features of solute-membrane interactions.

3.4 Conclusions

We demonstrated that, from a stochastic description of roto-translational diffusion of solutes in membranes, the traditional solubility-diffusion equation for solute permeability, in the form derived by Diamond, Szabo and Katz[2], is recovered in the limit of fast solute reorientation.

Our calculations of the permeability coefficients of benzene and drug-like solutes yielded results in good agreement with literature data from experiments and MD simulations. We noticed that calculated intrinsic permeabilities were mainly determined by the free energy profiles of solutes across the lipid bilayer, rather than by their diffusion properties in the membrane environment. The implicit membrane model we proposed in ref.[5] (Chapter 2), was found to provide a reliable description of the bilayer-water partitioning of the solutes under investigation, while reasonable estimates of their diffusion coefficients in different regions of the bilayer could be obtained by simple hydrodynamic considerations.

A different behaviour was predicted for hydrophilic and hydrophobic molecules. In line with what expected[2], the rate-limiting barrier to the permeation of polar solutes was found to reside in the inner region of the bilayer, while a significant contribution to benzene permeability came from solute translocation across the bilayer/water interfacial regions. It was in this latter case that the need of a proper choice of the bilayer boundaries was evidenced. According to the definition of the intrinsic permeability coefficient P of a solute, the integration limit L in the solubility-diffusion equation should be chosen in such a way that *i*) the concentration of the solute in $Z=L$ is equal to its concentration in bulk water and *ii*) the presence of the lipid bilayer affects the behaviour of the solute in $Z<L$ and not in $Z>L$. In fact, while calculated permeability coefficients of hydrophilic molecules do not depend on the choice of L, since local resistance in water is negligible for these solutes, the problem of the assessment of this parameter when dealing with hydrophobic solutes was recently highlighted[12]. The method we proposed, based on the analysis of the

dependence on L of the integrated resistance in the solubility-diffusion equation, provides a univocal definition of what is regarded in this field as the bilayer thickness. In our opinion, this would guarantee the correct quantitative comparison between intrinsic permeability coefficients derived from different calculations and experimental data.

Abbreviations

DMPC: 1,2-Dimyristoyl-sn-Glycero-3-Phosphocholine

DPPC: 1,2-Dipalmitoyl-sn-Glycero-3-Phosphocholine

MD: Molecular Dynamics

MW: Molecular Weight

3.5 References

[1] Lipinski, C.A. *Adv. Drug Del. Rev.* **1997**, *23*, 3-25.

[2] Diamond, J.M.; Katz, Y. *J. Membr. Biol.* **1974**, *17*, 121-154; Diamond, J.M.; Szabo, G.; Katz, Y. *J. Membr. Biol.* **1974**, *17*, 148-152.

[3] Marrink, S.-J.; Berendsen, H.J.C. *J. Phys. Chem.* **1994**, *98*, 4155-4168.

[4] Kramers, H.A. *Physica* **1940**, *7*, 284-304.

[5] Parisio, G.; Ferrarini, A. *J. Chem. Theory Comput.* **2010**, *6*, 2267-2280.

[6] Risken, H. The Fokker-Planck equation. Methods for solution and applications. 2nd ed.; Springer-Verlag: Berlin, 1989.

[7] Frezzato, D.; Polimeno, A.; Ferrarini, A; Moro, G.J. *Theor. Chem. Acc.* **2007**, *117*, 1017-1027.

[8] Karlsson, J.; Artursson, P. *Int. J. Pharm.* **1991**, *71*, 55-64.

[9] Bassolino-Klimas, D.; Alper, H.E.; Stouch, T.R. *Biochemistry* **1993**, *32*, 12624-12637.

[10] Alper, H.E.; Stouch, T.R. *J. Phys. Chem.* **1995**, *99*, 5724-5731.

[11] Walter, A.; Gutknecht, J. *J. Membr. Biol.* **1986**, *90*, 201-217.

[12] Fiedler, S.L.; Violi, A. *Biophys. J.* **2010**, *99*, 144-152.

[13] Xiang, T.-X.; Anderson, B.D. *J. Pharm. Sci.* **1994**, *83*, 1511-1518.

[14] Mayer, P.T.; Xiang, T.-X.; Anderson, B.D. *AAPS PharmSci* **2000**, *2*, E14.

[15] Bemporad, D.; Essex, J.W.; Luttmann, C. *J. Phys. Chem. B* **2004**, *108*, 4875-4884.

[16] Orsi, M.; Sanderson, W.E.; Essex, J.W. *J. Phys. Chem. B* **2009**, *113*, 12019-12029.

[17] Xiang, T.-X.; Anderson, B.D. *Adv. Drug Deliv. Rev.* **2006**, 58, 1357-1378.

[18] Aragon, S. *J. Comput. Chem.* **2004**, *25*, 1191-1205.

[19] CRC Handbook of Chemistry and Physics, 56th ed.; CRC Press: Cleveland, 1975.

[20] Orsi, M.; Essex, J.W. In Molecular simulations and biomembranes: from biophysics to function, Biggin, P.C.; Sansom, M.S.P. Eds., Royal Society of Chemistry 2010, pp. 77-91. Orsi, M.; Essex, J.W. *Soft Matter* **2010**, *6*, 3797-3808.

[21] Artursson, P.; Karlsson, J. *Biochem. Biophys. Res. Commun.* **1991**, *175*, 880-885.

[22] Kansy, M.; Seener, F.; Gubernator, K. *J. Med. Chem.* **1998**, *41*, 1007-1010. Kansy, M.; Avdeef, A.; Fischer, H. *Drug Discov. Today* **2004**, *1*, 349-355.

[23] The error was estimated as the variation of the permeability coefficient obtained with L=34Å and L=36Å.

Chapter 4*

Penetration of monomeric [60]Fullerenes into lipid membranes: effects of molecular shape and polarity

*This chapter is adapted from Parisio, G.; Bortolus, M; Maniero, A.L.; Ferrarini, A. manuscript in preparation. For Experimental Section see Appendix B.

4.1 Introduction

Carbon nanomaterials, which include fullerenes, metallofullerenes, carbon nanotubes and their derivatives, hold promising properties which make them good candidates for application in the biomedical field.[1-3] At the same time, the perspective of intensive production and use has raised concern on their potential health impact and environmental safety and there is increasing attention to their cellular effects.[4] In this context, the interaction of carbon nanoparticles with cell membranes has a special relevance. Small particles can access the cell via passive diffusion across the lipid bilayer. Fullerenes can be cytotoxic and C_{60} derivatives and their aggregates can cause membrane leakage due to lipid peroxidation.[5,6] Moreover, the embedding of carbon nanoparticles in liposomes allows their solubilization in aqueous environments and their delivery to cells.[1,2] Hence, the study of the partitioning and permeation of C_{60} and its derivatives across lipid bilayers has become of particular interest.[7,8]

The characterization of C_{60} incorporated in model lipid membranes such as vesicles and liposomes was the object of a few studies published in the 90s,[9-11] where, from the analysis of UV-Visible absorption spectra, the presence of C_{60} aggregates in the lipid phase was revealed even at low fullerene concentrations (C_{60}/lipid ratio = 0.1%),[10] and no information could be obtained on the behaviour of C_{60} as a single molecule.

Recently, the problem was addressed with the aid of computational tools. Several Molecular Dynamics (MD) studies appeared in the last few years on the translocation of fullerenes across lipid membranes.[12-18] Because of the high computational cost, only relatively short trajectories could be collected by all-atom (AA) simulations. This limit could be overcome by coarse-grained (CG) simulations, at the cost of a less detailed representation of solute, bilayer and water. Most of the calculations were performed on single C_{60} molecules placed and constrained at different depths in the membrane in order to obtain energy and distribution profiles of the solute across the bilayer,[15,16,18] its diffusion coefficient in the viscous membrane environment, and, finally, its permeability coefficient, which is a measure of the efficiency of the overall passive diffusion process.[12-14,17] Unconstrained simulations provided insight into the mechanism of migration from bulk water to the inner region of the bilayer.[14-

[16] In a few cases the formation of C_{60} aggregates[18] and their permeation[14] through the membrane were followed by simulations. Sometimes significant discrepancies emerge between the collected data, and it is difficult to ascertain the reliability of these results, since they mostly refer to different bilayer compositions and temperatures and are obtained with different force-fields. Undoubtedly the parameterization of the interactions of fullerenes with their environment is not a simple task.[19] On the other hand no experimental data directly comparable with the results of simulations are available.

An important and not yet clarified issue concerns the effects of polar functionalization, which has been shown to enhance the solubility of carbon nanoparticles in water and to lower their cytotoxicity[3,6]. The interaction between C_{60} polar derivatives and model membranes was investigated by MD,[12,15] but there is still a distinct lack of experimental data on these systems that can confirm the results of simulations.

In this work, we have focused on the behaviour of fullerenes as a single molecule inside lipid bilayers, combining a theoretical study and Electron Paramagnetic Resonance (EPR) experiments in oriented bicelles. The investigated systems are pristine C_{60} and the two N-substituted fulleropyrrolidines shown in Figure 1. The three molecules differ from each other in shape and polarity, therefore they appear suitable for investigating the effect of functionalization on the interaction of fullerenes with lipid bilayers.

Our theoretical analysis makes use of a so-called *implicit membrane model*, wherein the atomistic description of the solute is integrated with a continuum representation of the bilayer. In this kind of approaches the lower resolution, due to the absence of explicit solvent molecules, may be compensated by the advantages of a limited computational cost and by the ease to correlate interactions with their effects on solute behaviour. These methods have been widely applied to the problem of solvation in isotropic liquids,[20] but their extension to lipid bilayers poses some problems, due to the need of including in a consistent way the nonuniformity and order characteristics of the bilayer environment[21]. Recently, some of us developed a theoretical and computational methodology where such features are introduced in terms of the profiles of lateral pressure, density, dielectric permittivity and order parameters across the bilayer.[22] This method is applied here to the case of fullerenes.

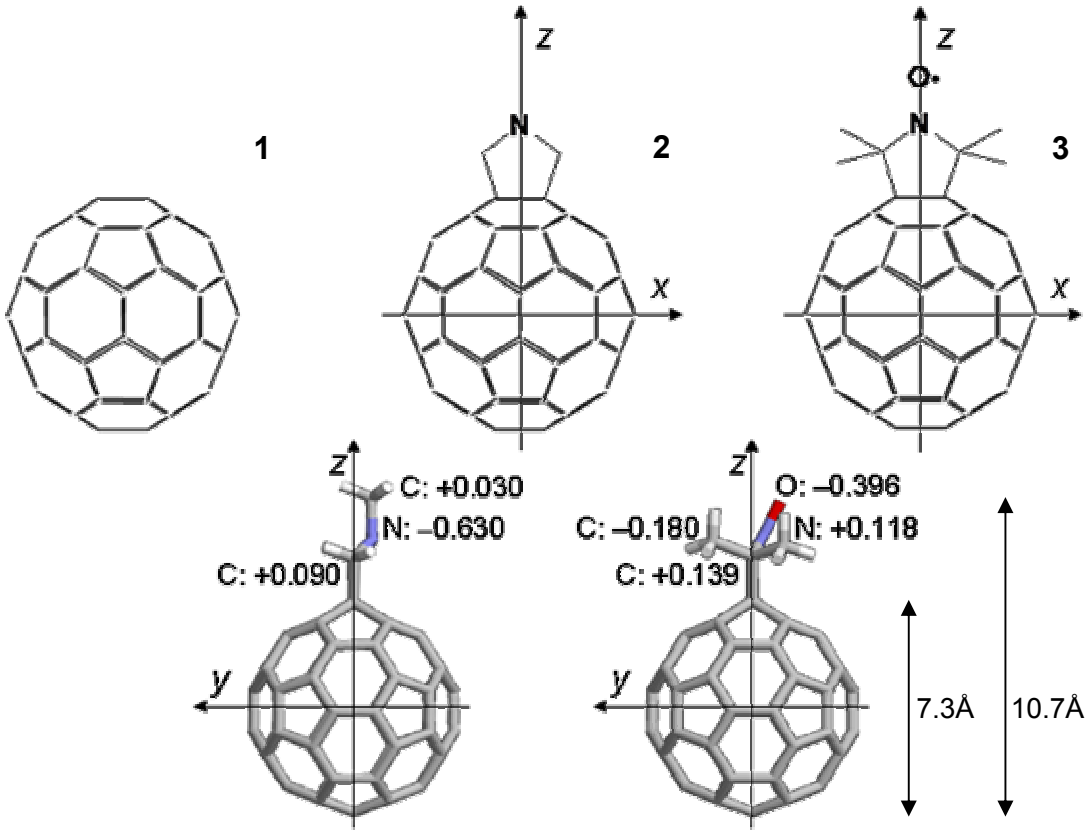

Figure 1: Molecular structure of C_{60} (**1**) and of the two fulleropyrrolidines considered in this study (**2**, **3**). (*x,y,z*) are the axes of the molecular reference frame, with the origin in the centre of the C_{60} cage. Atomic charges are reported (in electron units). Each hydrogen bears a charge equal to +0.060.

EPR spectroscopy is a well-proven technique for the study of solutes in membrane, with the valuable feature of a great sensitivity.[23] It can provide information on the molecular environment, orientation and dynamics of the paramagnetic probe, which may be either the solute itself or a spin-labelled lipid. We used the first approach for the nitroxide derivative **3** and the latter for the diamagnetic derivatives **1** and **2**; in this way the system could be characterized from the perspective of fullerene and from that of the bilayer. DHPC/DMPC bicelles[24] were used as model planar bilayers, offering the possibility of investigating solute preferential orientations. This is especially important to characterize the behaviour of solutes with anisotropic orientational distribution, as is the case of fullerenes, whose icosahedral symmetry is broken by substituents. In fact, **3** was found to show a considerable degree of orientational order in the nematic liquid crystal solvent 4,4'-azoxyanisole (PAA).[25] The compatibility of the fullerene structure with ordered environments was also demonstrated by the incorporation of fulleropyrrolidines in liquid crystals.[26]

4.2 Results and Discussion

4.2.1 Position and orientation of fullerenes inside bilayers

A lipid bilayer in the liquid crystal phase is a uniaxial environment, where the C_∞ symmetry axis, also indicated as the director **n**, is parallel to the bilayer normal **N**. Our description of the behaviour of a molecular solute in a lipid bilayer is based on the definition of a mean field potential U, exerted by the membrane environment, which determines the solute distribution across the bilayer. This potential is expressed as the superposition of four contributions, associated with: the work required to form a molecular shaped cavity (U_{cav}); the electrostatic (U_{el}) and dispersion (U_{disp}) interactions between the solute and the bilayer; the anisotropic interactions of the solute with the ordered acyl chains in the membrane interior (U_{ord}):[22]

$$U = U_{cav} + U_{el} + U_{disp} + U_{ord} \tag{1}$$

Due to the nonuniform and anisotropic nature of the bilayer environment, each term in eq.1 bears a dependence on the position, Z, of the solute along the bilayer normal **N**, and on its orientation Ω with respect to **N** (see Figure 1 in Chapter 2). The profile of the lateral pressure opposing the formation of the molecular cavity, whose high nonuniformity originates from the modulation of inter-lipid repulsions and attractions across the bilayer[27], enters the first term in eq.1. The gradients of density and dielectric permittivity along **N** affect the dispersion and the electrostatic term, respectively, the former described by a generalized London expression[28] and the latter by a generalized Born model[29]. From the order parameter profile, describing the average alignment of acyl chains to the bilayer normal[30], the orienting potential in the final term in eq.1 is derived, according to a theory originally proposed for liquid crystals[31]. The atomistic representation of the solute encompasses its geometry, charge distribution and polarizability. From the mean field potential $U(\Omega,Z)$, several equilibrium properties of the solute in the bilayer can be evaluated, like its orientational and positional distribution functions, as well as the free energy change upon transfer from water to bilayer.

We carried out calculations for compounds **1-3** in a liquid-crystalline lipid bilayer. Calculations were performed starting from molecular properties of the solutes and

phase properties of a DPPC bilayer at a temperature T=323K which were parameterized as reported in ref.[22].

Figure 2 shows the water-bilayer transfer free energy for the three fullerenes as a function of the position of the centre of their C_{60} cage (see Figure 1) across the bilayer normal **N**, and the corresponding position distribution functions; the profiles were obtained by averaging over all molecular orientations at each position. The location of the hydrophobic/hydrophilic interface, which can be identified with the average position of acyl chain carbonyl groups, as well as the average position of phosphate groups, are also shown in Figure 2. We can see that for all the three solutes the predicted transfer free energy is highly favourable to insertion in the bilayer. However the profiles are well far from the uniform distribution which would be found in a homogeneous isotropic liquid; all the fullerenes are predicted to preferentially locate the centre of their C_{60} cage in a well defined zone, i.e. a few Ångstrom wide region just below the hydrophobic/hydrophilic interface. No barrier to penetration is found, and the free energy profile reaches a depth of about -18 kcal mol^{-1}. Interestingly, the presence of a substituent, even polar, does not strongly differentiate the behaviour of the fullerenes in the lipid bilayer: the position distribution probability across the bilayer is very similar for pristine C_{60} and fulleropyrrolidine **2**, and only slightly broader and shifted towards the bilayer interior for the nitroxide derivative **3**. The behaviour of pristine C_{60} was investigated in various lipid bilayers by MD simulations, either at the AA or at the CG level; in general no barrier to fullerene penetration was found, (with the only exceptions of refs.[12,14]) and the following values were reported for the depth and position of the free energy minimum (unless differently specified, the bilayer was in the liquid crystal phase): ~ -8 kcal mol^{-1} and 11 Å in DPPC (AA)[12]; ~ -18 kcal mol^{-1} and 9 Å in DMPC in the presence of cholesterol (AA)[17]; ~ -21.5 kcal mol^{-1} and 11 Å (AA) or -19.5 kcal mol^{-1} and 9 Å (CG), both in DOPC[18]; ~ -20 kcal mol^{-1} and 18 Å in DPPC in the gel phase (AA)[16]; ~ -23 kcal mol^{-1} and 6 Å in DMPC (AA)[13]; ~ -24 kcal mol^{-1} and 10 Å in DPPC and similar in DOPC (CG)[14]; up to ~ -48 kcal mol^{-1} and 0 Å in DPPC (CG)[15]. Given the different chemical constitution of the bilayers, no strict quantitative agreement can be expected; however, the large differences, especially in terms of the minimum value reached by the free energy profile, indicate the uncertainty which mostly derives from the parameterization of interactions involving

fullerene[7]. In fact it was demonstrated that calculated free energies of transfer of C_{60} between apolar and polar solvents are extremely sensitive to the interaction potential used.[19] All this notwithstanding, we can notice that a transfer free energy minimum near -20 kcal mol^{-1}, as obtained from our calculations, was also found in several simulations. Especially remarkable is the agreement in predicting C_{60} as preferentially confined below the hydrophobic/hydrophilic interface, at least when the bilayer is in the liquid crystal phase. This seems to be a general results, not dependent on the specific features of a given model, provided that the nonuniform polarizability of the bilayer environment, involved in dispersion interactions with the fullerene cage[19], is suitably taken into account. The key role played by these interactions for fullerene derivatives is confirmed by the scarce effects of substituents on the positional distribution shown in Figure 2.

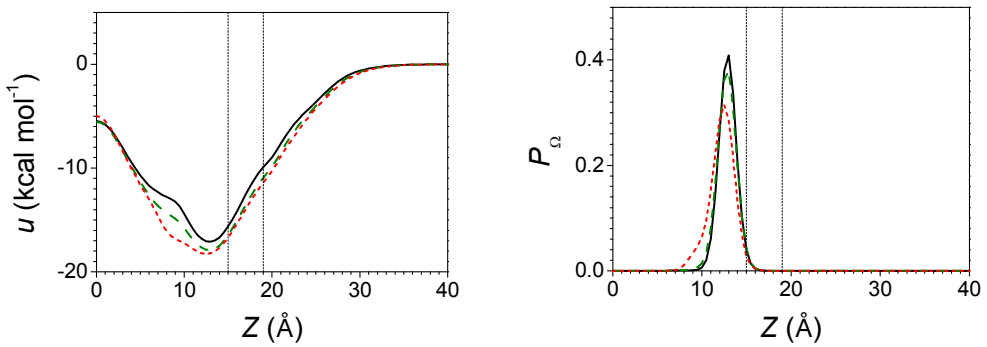

Figure 2: Transfer free energy $u(Z)$ (left) and position distribution function $P_\Omega(Z)$ (right) calculated for **1** (solid), **2** (dashed) and **3** (dotted) as a function of the position of the centre of the fullerene cage across the lipid bilayer. The coordinate Z=0 corresponds to the bilayer midplane. The vertical lines indicate the average position of carbonyl and phosphate groups. Given the symmetry of the system, only one half of the bilayer is shown.

To analyse in more detail the origin of the partitioning behaviour of fullerenes, we report in Figure 3 the transfer free energy profiles, and the corresponding position distribution functions, calculated for **3** by removing one term in eq.1 at a time. The results clearly show that dispersion interactions involving the highly polarizable C_{60} cage are the main responsible for the affinity of fullerenes for the membrane environment, especially for the region of the bilayer where the acyl tails are tighter[32]. The small differences between the free energy profiles in Figure 2 show that pyrrolidine substituents slightly enhance this affinity. Non-dispersion interactions concur to determine the position of the free energy minimum, and hence of the maximum of the fullerene distribution function inside the bilayer. In particular, the

cavity contribution favours locations close to the hydrophobic/hydrophilic interface, where the formation of a molecular cavity is promoted by the strongly negative lateral pressure[27]. On the contrary, anisotropic interactions between **3** and the ordered acyl tails are optimized by slightly deeper insertion of the molecule, so that a large part of its body resides in the most ordered region of the bilayer. Figure 3 also shows that, despite the presence of charges in the substituent, electrostatic interactions do not significantly affect the behaviour of **3**: they only slightly destabilize those locations in which the molecule either puts its polar head in an apolar environment or adopts an orientation which complies with electrostatic requirements, but does not optimize the other interactions (see below).

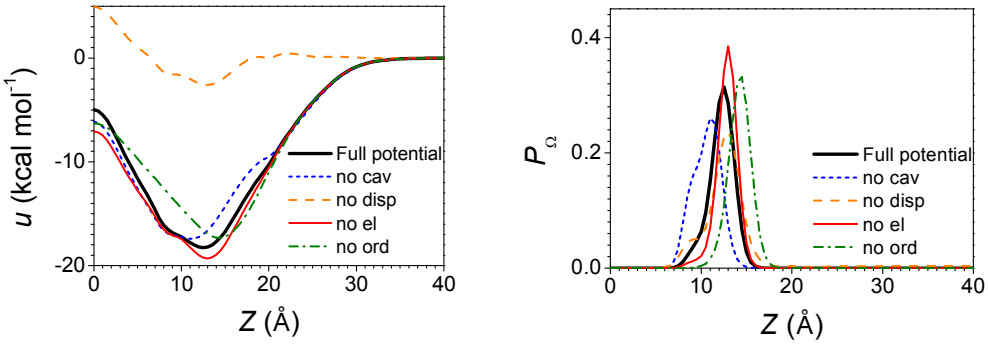

Figure 3: Transfer free energy $u(Z)$ (left) and position distribution function $P_\Omega(Z)$ (right) calculated for **3**, as a function of the position of the centre of the molecular frame across the lipid bilayer, by removing from eq. 1 one contributions at a time. The coordinate Z=0 corresponds to the bilayer midplane. Given the symmetry of the system, only one half of the bilayer is shown.

Analogous effects of the various contributions to the mean field potential in eq.1 were found for the other derivatives, with the difference that electrostatic effects are absent for **1** and play a role even weaker for **2** than for **3**, since the non-negligible charge on the nitrogen atom in **2** is buried by the bulky methyl substituent.

It is interesting to realize that, behind the similar positional distribution, a significantly different orientational behaviour is predicted for the fullerenes; the nonuniformity and anisotropy of the membrane environment result in the non-equivalence of the orientations of the anisometric derivatives, **2** and **3**, with some effects determined by the polarity of their substituents. The contour plots in Figure 4 show the orientational distribution of **3**, calculated at different depths within the region where, according to Figure 2, this derivative is predicted to preferentially reside. The orientation of the solutes with respect to the bilayer normal **N** is defined

as in ref.[22] (see Figure 1 in Chapter 2): β is the angle between the long molecular axis *z* (Figure 1) and **N**; the γ angle refers to molecular rotation around *z*.

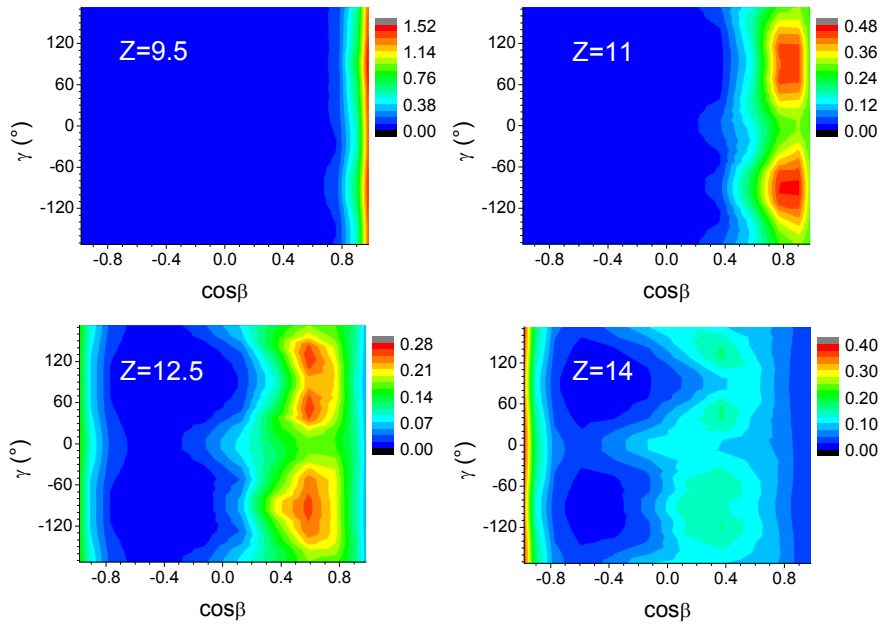

Figure 4: Orientational distribution $P(\Omega,Z)$ calculated for **3** at different positions, *Z*, of the solute along the bilayer normal. β is the angle between the long molecular axis, *z* (Figure 1) and the bilayer normal. The γ angle refers to molecular rotation around *z*.

We can see that the orientational distribution exhibits significant variations in a range of a few Ångstrom. In general, the molecule tends to align its long axis, *z*, to the bilayer normal, **N**, because in this way the interactions with the ordered acyl chains are optimized; however, all interactions contribute to modulate this tendency. When located in correspondence of the tail of the positional distribution at deeper positions (*Z*=9.5Å in Figure 4), **3** is preferentially oriented with the molecular *z* axis parallel to **N** and the polar head towards water (β~0). As the molecule moves to shallower positions (*Z*=11Å in Figure 4), the *z* axis tilts, in such a way that the pyrrolidine ring is still kept at the hydrophobic/hydrophilic interface, where the solute cavity is stabilized by lateral pressure, and the polar nitroxide group resides in the hydrophilic region of the bilayer. Beyond a distance of about 11.5Å from the bilayer midplane also the antiparallel orientation (β~π), with the nitroxide directed towards the bilayer core, acquires some probability (*Z*=12.5Å in Figure 4): the cost for bringing the polar group in the hydrophobic region of the bilayer is compensated by the gain in dispersion and anisotropic interactions with the ordered acyl chains, when a large

portion of the molecular body lies along them. This antiparallel orientation prevails when the centre of the C_{60} cage of **3** approaches the hydrophobic/hydrophilic interface (Z=14Å in Figure 4). We can also see in Figure 4 that, irrespective of depth, the orientational distribution is scarcely affected by rotation about the molecular long axis, which means that **3** approximately behaves as a uniaxial particle. The orientational behaviour predicted for **2** is similar to that just discussed for **3**, although with a weaker effect of electrostatics, due to the screening effect of the methyl substituent on the high charge on the nitrogen atom. As a consequence, a non-negligible contribution of the antiparallel orientation is found across the whole peak of the position distribution of **2**.

4.2.2 EPR experiments in oriented bicelles

Bicelles are made of long-chain (DMPC) and short-chain (DHPC) lipids and exist in a fluid liquid-crystalline phase at temperatures between 308K and 318K.[24] A schematic representation is reported in Figure 5: dilute bicellar systems are composed of planar bilayer disks, while concentrated systems (our case) are parallel perforated bilayer planes, where the planar region is constituted primarily by DMPC and the edge regions by DHPC.[33] Bicelles have a natural tendency to macroscopically orient in strong magnetic fields with the bilayer normal **N** perpendicular to the external magnetic field ($\mathbf{B_0}$). However, at the magnetic fields reached by a typical X-band EPR spectrometer (working field 0.35T, maximum field up to 1.2T), no macroscopic orientation is observed, unless the system is doped by trivalent lanthanide salts. Lanthanide ions are thought to bind to the polar heads of the lipids forming complexes that possess strong positive or negative magnetic anisotropies, which allow the bicelle-lanthanide system to orient with **N** parallel or perpendicular to $\mathbf{B_0}$ depending on the sign of the magnetic anisotropy. Bicelles are therefore a very versatile bilayer system that can achieve strong macroscopic orientation in fluid solutions at physiological temperatures.

The EPR spectrum of a nitroxide is given by three lines, whose distance is a function of the orientation of the paramagnetic probe with respect to the static magnetic field $\mathbf{B_0}$. In an ordered uniaxial sample this distance (hyperfine splitting) depends on the orientation of the C_∞ axis with respect to $\mathbf{B_0}$ and on the degree of order of the spin probe. The lineshape reflects the anisotropy of magnetic tensors and the

reorientational dynamics of the probe, which is responsible for the partial averaging of the magnetic tensors.

4.2.2.1 Nitroxide fullerene derivative

Several samples were prepared with different amounts of **3** loaded into DMPC/DHPC bicelles. At higher fullerene loading the EPR spectra exhibited strong line broadening, due to spin-spin exchange interactions, occurring when paramagnetic probes are at close range; however, three distinct broad lines could always be distinguished, which do not reach the single line limit expected for small fullerene nanoclusters. With lower loading (**3**:lipid molar ratio ~ 1:1500) no broadening could be detected, which is an indication that **3** is in large amount present as a monomer in the samples.

Three types of samples were prepared: isotropic (without any lanthanide ions); oriented with the bilayer normal **N** parallel to the magnetic field $\mathbf{B_0}$ by adding Tm^{3+}; oriented with **N** perpendicular to $\mathbf{B_0}$ by adding Dy^{3+}. For the two oriented samples two series of spectra were recorded: the first immediately after the orientation procedure (see Experimental Section) and the second after rotating the sample tube by 90° relative to $\mathbf{B_0}$. The EPR spectra are reported in Figure 5, where we can see that the lineshape depends on the orientation of the bicelles with respect to the magnetic field, which proves the anisotropic orientational distribution of **3** within the samples. The presence of a single spectral component showing a partial orientation, that follows the orientation of the bilayer, confirms that **3** is incorporated into the lipid bilayer.

The analysis of the spectra recorded under different conditions provides insights into the orientation of **3** in the bilayer. The observed hyperfine splitting ($2A_{exp}$) in the isotropic phase is equal to 3.19 mT (Figure 5E), it is smaller when $\mathbf{N}\|\mathbf{B_0}$ (2.66 mT, Figure 5A), and slightly larger when $\mathbf{N}\perp\mathbf{B_0}$ (3.25 mT, Figure 5C). These features are compatible with a preferred orientation in which **3** alignes the long molecular axis *z* (Figure 1), and therefore the N-O bond, parallel to the bilayer normal **N**. In fact, a similar anisotropic orientational distribution of **3** was found in the nematic liquid crystal phase of PAA, where the molecule preferentially alignes with its long axis parallel to the phase director **n**.[25]

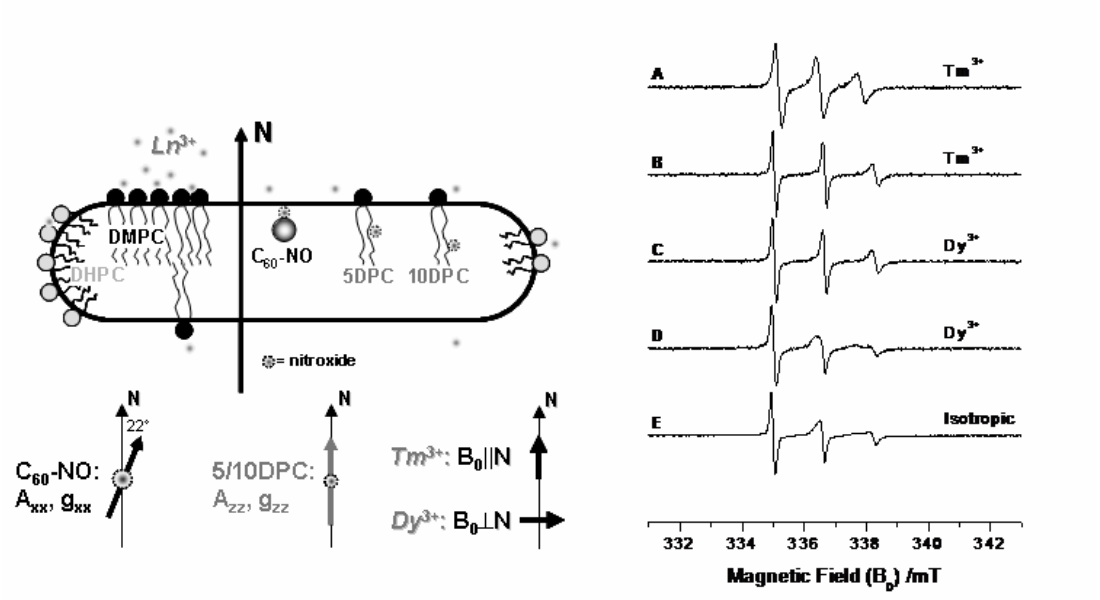

Figure 5: Left: cartoon of the membrano-mimetic system under study. On the bottom the principal axes systems of the magnetic tensors of the spin labels relative to the bilayer normal **N** are shown. Right: EPR spectra of **3** in bicelles at 308K, recorded under different conditions. All spectra are normalised to unit intensity for ease of comparison. Oriented bicelles doped with Tm^{3+}, $\mathbf{N}||\mathbf{B}_0$: (A) sample tube in the initial position (B) sample tube rotated by 90˚. Oriented bicelles doped with Dy^{3+}, $\mathbf{n}\perp\mathbf{B}_0$: (C) sample tube in the initial position, (D) sample tube rotated by 90˚. (E) Isotropic bicelles.

For the sake of comparison, Figure 6 shows the EPR spectrum of **3** in bicelles with $\mathbf{N}||\mathbf{B}_0$, together with that recorded in the nematic phase of the cyanobiphenyl mixture E7[34] at T=308K, which also orients with the director $\mathbf{n}||\mathbf{B}_0$.

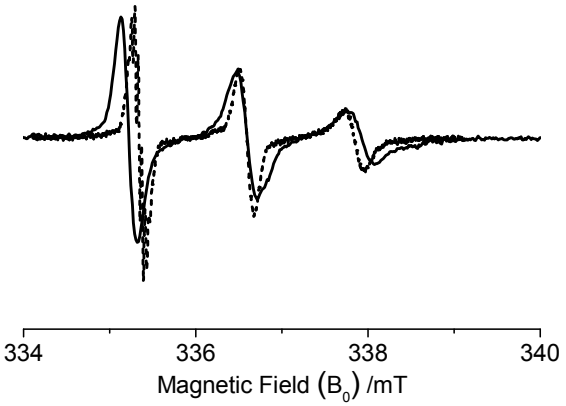

Figure 6: Spectra of **3** in bicelles with $\mathbf{N}||\mathbf{B}_0$ (solid line) and in the liquid crystal E7 at T=308K, with the director $\mathbf{n}||\mathbf{B}_0$ (dotted line).

The two spectra look similar, which indicates the analogy of the conditions experienced by the fullerene derivative in the two environments, yet some differences can be noticed. The nitrogen hyperfine splitting in the spectrum of **3** in E7 is a little smaller ($2A_{exp}$=2.46 mT) than that found in bicelles ($2A_{exp}$=2.66 mT),

which may be ascribed to a slightly higher molecular order in the nematic than in the lipid bilayer. Moreover, the spectrum recorded in bicelle exhibits some inhomogeneous broadening, whose origin cannot be easily identified: possible reasons could be the non perfect alignment of bicelles with respect to the magnetic field, as well as the nonuniformity of the bilayer interior, in particular the variation of molecular order (see Figure 4) and of magnetic interactions[35] with the insertion depth. The spectral lineshape in E7 could be accurately simulated using the methodology based on the stochastic Liouville equation in a uniaxial environment[36] (see Experimental Section). From this analysis an average orientational order parameter $S_{ii} = \langle(3\cos^2\beta - 1)/2\rangle = 0.46$ (where β is the angle between the long molecular axis z and the phase director **n**) and rotational diffusion coefficients $D_{\perp}^{R}=1.7\cdot10^{8}$ s^{-1} (perpendicular to the molecular z axis) and $D_{\parallel}^{R}=3.6\cdot10^{8}$ s^{-1} (parallel to the z axis) were obtained. The value $D^{R}=3.6\cdot10^{8}$ s^{-1} would be calculated from the Stokes-Einstein equation[37] for a sphere of radius equal to 5.4Å at the temperature T=300K in a medium of viscosity $\eta \sim 2.9\cdot10^{-3}$ Pa·s, which appears reasonable for the nematic phase of E7[38]. The available methodology for the simulation of EPR spectra cannot account for the more complex bilayer environment, so we cannot expect analogously accurate prediction for the spectra recorded in bicelles; however, from the similarity of the lineshapes shown in Figure 5 we can infer that the motional parameters determined for **3** in E7 should be close to those appropriate for the same solute in the lipid bilayer. Simple arguments provide further support to this conclusion. Since diffusion coefficients in the hydrocarbon core of the bilayer have been shown to be similar to those in alkane solvents[39], the values $D^{R}=3.2\cdot10^{8}$ s^{-1} and $D^{T}=1.2\cdot10^{-6}$ cm^2 s^{-1}, obtained from the Stokes-Einstein relations with the viscosity coefficient of hexadecane $\eta \sim 3.3\cdot10^{-3}$ Pa·s,[40] can be taken as reasonable for the rotational and translational diffusion coefficients, respectively, of **3** in bicelles. From the latter, in particular, a time $t = \langle r^2\rangle/2D^{T} \sim10^{-9}$ s for a root mean square displacement $\langle r^2\rangle^{-1/2} = 5$Å along the bilayer normal can be evaluated. These estimates rule out the possibility that the distribution of the spin probe spanning depths with different molecular order across the bilayer results in inhomogeneous line broadening. On the contrary, they suggest that, on the timescale of EPR experiments, the nitroxide probes a wide range of positions and orientations, and that the hyperfine

splittings in the spectral lineshapes reflects the average order experienced by the molecule in the bilayer. An average orientational order parameter equal to 0.23 was obtained for **3** from the calculated positional and orientational distributions shown in Figures 2 and 4, in line with the value which can be estimated from the hyperfine splitting in the spectrum reported in Figure 5A.

4.2.2.2 Diamagnetic fullerene derivatives in bicelles with spin labeled lipids

No direct EPR experiment could be performed on fullerenes **1** and **2**, which are diamagnetic, instead, they were investigated indirectly, through their effect on spin labeled lipids embedded in the bicelles. Two kinds of spin probes were used, either 5DPC or 10DPC, differing for the position of the paramagnetic doxyl moiety along the acyl chain of the labelled lipid (Figure 5). The spin label is covalently linked to the C_5 and C_{10} acyl chain site, respectively in the former and in the latter, residing in the ordered region near the hydrophobic/hydrophilic interface, and in the more disordered and fluid region close to the tail ends, respectively in the two cases. Figure 7 shows the spectra recorded for 5DPC and 10DPC with $\mathbf{N}||\mathbf{B_0}$; also those in isotropically oriented bilayers and with $\mathbf{N}\perp\mathbf{B_0}$ were recorded, but they are not reported here as they do not add anything to the discussion. The spectra of 5DPC and 10DPC in the absence of fullerenes, Figure 7A/D, are identical to those reported in the literature[24]; their differences reflect the different order and mobility of the two spin labels: that of 5DPC resides in a more ordered region and undergoes slower dynamics.

We can see that the overall lineshapes are not modified by incorporation of fullerenes (see for comparison the effects produced by cholesterol as a function of concentration in ref.[41]). Only for 5DPC some additional spectral features can be detected in the presence of **1** and **2**, which are highlighted by arrows in Figure 8B/C. Exactly the same effects are found for **1** and **2**, in agreement with our prediction of very similar behaviour for C_{60} and its apolar monoadduct. Also the emergence of some effect at the level of the acyl chain C_5 position, but not at that of C_{10}, is in agreement with our prediction that fullerenes would be localized in the region below the hydrophobic/hydrophilic interface.

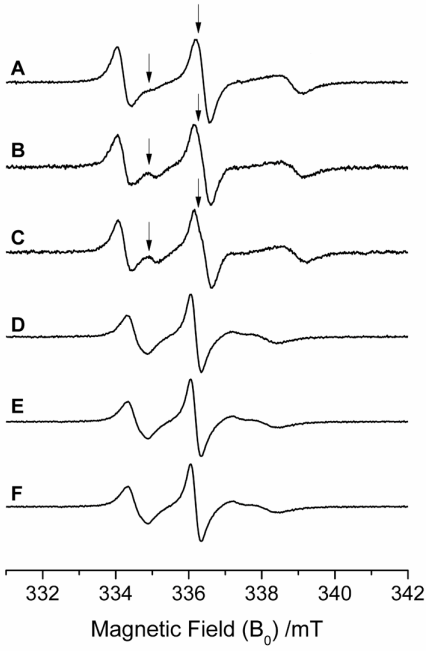

Figure 7: EPR spectra of 5DPC (A,B,C) and 10DPC (D,E,F) in bicelles oriented with $\mathbf{N}||\mathbf{B_0}$. (A,D) Pure bicelles; (B,E) bicelles incorporating **1;** (C,F) incorporating **2**.

4.2.3 Bilayer permeability

The membrane permeability coefficient P of a solute diffusing under the concentration gradient Δc, intended as the difference in bulk water concentration at the two sides of the lipid bilayer, is defined as the ratio $P = -J/\Delta c$, where J is the flux of solute. According to the inhomogeneous solubility-diffusion model the permeability coefficient across a lipid bilayer can be calculated as:[42]

$$P = \left(\int_{-L}^{L} \frac{\exp\left(u(Z)/k_B T\right)}{D^T(Z)} \, \mathrm{d}Z \right)^{-1} \tag{2}$$

where $u(Z)$ is the free energy of transfer from water to bilayer (i.e. u=0 in bulk water) and D^T is the translational diffusion coefficient of the permeating species in the direction of the bilayer normal; k_B is the Boltzmann constant and T is the temperature. The integration limits, L and –L (the coordinate Z=0 corresponds to the bilayer midplane, and a symmetrical bilayer is considered), are taken at the water/bilayer interfaces, so that the integration is performed over the entire bilayer thickness. The function within the integral represents the *local resistance*: high diffusion coefficient and/or high affinity for the bilayer (i.e. low u values) yield low resistance, thus high permeability.

Figure 8 shows the profile of $\exp(u(Z)/k_BT)$ across the bilayer, calculated for **1**. We can see that the exponential is significantly different from zero only when most of the molecule resides out of the lipid bilayer. Then, since the diffusion coefficient is expected to have a much weaker position dependence than the numerator in eq.2,[39,43] an approximate expression for the permeability coefficient of C_{60} can be written, $P \approx D_w^T \left(\int_{-L}^{L} \exp\left[u(Z)/RT\right] \mathrm{d}Z \right)^{-1}$, where only the diffusion coefficient of **1** in water, D_w^T, appears, as it is taken to describe the transport properties of the region of interest (Z>25Å) in Figure 8. Taking $\eta = 10^{-3}$ Pa·s for the viscosity coefficient of water[40], $D_w^T \sim 4.1 \cdot 10^{-6}$ cm^2 s^{-1} is obtained from the Stokes-Einstein equation for a sphere of radius equal to 5.4Å at the temperature T=300K, in line with the results of different MD simulations (all given in unit of cm^2 s^{-1} and denoted by *w*; diffusion coefficients calculated for C_{60} in membranes from MD simulations are also reported for comparison and denoted by *m*): $2.7 \cdot 10^{-6}$ (*m*)[12], $\sim 1 \cdot 10^{-5}$ (*w*), $\sim 1.5 \cdot 10^{-7}$ (*m*)[13]; $\sim 3 \cdot 10^{-6}$ (*w*), $\sim 1 \cdot 10^{-6}$ (*m*)[14]; $1.6 \cdot 10^{-6}$ (*w*), $1 \cdot 10^{-8}$-$1 \cdot 10^{-7}$ (*m*)[17].

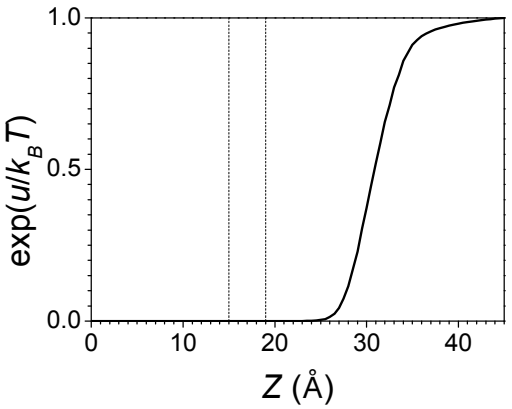

Figure 8: Position dependence of the exponential term appearing in eq.2, calculated for **1** as a function of the position of its centre across the lipid bilayer. The coordinate *Z*=0 corresponds to the bilayer midplane. The vertical lines indicate the average position of carbonyl and phosphate groups. Given the symmetry of the system, only one half of the bilayer is shown.

Taking *L*=42Å, an integrated area under the profile reported in Figure 8, $\int_{-L}^{L} \exp\left(u(Z)/k_BT\right) \mathrm{d}Z = 2\int_{0}^{L} \exp\left(u(Z)/k_BT\right) \mathrm{d}Z \sim 0.21 \cdot 10^{-6}$ cm is obtained. Thus a permeability coefficient $P \sim 19$ cm s^{-1} is estimated for C_{60} from our calculations. The consideration reported here for **1** could be extended to the monoadducts **2** and **3**, since profiles very similar to that reported in Figure 8 were obtained for the two

derivatives, and also their translational diffusion coefficients, calculated by a molecular-surface-based model accounting for their structural features[44], resulted close to the value estimated for C_{60}, with negligible anisotropy (lower than 10%).

It is worth comparing our predictions with the data reported in the literature. A permeability coefficient $P \sim 100$ cm s^{-1} was obtained for C_{60} in DMPC from all-atom MD simulations[13], whereas a significantly lower estimate, $P = 0.06$ cm s^{-1}, was given from MD simulations in DOPC with a coarse-grained force-field[14]. Also, $P = 330$ cm s^{-1} was reported from all-atom MD of C_{60} in DMPC containing cholesterol[17], in a work where the strong dependence of the result on the choice of the integration limits in eq.2 was highlighted: an increase of P by orders of magnitude was evidenced for a few Ångstrom decrease of L. In our calculations the ambiguity in the definition of the bilayer boundaries, especially critical in the case of hydrophobic solutes, was removed, on the basis of the analysis of the dependence on L of the integral $\int_0^L \exp\left(u(Z)/k_BT\right)\mathrm{d}Z$, approaching linearity as L shifts towards bulk water. The variety of results reported in the literature makes it difficult to establish the reliability of estimated permeability coefficients. In any case a major problem, usually ignored in calculations, derives from the fact that the permeation of molecular fullerene across lipid bilayers is likely to be a more complex process, involving the dissolution of the aggregates formed in water. This seems to be a general problem dealing with hydrophobic solutes, which spontaneously penetrate the lipid bilayer, without appreciable free energy barrier. In these cases, according to the solubility-diffusion model, at least in its original form which is generally used in the literature, permeability would be determined by the partition and diffusion properties of molecular solutes in water. Actually, however, aggregation is very likely to take place and hydrophobic species are expected to dissolve in water as single molecules to a very low extent. Hence, a more realistic description of the permeation process should take into account the thermodynamics of aggregation and the kinetics of breaking and formation of aggregates at the water/bilayer interfaces. For these reasons, we think that permeability predictions for fullerenes must be taken with caution; they may be used to compare trends for different solutes examined under the same conditions, but they cannot be expected to give realistic numerical values.

4.3 Conclusions

Combining a recent implicit membrane model, for the description of solute partitioning into lipid bilayers, and EPR spectroscopy, we characterized the single molecule behaviour of pristine fullerene (**1**) and two of fulleropyrrolidine derivatives (**2** and **3**) within lipid bilayers, in terms of confinement, order and mobility.

The theoretical prediction is that the presence of a substituent, even strongly polar, does not substantially affect the fullerene distribution in the bilayer. The distribution profiles calculated for the three derivatives are similar; in all cases high affinity for the bilayer interior is predicted, whose main responsibility can be ascribed to the highly polarizable C_{60} cage. Also diffusion properties are predicted to be very similar for the three fullerene derivatives. These results, obtained by atomistic modelling of fullerene derivatives with a limited degree of functionalization, are in general agreement with recent coarse-grained MD simulations of C_{60}, which showed that surface derivatization may have a profound effect on the interaction of fullerenes with a lipid bilayer, but to this purpose at least 50% of the surface must assume a polar character[15].

Actually the EPR spectra of **3** show that at low concentration it penetrates the bilayer as a single molecule, while no direct assessment could be made on the aggregation state of **1** and **2** in bicelle.

In contrast to the simple picture of the bilayer as an oil slab, the distribution of fullerenes is predicted to be strongly nonuniform: for all derivatives the centre of the C_{60} cage is confined in a zone a few Ångstrom wide, just below the interface between the hydrophobic tail region and the hydrophilic headgroup region of the bilayer. This result is in line with the experimental result that the presence of **1** and **2** only affects the EPR lineshape of nitroxide spin labels linked to acyl chain carbons near the hydrophobic/hydrophilic interface. Confinement of bare C_{60} in a restricted region was also found in MD simulations.[12-18] Our calculations indicate that this as a general behaviour, scarcely affected by the presence and the nature of substituents.

On the other hand, substituents, breaking the symmetry of the C_{60} core and introducing charge polarity in the molecule, induce some orientational preferences of solutes with respect to the bilayer normal. A strong orientational-positional coupling is predicted both for **2** and **3**, as a result of their interactions with the highly

nonuniform bilayer environment, which makes the orientational behaviour of these molecules in bicelles more complex than in nematic liquid crystals. This difference is confirmed by comparison of the EPR spectra of **3** in the two environments.
An estimate was provided of the membrane permeability coefficient of C_{60}, based on the traditional heterogeneous solubility-diffusion model, although stressing some critical aspect of this approach when applied to hydrophobic solutes.

Abbreviations

AA: all-atom
CG: coarse-grained
DHPC: 1,2-dihexanoyl-sn-glycero-3-phosphocholine
DMPC: 1,2-dimyristoyl-sn-glycero-3-phosphocholine
DOPC: 1,2-dioleoyl-sn-glycero-3-phosphocholine
DPPC: 1,2-dipalmitoyl-sn-glycero-3-phosphocholine
EPR: Electron Paramagnetic Resonance
MD: Molecular Dynamics
PAA: 4-4'-azoxyanisole
5DPC: 1-palmitoyl-2-stearoyl-(5-doxyl)-sn-glycero-3-phosphocholine
10DPC: 1-palmitoyl-2-stearoyl-(10-doxyl)-sn-glycero-3-phosphocholine

4.4 References

[1] Jensen, A.W.; Wilson, S.R.; Schuster, D.I. *Bioorg. Med. Chem.* **1996**, *4*, 767-779.
[2] Bosi, S.; Da Ros, T.; Spalluto, G.; Prato, M. *Eur. J. Med. Chem.* **2003**, *38*, 913-923.
[3] Johnston, H.J.; Hutchison, G.R.; Christensen, F.M.; Aschberger, K.; Stone, V. *Toxicol.. Sci.* **2010**, *114*, 162-182.
[4] Colvin, V.L. *Nature Biotechnol.* **2003**, *21*, 1166-1170.
[5] Sayes, C.M.; Gobin, A.M.; Ausman, K.D.; Mendez, J.; West, J.L.; Colvin, V.L. *Biomaterials* **2005**, *26*, 7587-7595.

[6] Sayes, C.M.; Fortner, J.D.; Guo, W.; Lyon, D.; Boyd, A.M.; Ausman, K.D.; Tao, Y.J.; Sitharaman, B.; Wilson, L.J.; Hughes, J.B.; West, J.L.; Colvin, V.L. *Nano Lett.* **2004**, *4*, 1881-1887.

[7] Monticelli, L.; Salonen, E.; Ke, P.C.; Vattulainen, I. *Soft Matter* **2009**, *5*, 4433-4445.

[8] Ke, P.C.; Qiao, R. *J. Phys.: Cond. Matt.* **2007**, *19*, 373101:1-25.

[9] Hungherbühler, H.; Guldi, D.M.; Asmus, K.-D. *J. Am. Chem. Soc.* **1993**, *115*, 3386-3387.

[10] Bensasson, R.V.; Bienvenue, E.; Dellinger, M.; Leach, S.; Seta, P. *J. Phys. Chem.* **1994**, *98*, 3492-3500.

[11] Williams, R.M.; Crielaard, W.; Hellingwerf, K.J.; Verhoeven, J.W. *Recl. Trav. Chim. Pays-Bas* **1996**, *115*, 72-76.

[12] Qiao, R.; Roberts, A.P.; Mount, A.S.; Klaine, S.J.; Ke, P.C. *Nanolett*. **2007**, *7*, 614-619.

[13] Bedrov, D.; Smith, G.D.; Davande, H.; Li, L.W. *J. Phys. Chem. B* **2008**, *112*, 2078-2084.

[14] Wong-Ekkabut, J.; Baoukina, S.; Triampo, W.; Tang, I.M.; Tieleman, D.P.; Monticelli, L. *Nat. Nanotech*. **2008**, *3*, 363-368.

[15] D'Rozario, R.S.G.; Wee, C.L.; Wallace, E.J.; Sansom, M.S.P. *Nanotechnol*. **2009**, *20*, 115102:1-7.

[16] Redmill, P.S.; McCabe, C. *J. Phys. Chem. B* **2010**, *114*, 9165-9172.

[17] Fiedler, S.L.; Violi, A. *Biophys. J.* **2010**, *99*, 144-152.

[18] DeVane, R.; Jusufi, A.; Shinoda, W.; Chiu, C.; Nielsen, S.O.; Moore, P.B.; Klein, M.L. *J. Phys. Chem. B* **2010**, *114*, 16364-16372.

[19] Maciel, C.; Fileti, E.E.; Rivelino, R. *J. Phys. Chem. B* **2009**, *113*, 7045-7048.

[20] Chen, J.; Brooks, C.L.; Khandogin, *J. Curr. Opin. Struct. Biol.* **2008**, *18*, 140-148.

[21] Grossfield, A. *Curr. Top. Membr.* **2008**, *60*, 131-157.

[22] Parisio, G.; Ferrarini, A. *J. Chem. Theory Comput.* **2010**, *6* , 2267-2280.

[23] Hemminga, M.A.; Berliner, L. ESR Spectroscopy in Membrane Biophysics; Springer: New York, 2007.

[24] Cardon, T.B.; Tiburu, E.K.; Lorigan, G.A. *J. Magn. Res.* **2003**, *161*, 77-90.

[25] Mazzoni, M.; Franco, L.; Ferrarini, A.; Corvaja, C.; Zordan, G.; Scorrano, G.; Maggini, M. *Liq. Cryst.* **2002**, *29*, 203-208.

[26] Deschenaux, R.; Donnio, B.; Guillon, D. *N. J. Chem.* **2007**, *31*, 1064-1073.

[27] Cantor, R. S. J. Phys. Chem. 1997, *101*, 1723-1725.

[28] Gallicchio, E.; Levy, R.M. *J. Comp. Chem.* **2003**, *25*, 479-499.

[29] Tanizaki, S.; Feig, M. J. *Chem. Phys.* **2005**, *122*, 124706:1-13.

[30] Seelig, J. *Q. Rev. Biophys.* **1977**, *10*, 353-418.

[31] Ferrarini, A.; Moro, G. J.; Nordio, P. L.; Luckhurst, G. R. *Mol. Phys.* **1992**, *77*, 1-15.

[32] Nagle, J.F.; Tristram-Nagle, S. *Biochim. Biophys. Acta* **2000**, *1469*, 159-195.

[33] Nieh, M.-P.; Glinka, C.J.; Krueger, S. *Langmuir* **2001**, *17*, 2629-2638.

[34] Raynes, P.; Tough, R.J. A.; Davies, K.A. *Mol. Cryst. Liq. Cryst.* **1979**, *56*, 63-68.

[35] Marsh, D. *J. Magn. Res.* **2002**, *157*, 114-118.

[36] Schneider, D.J.; Freed, J. H. In Biological Magnetic Resonance, Vol.8; Berliner, L.J.; Reuben, J.; Eds.: Plenum Press, New York, 1989. Budil, D.E., S. Lee, Saxena, S.; Freed, H.J. *J. Magn. Reson.* **1996,** *120*, 155-189.

[37] Tanford, C. Physical Chemistry of Macromolecules; John Wiley & Sons, Inc.: New York, 1961.

[38] Bosco, A.; Jongejan, M.G.M.; Eelkema, R.; Katsonis, N.; Lacaze, E.; Ferrarini, A.; Feringa, B.L. *J. Am. Chem. Soc.* **2008**, *130*, 14615-14624.

[39] Xiang, T.-X.; Anderson, B.D. *Adv. Drug Deliv. Rev.* **2006**, *58*, 1357-1378.

[40] CRC Handbook of Chemistry and Physics, 56th ed.; CRC Press: Cleveland, 1975.

[41] Dave, P.C.; Nusair, N.A.; Inbaraj, J.J.; Lorigan, G.A. *Biochim. Biophys. Acta* **2005**, *1714*, 141-151.

[42] Diamond, J.M.; Katz, Y. *J. Membr. Biol.* **1974**, *17*, 121-154; Diamond, J.M.; Szabo, G.; Katz, Y. *J. Membr. Biol.* **1974**, *17*, 148-152.

[43] Orsi, M.; Essex, J.W. *Soft Matter* **2010**, *6*, 3797-3808.

[44] Aragon, S. *J. Comput. Chem.* **2004**, *25*, 1191-1205.

Chapter 5

Effects of size and shape on solute distribution in lipid bilayers

5.1 Introduction

In addition to the quite obvious effect of polarity, molecular size and shape are also expected to affect the behaviour of a solute within a lipid bilayer. Due to the ordering of the acyl chains the interactions of sphere-like and rod-like solutes with their environment will be reasonably different in the interior of the bilayer, as well as the accomodation of large and small solutes will be favoured or unfavoured by the chain packing, due to short-range attractive and repulsive interactions, to a different extent at different depths. Reversed-phase chromatography and permeability experiments revealed the selectivity of stationary phases and lipid bilayers, both showing chain ordering and depth-dependent molecular organization, for the size and shape of partitioning or permeating molecules. An interpretation for these results was provided by the model developed by Xiang and Anderson, where the effect of the size and shape of solutes on their partitioning in the bilayer interphase was described through the lateral pressure profile across the chain region.[1]

According to the implicit membrane model for solute partitioning we presented in ref.[2] (Chapter 2), the effect of the size and shape of a solute on its coupled positional-orientational-conformational distribution is modulated by lateral pressure as well as density and order profiles across the bilayer. The computational methodology we proposed for the numerical evaluation of all the contributions to the mean field potential

$$U = U_{cav} + U_{el} + U_{disp} + U_{ord} \tag{1}$$

was based on the computation of the solute molecular surface; actually, however, the sensitivity to the size and shape of the solute can reasonably be expected to be different for each term in eq.1. While electrostatic interactions can be assumed to be nearly independent from the solute size and shape, as long as molecular dimensions and conformational changes do not affect the screening of charged groups from the dielectric, dispersion interactions approximately scale with the molecular surface area. A major effect of solute structure is introduced by the cavity and order contributions, which is mainly reflected by the orientational and conformational distributions of apolar molecules.

In order to assess how the contributions in eq.1 determine different distributions for solutes with different size and shape, we applied our partition model to the four compounds in Figure 1.

We considered highly symmetrical and rigid aromatic hydrocarbons, whose size and shape do not vary upon conformational change, and whose behaviour is presumably unaffected by electrostatic interactions with the environment due to the absence of polar groups. We chose to compare the bulky C_{60} nanoparticle with the planar coronene, pyrene and DPH membrane probes. This choice allowed us to explore changes in the distribution of solutes with decreasing symmetry and dimensions, going from spherical to rod-like particles. Moreover, the comparison of our results with the data available from the literature provided a further test of the reliability of our model.

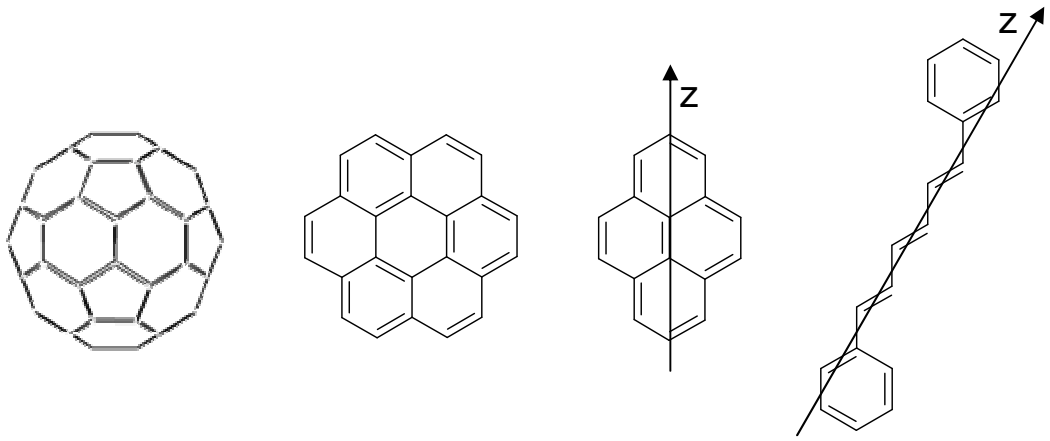

Figure 1: (From left to right) Molecular structure of C_{60}, coronene, pyrene and DPH. The *z* axis of the molecular reference frame is shown for pyrene and DPH. For all planar molecules the *y* axis of the molecular reference frame was taken perpendicular to the molecular plane.

The discussion of the results of our calculations on C_{60}, in light of those reported in the literature from MD simulations, was tackled in Chapter 3 even if with some difficulty, due to the variability and poor agreement between data obtained from different MD simulations. On the other hand a large amount of experimental data can be found in the literature on the distribution of the membrane fluorescent probe DPH in lipid bilayers. The widespread use of DPH as a probe of membrane polarity, order and fluidity has promoted the investigation of its membrane partitioning, with particular interest for its favourite location and orientation within the bilayer.[3] Time resolved fluorescence decay and fluorescence anisotropy of DPH report on the

micro-environment where the probe resides within the membrane. The response of the probe reflects membrane micro-heterogeneity, orientational order and dynamics, and is sensitive to the lipid composition and phase of the bilayer or of coexisting domains, to temperature and pressure conditions, to the presence of cosolutes. Hence, for the correct interpretation of its spectroscopic behaviour, the detailed knowledge of the distribution of the probe across the bilayer, and of how it changes under the influence of so many factors, is required. Thanks to their unusually long fluorescence lifetime, pyrene and coronene are also used as probes of lipid dynamics in membranes, but not so many studies have appeared concerning their distribution in lipid bilayers.

According to simple considerations on its apolar nature and elongated shape, DPH may be expected to reside in the most inner and hydrophobic part of a lipid bilayer, aligned with the ordered acyl chains.[4] However, both steady-state experiments on oriented planar liquid-crystalline bilayers and time-resolved fluorescence anisotropy studies suggested a bimodal orientational distribution of DPH in lipid bilayers.[5,6] Two spectroscopic contributions were recognized, which could be attributed to probe molecules differently oriented with respect to the bilayer normal, and the coexistence of two populations, one constituted by the probe molecules aligned parallel to the bilayer normal, the other constituted by the probe molecules lying perpendicular to the bilayer normal, was hypothesised. A bimodal coupled positional-orientational distribution of DPH was suggested by neutron diffraction experiments[7] and MCD simulations[8,9], which, however, supported different descriptions of the two populations. According to the two-population model, which was proposed on the basis of the results of MCD simulations, part of the DPH molecules would lie parallel to the bilayer surface in the centre of the bilayer, part would be intercalated parallel to the bilayer normal between the hydrocarbon chains closer to the polar headgroups.[8,9] The neutron diffraction study by Pebay-Peroula *et al.* revealed different distributions of DPH in the gel and liquid crystal phase of a DPPC bilayer. A population of probes lying parallel to the bilayer surface, just below the lipid headgroups, was found both above and below the bilayer transition temperature, while the orientation of the probes residing at the bilayer centre seemed to change from parallel to the acyl chains in the gel phase to perpendicular to them in the liquid crystal phase.[7] The bimodal positional distribution of DPH between the hydrophobic

and hydrophilic regions of the membrane was also proposed as an explanation of the two-componental fluorescence decay observed for DPH in soybean PC.[10] In contrast with the accepted view of a bimodal, although not fully characterized, distribution of DPH in lipid bilayers, according to the results of a recent MD simulation of the probe in a liquid-crystalline DPPC bilayer, DPH was stated to reside in the hydrophobic region of the bilayer, with a one-peak distribution at an average distance of 7.5Å from the bilayer centre.[11] Almost the same average distance of the probe from the bilayer midplane, 7.8Å, had been obtained from the parallax analysis of fluorescence quenching data on DPH in a DOPC bilayer.[12] Such an excellent agreement, however, should not sound so meaningful, given the structural differences between bilayers of 16-carbon saturated chain (DPPC) and 18-carbon unsaturated chain (DOPC) lipids. Moreover, since no information on the shape of the distribution profile of the probe around its average location can be gained from the quenching analysis, this can provide only little support to the results of the MD simulation.

We report here the distributions we calculated for the compounds in Figure 1 in a model saturated liquid-crystalline lipid bilayer. We found DPH to be characterized, with respect to the other solutes we considered, by a bimodal distribution, and could ascribe the distinctive behaviour of this probe to its elongated shape.

5.2 Results and Discussion

Calculations were performed starting from molecular properties of the solutes and phase properties of a DPPC bilayer at a temperature T=323K which were parameterized as reported in ref.[2] (Chapter 2). The position Z and orientation Ω of the molecules in the bilayer were defined, with respect to the molecular frames in Figure 1, as shown in Figure 1 of Chapter 2.

The water-bilayer transfer free energy profiles $u(Z)$ and the corresponding position-dependent distribution functions $P_{\Omega}(Z)$ calculated for the compounds in Figure 1 show common features (Figure 2). High affinity for the membrane environment is predicted for all these hydrophobic solutes with respect to bulk water. However, far from being uniform across the whole hydrophobic region inside the bilayer, or from decreasing monotonically with increasing depth towards the lowest-dielectric bilayer

core, the free energy profiles of all the compounds reach a minimum more than 10Å above the bilayer centre (Figure 2 left). The lowest energies are found for C_{60}, whose dispersion interactions with the surrounding are mediated by the most extended molecular surface. Correspondingly all the solutes are mainly localized in a well defined region just below the hydrophobic/hydrophilic interface, which can be traced at the average position of the carbonyl groups of the lipid molecules (Figure 2 right). However, different distribution widths are found, reflecting the different selectivity of the solutes for this specific micro-environment within the bilayer. The narrowest distribution is found for the bulky C_{60} molecule. The distribution peaks of coronene and pyrene are progressively broader. Finally, an even broader distribution with the appearance of a second peak is observed for DPH.

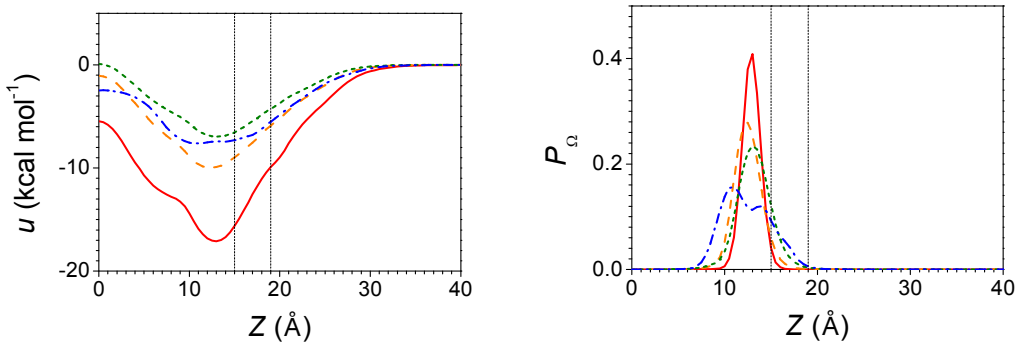

Figure 2: Transfer free energy $u(Z)$ (left) and position distribution function $P_\Omega(Z)$ (right) calculated for C_{60} (solid line), coronene (dashed line), pyrene (dotted line) and DPH (dash-dotted line) as a function of the position of the molecular centre of mass across the lipid bilayer. The coordinate Z=0 corresponds to the bilayer midplane. The vertical lines indicate the average position of carbonyl and phosphate groups. Given the symmetry of the system, only one half of the bilayer is shown.

A relation between the molecular shape of a solute and the shape of its distribution profile seems to exist, which can be rationalized by investigating the effect of each contribution to the mean field potential in eq.1. Figure 3 shows how the free energy and distribution profiles calculated for DPH would have changed if each one of the terms on the right-hand side of eq.1, only one at a time, had not been taken into account. As can be seen, while dispersive interactions are the main responsible for the high affinity of the probe for the membrane environment (Figure 3 left), the shape of the distribution profile is heavily affected by the order contribution to the mean field potential (Figure 3 right). In the absence of anisotropic interactions with the acyl chains, DPH would be found closer to the headgroups and its distribution

would be described by a single narrow peak. Analogous calculations were performed for pyrene, coronene and C_{60} (results not shown).

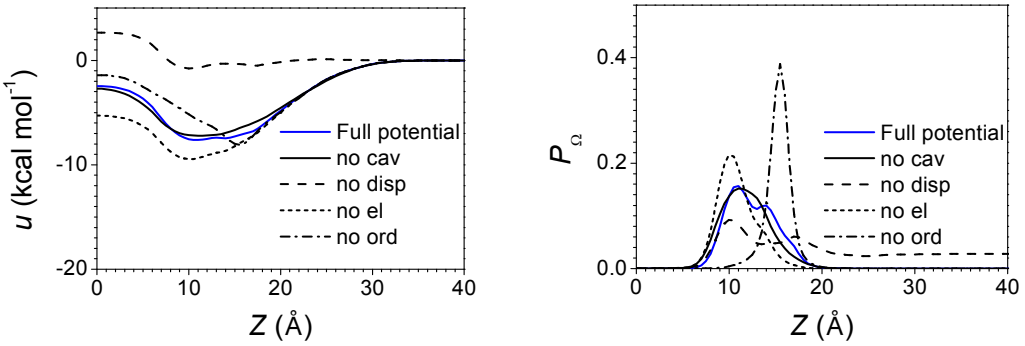

Figure 3: Transfer free energy $u(Z)$ (left) and position distribution function $P_\Omega(Z)$ (right) calculated for DPH, as a function of the position of the molecular centre of mass across the lipid bilayer, by removing one of the contributions in eq.1 at a time. The coordinate Z=0 corresponds to the bilayer midplane. Given the symmetry of the system, only one half of the bilayer is shown.

Overall, a double effect of the order contribution on the distribution profile could be seen: i) a similar shift of the peak position towards the interior of the bilayer was found for all solutes, which was ascribed to the energetically favourable anisotropic interactions of the solutes with the acyl chains in the most ordered region of the bilayer; ii) a significant broadening of the distribution was observed for all anisotropic solutes, more evident for DPH than for pyrene and coronene, which was ascribed due the ordering effect of the aligned acyl chains on the orientational distribution of the solutes. The opposite orienting effects of the cavity and order contributions, which are strong at and in the close vicinity of the hydrophobic/hydrophilic interface, were identified as the responsible of the presence of two distinct contributions to the distribution of DPH. The analysis of the orientational distributions in Figures 4 and 5 will help understanding these last considerations.

In correspondence of their distribution maximum (Figure 2 right), coronene and pyrene were found to preferentially align their molecular plane perpendicular to the bilayer plane ($\gamma = 0, \pm\pi$), the long molecular axis of pyrene being preferentially aligned to the bilayer normal ($\beta = 0, \pi$) (Figure 4). In this orientation the anisotropic interactions between the planar molecules and the ordered acyl chains are optimized and bring an energetically favourable contribution to the partition of the solutes in the hydrophobic region of the bilayer. Slight changes of position of the solutes in this orientation within the ordered region of the bilayer, causes only minor variations in

their free energies. The action of the orienting potential of the acyl chains is amplified on the rod shaped DPH probe, while it is much less effective on the spherical C_{60} particle. The selectivity of coronene and pyrene for a specific micro-environment is thus reduced with respect to C_{60} and their distribution is broader. In the absence of anisotropic interactions with the acyl chains both the planar molecules would lie parallel to the bilayer plane at the hydrophobic/hydrophilic interface, where the deep negative well in the lateral pressure profile highly favours the process of solute cavity formation. The reduced thickness of the region occupied by the solutes in this orientation, and the modulation of the lateral pressure profile, would enhance selectivity and make distributions narrower (results not shown).

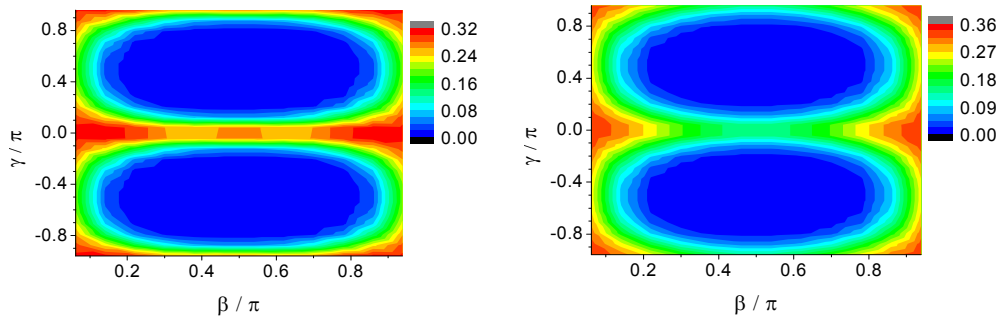

Figure 4: Orientational distribution $P(\Omega,Z)$ calculated in the preferred position Z=12.5Å for coronene (left) and Z=13Å for pyrene (right). β is the angle between the long molecular axis, z, and the bilayer normal. The γ angle refers to molecular rotation around z.

The calculated orientational distributions of DPH in correspondence of the two maxima in its distribution (Figure 2 right) are represented in Figure 5. The orienting potential generated by the ordered acyl chains, dominating in the hydrophobic region (in correspondence of the distribution maximum at Z=11Å), induces the alignment of the rod-like DPH molecule with its long axis parallel to the bilayer normal (β = 0, π in Figure 5 left). The orienting effect of the cavity contribution, dominating at the hydrophobic/hydrophilic interface (in correspondence of the distribution maximum at Z=14Å), favours the perpendicular orientation of DPH (β = π/2 in Figure 5 right), with the aromatic plane of the molecule lying preferentially parallel to the bilayer plane (γ = 0, ±π). Together, the distribution profile in Figure 2 and the orientational distributions in Figure 5 describe a bimodal coupled positional-orientational distribution of DPH in the lipid bilayer, where two distinct contributions can be recognised. One of these is due to probes aligned parallel to the bilayer normal,

which are located deeper in the hydrophobic region of the bilayer, the other comes from probe molecules lying parallel to the bilayer surface, located closer to the headgroups region.

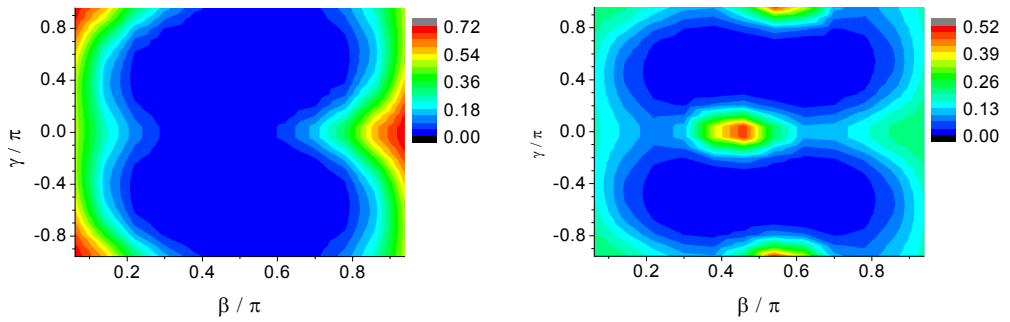

Figure 5: Orientational distribution $P(\Omega,Z)$ calculated for DPH in correspondence of the two distribution maxima at Z=11Å (left) and Z=14Å (right). β is the angle between the long molecular axis, z, and the bilayer normal. The γ angle refers to molecular rotation around z.

However, although strong support to the hypothesis of a bimodal distribution of DPH in lipid bilayers is provided from experimental data, poor agreement is found with what is reported in the literature concerning the details of this distribution. In fact, despite minor discrepancies, the partitioning of DPH in the bilayer centre was suggested both by neutron diffraction[7] and MCD[8,9] studies. According to the two-population model, in particular, excluded volume effects would be responsible of the distribution of the probe in the loosely packed core of the bilayer. If this is the case, a more rigorous treatment of the density fluctuations producing molecular-scaled cavities in the bilayer, which is typical of the SPT approach[13] but is not included in our model, could probably take into such microscopic effects.

A preferred position far from the middle of the bilayer was suggested for pyrene on the basis of the results of MD simulations[14,15], where the probe was found to be located in the upper acyl chain region, under the headgroups, preferentially oriented with its long axis parallel to the bilayer normal. This, in agreement with ^{2}H-NMR and fluorescence quenching experiments[14], confirms our results. The average order parameters $S_{ii} = \langle(3\cos^2\theta_i - 1)/2\rangle$, where θ_i is the angle between the ith molecular axis and the bilayer normal, describing the average orientation of the pyrene molecule in the bilayer phase, were calculated, and are reported in Table 1 with those obtained in refs.[14,15]. The good agreement found with literature data provides further support to our results.

	This work DPPC 323K	^{2}H-NMR[14] POPC 300K	MD[14] POPC 300K	MD[15] DPPC 325K
S_{xx}	0.05		0.07	
S_{yy}	-0.36	-0.42	-0.40	
S_{zz}	0.31		0.33	0.27
S_{zz}-S_{xx}	0.26	0.25	0.26	

5.3 Conclusions

Our analysis of the membrane distributions of the solutes in Figure 1 highlights the effects of apolar interactions, modulated by solute size and shape and by the structural properties of the lipid bilayer. As expected dispersion interactions drive the partitioning of hydrophobic solutes in membrane. There, however, the lipid density gradient confines them within the well defined region where the lipid chains are most tightly packed. Non obvious effects are due to the cavity and order contributions to the mean field potential we have defined[2] (Chapter 2), which represent the most innovative aspects of our implicit membrane model with respect to traditional approaches. The inclusion of the depth-dependent ordering of lipid tails and of the highly inhomogeneous lateral pressure profile in our representation of the lipid bilayer, has been shown here to produce important modifications in the predicted positional and orientational distribution of solutes, the most striking example being that of the elongated DPH molecule. In this case, indeed, the subtle interplay of pressure and order effects results in a bimodal distribution of the probe, i.e. in the existence of two favourite configurations differing for both probe position and orientation. This uncommon feature of the membrane distribution of DPH is also suggested by experimental findings, while no support to this picture has been provided by MD simulations. More than a mere qualitative agreement with literature data is found in the case of pyrene, whose average order parameters in lipid bilayers are well reproduced by our calculations.

Abbreviations

DOPC: 1,2-dioleoyl-sn-glycero-3-phosphocholine

DPH: 1,6-diphenyl-1,3,5-hexatriene

DPPC: 1,2-dipalmitoyl-sn-glycero-3-phosphocholine

NMR: Nuclear Magnetic Resonance

MD: Molecular Dynamics

MCD: Monte Carlo Dynamics

POPC: 1-palmitoyl-2-oleoyl-sn-glycero-3-phosphocholine

SPT: Scaled Particle Theory

5.4 References

[1] Xiang, T.-X.; Anderson, B.D. *Biophys. J.* **1994**, *66*, 561-573.

[2] Parisio, G.; Ferrarini, A. *J. Chem. Theory Comput.* **2010**, *6* , 2267-2280.

[3] Alakoskela, J.-M. Interactions in lipid-water interface assessed by fluorescence spectroscopy, Academic dissertation, Helsinki 2005.

[4] Andrich, M.P.; Vanderkooi, J.M. *Biochemistry* **1976**, *15*, 1257-1261.

[5] Ameloot, M.; Hendrickx, H.; Herreman, W.; Pottel, H.; van Cauwelaert, F.; van der Meer, W. *Biophys. J.* **1984**, *46*, 525-539.

[6] Straume, M.; Litman, B.J. *Biochemistry* **1987**, *26*, 5113-5120.

[7] Pebay-Peroula, E.; Dufourc, E.J.; Szabo, A.G. *Biophys. Chem.* **1994**, *53*, 45-46.

[8] Van der Heide, U.A.; van Ginkel, G.; Levine, Y.K. *Chem. Phys. Lett.* **1996**, *253*, 118-122.

[9] Van Zandvoort, M.A.M.J.; Gerritsen, H.C.; Levine, Y.K. *J. Phys. Chem. B* **1997**, *101*, 4142-4148.

[10] Konopasek, I.; Kvasnicka, P.; Herman, P.; Linnertz, H.; Obsil, T.; Vecer, J.; Svobodova, J.; Strzalka, K.; Mazzanti, L.; Amler, E. *Chem. Phys. Lett.* **1998**, *293*, 429-435.

[11] Repáková, J.; Čapková, P.; Holopainen, J.M.; Vattulainen, I. *J. Phys. Chem. B* **2004**, *108*, 13438-13448.

[12] Kaiser, R.D.; London, E. *Biochemistry* **1998**, *37*, 8180-8190.

[13] Pierotti, R.A. *Chem. Rev.* **1976**, *6*, 717-726.

[14] Hoff B.; Strandberg, E.; Ulrich, A.S.; Tieleman, D.P.; Posten, C. *Biophys. J.* **2005**, *88*, 1818-1827.
[15] Čurdová J.; Čapková, P.; Plášek J.; Repáková J.; Vattulainen, I. *J. Phys. Chem. B* **2007**, *111*, 3640-3650.

Chapter 6*

Fluorescent probes Prodan and Laurdan in lipid bilayers: partitioning and spectroscopic behaviour

*This chapter is adapted from Parisio, G.; Marini, A.; Mennucci, B.; Ferrarini, A. manuscript in preparation.

6.1 Introduction

Polarity sensitive fluorescence probes are chromophores which exhibit a change of the emission characteristics as a function of the local polarity of their environment. For this property they are extremely useful to investigate lipid membranes. The naphthalene derivatives Prodan (6-propionyl-2-dimethylaminonaphtahlene) and Laurdan (6-lauroyl-2-dimethylaminonaphtahlene) are important examples in this field.[1-6] Their molecular structure, together with that of the shorter homologue Acdan (6-acetyl-2-dimethylaminonaphtahlene), is shown in Figure 1. The naphthalene core of these probes is substituted on opposite sides by an electron-donor dialkylamino group and an electron-accepting carbonyl group, which give the fluorophores an ICT character.[7]

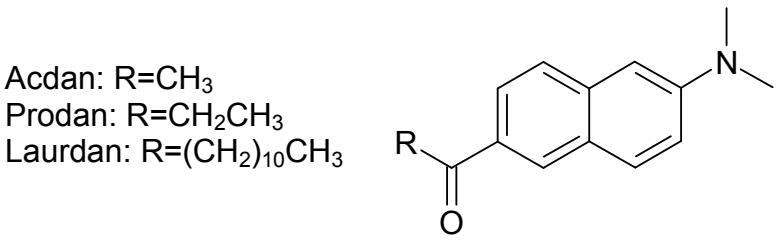

Figure 1: Molecular structure of Acdan, Prodan and Laurdan.

These probes in isotropic liquids exhibit a fluorescence emission extremely sensitive to the polarity of the environment, which shifts from about 430 nm to about 530 nm on changing the solvent from cyclohexane to water.[8-10] Within polar solvents a distinction can be made between protic and non-protic systems: whereas in the former case a generic mechanism of solvent reorganization explains Stokes shifts which scale with solvent dielectric permittivity, a major role of hydrogen bonding has been invoked to account for the dramatic effects on emission spectra observed in the latter case.[11]

The fluorescence spectra of 6-acyl-2-dimethylaminonaphtahlene dyes in lipid bilayers exhibit two bands, centred at about 440 nm and 490 nm, respectively.[1,12-14] In some cases additional emission at about 520 nm is found, which is ascribed to dyes partitioning in water.[15] Remarkable changes are observed on going from the liquid crystalline to the gel phase, as well as under changes of lipid composition; therefore these probes have been devised as suitable to monitor phase transitions and

to assess the lateral heterogeneity of bilayers.[6] Moreover, they have been proposed as reporters of changes in bilayer organization induced by pressure[1,16], by bilayer curvature[17] and strains[18], as well as by addition of cholesterol[12,19,20], local anesthetics and alcohols[1,15,20,21]. Different explanations have been proposed for the spectral features of the fluorescence emission and, in general, for the results of fluorescence experiments in membranes. The origin of the red-shift is controversial: it is generally believed to reflect changes in polarity of the probe micro-environment related to the amount of water accessible to the probe[12]; a crucial role of the mobility of water and/or lipids has been stressed[1,21-25]. From the influence of the chemical structure of phospholipid headgroups and from the absence of very fast contributions, on the picosecond timescale, to the solvent relaxation, some authors inferred that water should not be intended as free, but rather as hydration water bound to the lipid headgroups.[5,26-28] Another issue concerns hydrogen bonding[21,29,30]: it has been argued that a generic dipolar effect could not be sufficient to produce fluorescence shifts as large as those observed in experiments, and the presence of two forms of the probe, H-bonded and non H-bonded, has been hypothesized, the former of which would be responsible for the emission at around 490 nm.

A major point, for the translation of spectroscopic data into physical information on the system, is the knowledge of the location of the probe within the membrane.[26] After numerous solvent relaxation studies and quenching experiments, the distribution of Prodan and Laurdan in lipid bilayers is still not fully known.[14] Despite the presence of the same chromophore, differences in the behaviour of Prodan and Laurdan in lipid bilayers were evidenced by fluorescence[31] and FTIR studies[15,32]. Such differences are generally ascribed to a different position of the two probes, which would be a consequence of the different length of their acyl tails. From its higher perurbative effect in the chain region[32], and its lower sensitivity to the type of polar headgroup[31], Laurdan was inferred to reside deeper in the bilayer than Prodan. For the latter a heterogeneous distribution was proposed[27], as well as relocation between regions more or less rich in water under changes in the bilayer organization caused by phase transition[1,15,31,32]. Recently, MD simulations of Laurdan in a DOPC bilayer were reported[33]; however the results appear still preliminary, affected by the limited statistical sampling due to the prohibitive time-scale of conformational, rotational and translational motions[34].

Clearly, for the correct interpretation of the spectroscopic response of fluorescent probes in membrane, the simultaneous knowledge of the structure of their emitting state is needed. Several QM studies have been carried out to characterize the electronic states of Prodan and Laurdan, their geometry and spectroscopic properties.[35]

Here we present our analysis of the distribution properties of Acdan, Prodan and Laurdan in a liquid-crystalline lipid bilayer. Our approach, based on a mean field theory with an implicit bilayer model and an atomistic representation of the probe[36], can be seen as complementary to molecular simulations. There is the drawback that the details and specific aspects of solute/solvent interactions, are lost. However, if these do not play a major role, and the key effects of the bilayer environment can be described by its phase properties, the distribution of the solute, and in general all its equilibrium properties, can be obtained with good accuracy and with the advantage of a low computational cost. On the basis of our results, combined with those of QM calculations of the spectroscopic properties of the probes in different environments, we were able to provide an interpretation of the fluorescence emission behaviour of Prodan and Laurdan in membrane.

6.2 Results

Calculations were performed starting from molecular properties of the solutes and phase properties of a DPPC bilayer at a temperature T=323K which were parameterized as reported in ref.[36].

The fluorophores under investigation have some flexibility, which is limited in the case of Acdan and Prodan, and much more relevant for Laurdan. Flexibility is introduced into our model in terms of conformers, which correspond to the minima of the torsional potential $V(\chi)$[37]. Two equivalent states were taken for the C_{ar}-C(O)R bond, with the R-C=0 plane on the naphthyl plane and the C=O bond either on the side of the α or of the β carbon of the adjacent ring (the two conformers are related by a π rotation around the C_{ar}-C(O)R bond). These two conformational states will be henceforth denoted as I and II and are represented in Figure 2.

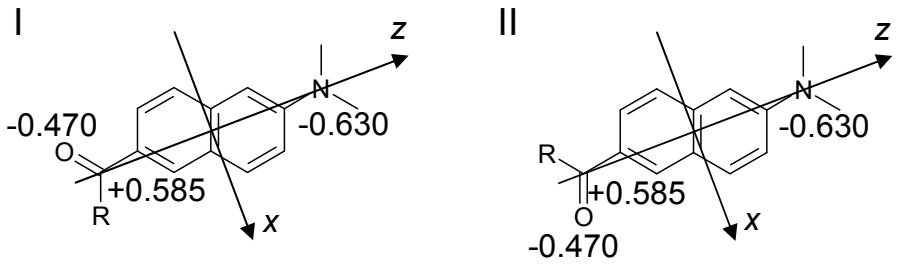

Figure 2: Molecular structure of I and II conformers of the probes under investigation. The highest atomic charges are reported and the molecular reference frame taken for Acdan and Prodan is shown; in the case of Laurdan the molecular *x* axis is taken pointing in the opposite direction.

In the case of Laurdan, also the flexibility of the acyl chain was taken into account. For each one of the C-C bonds along the acyl chain the three states usually denoted as *trans*, *gauche*$_+$ and *gauche*$_-$ were considered. For simplicity, only conformers with a single *gauche* state along the acyl chain, which are those with higher probability, were included in our analysis. Thus, a total number of 42 conformers was taken for Laurdan. From QM calculations at the DFT/B3LYP/6-31g** level the all-*trans* I and II conformers, with the same energy, resulted the most stable states; conformers with the C(O)-CH_2 in a gauche state were found to be slightly higher in energy (0.13 kcal mol^{-1}) and all other conformers with a single gauche in other bonds are even higher (0.51 kcal mol^{-1}).

The position Z and orientation Ω of the probes in the bilayer were defined, with respect to the molecular frames in Figure 1, as shown in Figure 1 of Chapter 2. The highest atomic charges on solute molecules are also reported in Figure 1.

Figure 3 shows the water/bilayer transfer free energy profile, $u(Z)$, calculated for Acdan and Prodan, with Z being the position along the bilayer normal of the origin of the molecular frame defined in Figure 2. Both exhibit a well about 8 kcal mol^{-1} deep in the range of 10-18Å distance from the midplane. The free energy profiles calculated for the two probes look very similar, with only slightly lower values in the case of Prodan. The corresponding position distribution functions, $P_{\Omega,\chi}(Z)$, which are also shown in Figure 3 indicate a preference of the two probes to locate the centre of their naphthalene mojety in the region between 10Å and 18Å. The absence of solute in the central region of the bilayer is predicted.

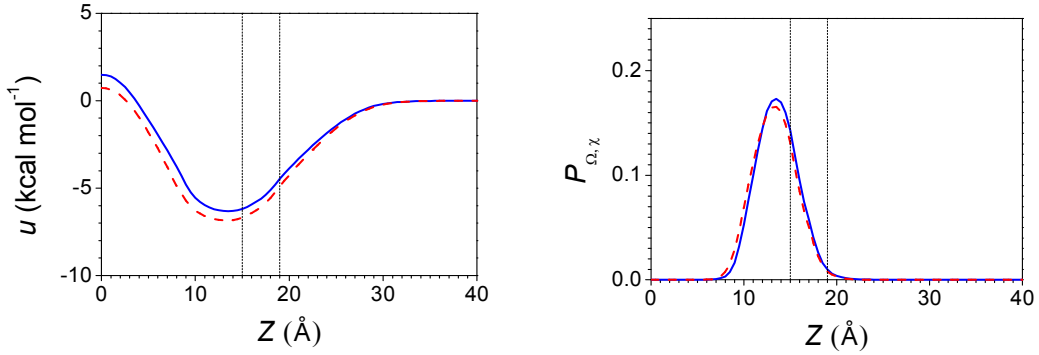

Figure 3: Transfer free energy $u(Z)$ (left) and position distribution function $P_{\Omega,\chi}(Z)$ (right) calculated for Acdan (solid line) and Prodan (dashed line), as a function of the position of the centre of the molecular frame across the lipid bilayer. The coordinate Z=0 corresponds to the bilayer midplane. the vertical lines indicate the average position of carbonyl and phosphate groups. Given the symmetry of the system, only one half of the bilayer is shown.

To shed light on the origin of the position distribution of the probes inside the bilayer, we report in Figure 4 the transfer free energies and distribution profiles calculated for Prodan by excluding a single contribution to the mean field potential

$$U = U_{cav} + U_{el} + U_{disp} + U_{ord} \tag{1}$$

at a time. Analogous results were obtained for Acdan.

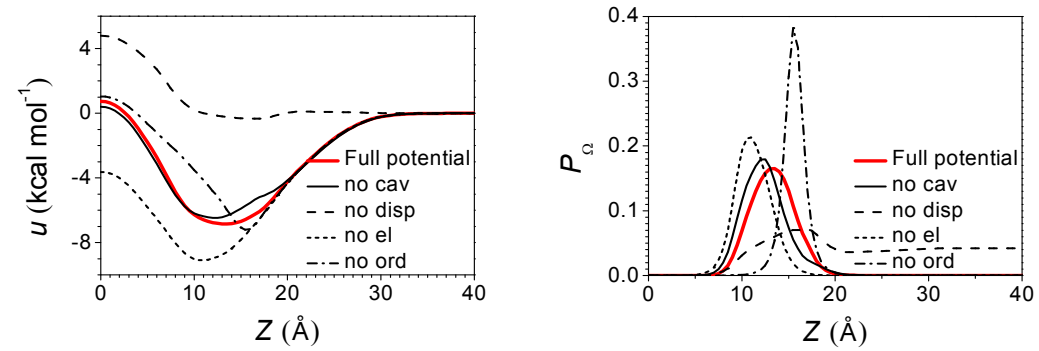

Figure 4: Transfer free energy $u(Z)$ (top) and position distribution function $P_{\Omega}(Z)$ (bottom) calculated for conformer I of Prodan as a function of the position of the centre of the molecular frame across the lipid bilayer, by removing one of the contributions appearing in eq.1 at a time. The coordinate Z=0 corresponds to the bilayer midplane. Given the symmetry of the system, only one half of the bilayer is shown.

We can see that dispersion interactions are the main responsible for the partitioning of Prodan in the bilayer; in their absence the free energy profile would be nearly flat and would only exhibit an appreciable increase for insertion of the probe deeper in the bilayer, in which case the molecular charges would reside in the most apolar region. The cavity term has a weaker influence on the free energy profile; among the

most probable positions, it favours those closer to the exterior, which allow the probe to keep a large part of its body at the hydrophilic/hydrophobic interface, generally identified with the carbonyl region of the bilayer. Electrostatic probe-environment interactions favour position which allow the molecular charges, which are mainly located in the carbonyl and amino groups, to reside close to water. The ordering of the acyl chains promotes locations of the probe deeper in the bilayer and has the overall effect of broadening its distribution. Analogous effects were found for cholesterol[36], but were differently tuned by the molecular shape and charge distribution; the result is a broader distribution for Prodan.

To fully understand the behavior of the probes inside the bilayer we must take into account also their orientational preferences. Figure 5 shows the orientational distribution function $P(\Omega,Z)$ calculated for the I and II conformers of Acdan and Prodan at their most probable position (in correspondence of the maximum of the curve shown on the left-hand side of Figure 3).

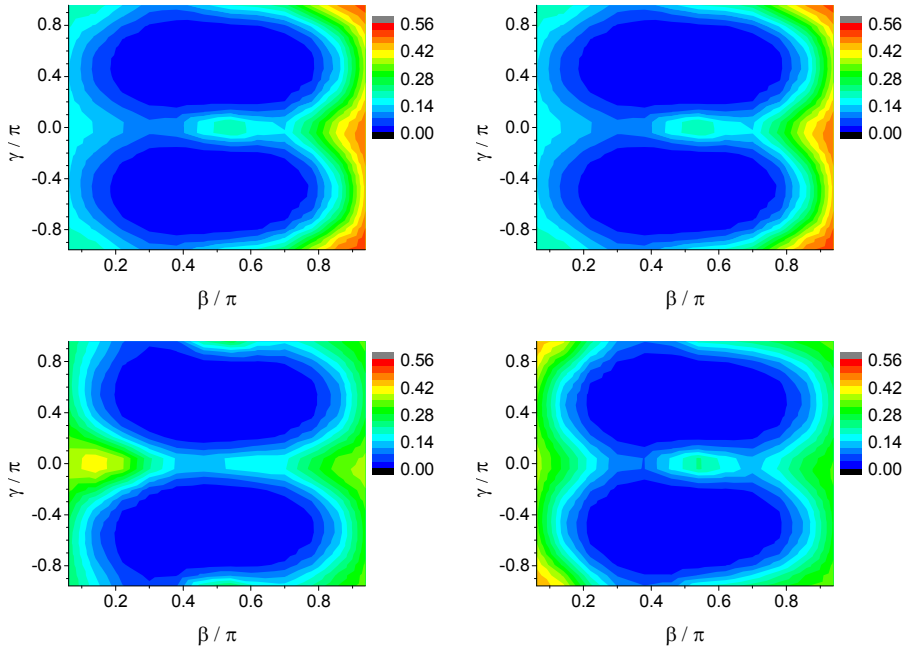

Figure 5: Orientational distribution $P(\Omega,Z)$ calculated in the preferred position Z=13.5Å for Acdan (I: top right; II: top left) and for Prodan (I: bottom right; II: bottom left). β is the angle between the long molecular axis, z, and the bilayer normal. The γ angle refers to molecular rotation around z.

Both probes exhibit a clear preference for keeping the molecular z axis parallel to the bilayer normal. However, for Acdan the orientation with the carbonyl group pointing towards water is much more probable than the opposite orientation, with the carbonyl

group pointing towards the bilayer core. On the contrary, for Prodan the two orientations are almost equally probable. This difference can be easily explained, considering that the ethyl chain increases the hydrophobic character of the carbonylic end of Prodan, decreasing the exposure of the polar group to the dielectric.

A global view of the orientational behaviour across the distribution peak, is obtained from inspection of the profiles of the first and second rank order parameters $\langle P_1 \rangle = \langle \cos\beta \rangle$ and $S_{ii} = \langle (3\cos^2\theta_i - 1)/2 \rangle$, where θ_i is the angle between the ith molecular axis and the bilayer normal ($\theta_z = \beta$), which are shown in Figure 6.

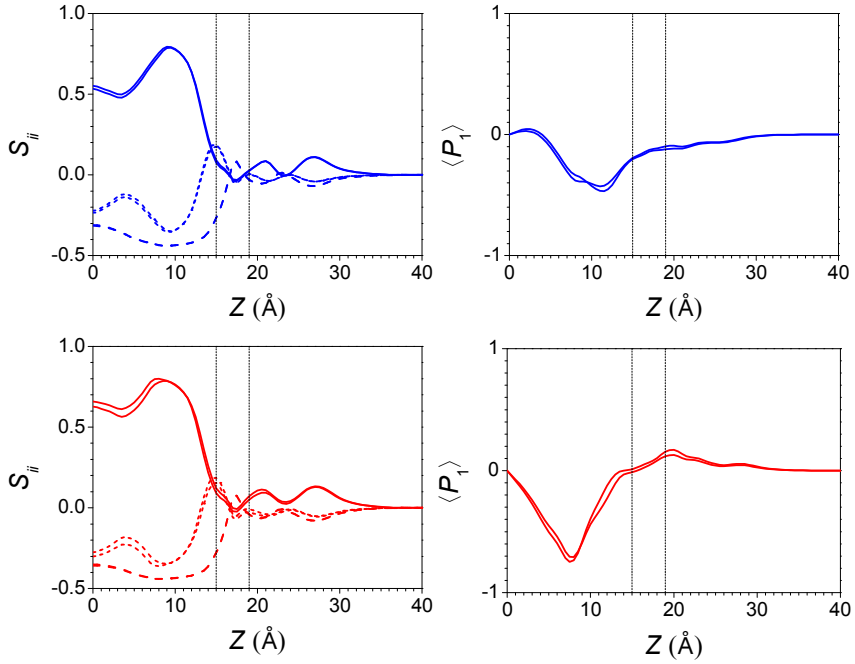

Figure 6: Orientational order parameters S_{ii} (left: S_{xx} dotted, S_{yy} dashed and S_{zz} solid) and $\langle P_1 \rangle$ (right) calculated for Acdan (top) and Prodan (bottom) as a function of the position of the centre of the molecular frame across the lipid bilayer. For each solute the results obtained for the I and II conformers are shown. The coordinate Z=0 corresponds to the bilayer midplane. The vertical lines indicate the average positions of carbonyl and phosphate groups. Given the symmetry of the system, only one half of the bilayer is shown.

Again we can recognize a close similarity between Acdan and Prodan, although some differences appear. The Saupe matrix profiles indicate that both probes in the hydrophobic region of the bilayer preferentially align their z axis to the bilayer normal across the whole bilayer, and have only a small preference for keeping the y rather than the x axis perpendicular to the normal.The negative $\langle P_1 \rangle$ value predicted for Acdan indicates that this probe everywhere has at least a weak preference to orient with its carbonyl end pointing towards the exterior of the bilayer. The polar

order parameter of Prodan shows a stronger dependence on the position of the probe, being close to zero or even slightly positive in the hydrophilic region of the bilayer and reaching strongly negative values in the deeper hydrophobic region.

The situation is very different in the case of Laurdan, because of the strong effects of the long acyl chain. Figure 7 shows the torsional potential V and the average effective torsional potential V' in the bilayer calculated for all conformers. We can see that the bilayer can introduce profound differences between conformers; in general, those of type I are predicted to be stabilized with respect to those of type II. Interestingly, conformers with all-trans acyl chain are no longer the most stable.

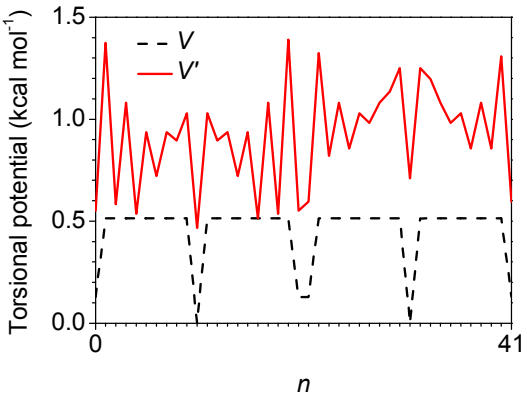

Figure 7: Torsional potential V and effective torsional potential V' in the bilayer environment calculated for the conformers of Laurdan; n is the conformer label.

Figure 8 shows the probability distributions $P_\Omega(Z)$ calculated for all single conformers. We can see that they look similar, with the maximum at a distance of about 15.5Å from the midplane. Some distinction between different conformers can be made when considering their orientational distribution, $P(\Omega,Z)$, calculated at Z=15.5Å, corresponding to the maximum of the average position probability distribution on the left-hand side of Figure 8. L-shaped conformers of Laurdan are predicted to preferentially keep the aromatic plane parallel to the acyl chains; the z molecular axis tends to stay perpendicular to the bilayer normal and the x axis approximately parallel to the normal (I) or antiparallel to it (II). These different orientations allow the conformers to direct the polar CO group towards the polar interface, and the apolar tail towards the hydrophobic core of the bilayer. Examples are shown in Figure 9 for one I and one II conformer. More elongated conformers preferentially align their long axis roughly parallel to the bilayar normal.

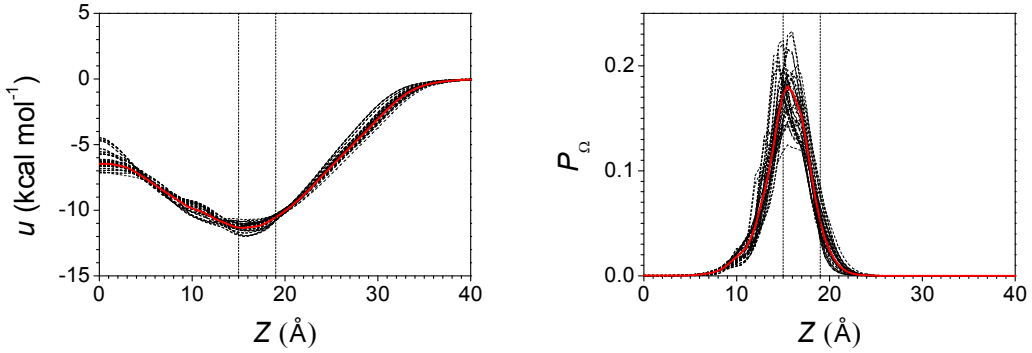

Figure 8: Transfer free energy $u(Z)$ (left) and position distribution function $P_{\Omega}(Z)$ (right) calculated for each single conformer of Laurdan (dotted line) as a function of the position of the centre of the molecular frame across the lipid bilayer. The solid lines represent the transfer free energy $u(Z)$ (bottom) and the position distribution function $P_{\Omega,\chi}(Z)$ (top) obtained after averaging over all the conformers. The coordinate Z=0 corresponds to the bilayer midplane. The vertical lines indicate the average positions of carbonyl and phosphate groups. Given the symmetry of the system, only one half of the bilayer is shown.

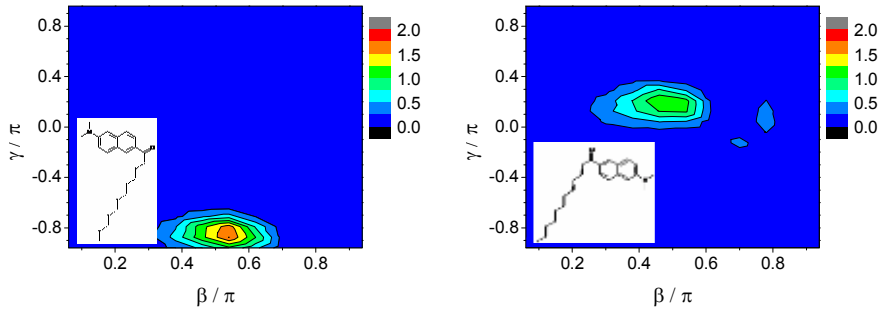

Figure 9: Orientational distribution $P(\Omega,Z)$ calculated in the preferred position Z=15.5Å for the I- (left) and the II- (right) conformers of Laurdan shown in the insets. β is the angle between the long molecular axis, z, and the bilayer normal. The γ angle refers to molecular rotation around z.

Figure 10 gathers the first and second rank order parameters $\langle P_1 \rangle$ and S_{ii} of all conformers at two different depth within the bilayer; a significant dependence of order from position across the distribution peak appears. The results relative to the position of maximum probability (on the top of Figure 10) are in line with the comments reported just above: the positive S_{xx}, together with the negative S_{zz} and S_{yy} values, similar to each other, indicate the preferential alignment of the of the L-shaped conformers with their x molecular axis parallel to the bilayer normal and the z axis parallel to the bilayer plane, which also explains the small $\langle P_1 \rangle$ order parameters. A completely different behaviour is predicted when the centre of the naphthalene mojety is located deeper in the bilayer (on the bottom of Figure 10): in this case the L-shaped conformers of Laurdan preferentially align their z axis to the bilayer normal (positive S_{zz}), antiparallel to it (negative $\langle P_1 \rangle$). The alignment of elongated

conformers to the bilayer normal is stronger when they are inserted deeper in the bilayer.

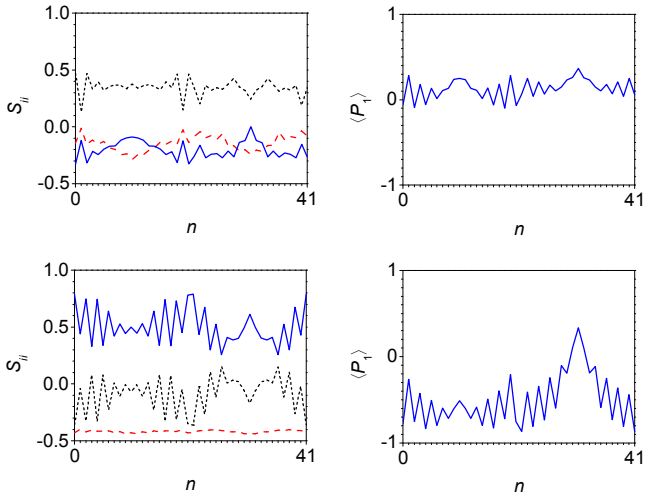

Figure 10: Orientational order parameters S_{ii} (left: S_{xx} dotted, S_{yy} dashed and S_{zz} solid) and $\langle P_1 \rangle$ (right) calculated for all conformers of Laurdan at Z=15.5Å (top) and Z=10Å (bottom); n is the conformer label.

6.3 Discussion

In the following we shall discuss the main results of our calculations in the light of the experimental findings reported in the literature. In most cases, however, rather than carrying out a direct comparison, we can only ascertain whether our results are compatible with the experimental findings. In fact, calculations can provide detailed insights into the probe distribution in the lipid bilayer, which is generally not accessible experimentally. Moreover the averaged properties which can be revealed by experiments depend on specific lipid composition of the bilayer and experimental conditions. Anyway a wealth of data is available for Laurdan and Prodan, whereas Acdan has been very scarcely investigated.

The three probes are predicted to be inhomogeneously distributed across the bilayer, as shown by the profiles collected in Figure 11. Preferential location of the naphthalene cores in the glycerol region is in accord with the general belief for Prodan and Laurdan.[4,16,27,38-40] In particular, it is generally stated that Prodan resides closer to the water/bilayer interface than Laurdan. The location of the two probes was inferred, with different motivations, from FTIR experiments at various

pressures[1,32] as well as from both steady-state and time-dependent fluorescence measurements of solvent relaxation, and parallax analysis of fluorescence quenching experiments[27]; however the capability of these methods to provide information allowing the unambiguous assessment of probe positions may be questionable. The weaker sensitivity of Laurdan to changes in the bilayer headgroup region[31] and its stronger perturbing effect[32] than Prodan, were ascribed to its deeper location. We suggest that both may derive from the higher affinity of Laurdan for the hydrophobic region of the bilayer, determined by its longer acyl chain. From the transfer free energy profiles collected in Figures 11, the following ranking of affinity for the membrane environment is found: Laurdan > Prodan > Acdan, in agreement with the commonly accepted view, which is based on simple considerations on the hydrophobic character of the acyl chains of the probes and has been supported by experimental evidences in various conditions[1,2,15,32].

It is worth pointing out that a non-uniform distribution of the probes within the bilayer does not mean that these are anchored at a given site; they are rather predicted to span a range of positions, which may be as broad as 1 nm. A heterogeneous localization of Prodan was inferred by fluorescence quenching experiments.[27] Concerning our results, a broad distribution inside lipid bilayers is generally a feature sheared by most molecules with elongated shape; we obtained a similar result for also for cholesterol[36], in agreement with experimental findings[41,42]. Vertical displacements may have some relevance for the interaction of the fluorescent probes with water.

Differences between the behaviour of the three probes investigated were found, stronger than those exhibited by their position distribution. In particular, while Prodan shows no pronounced preference for insertion of its aminic or acylic end, Acdan is predicted to have a clear preference for the orientation with its carbonyl group pointing towards water. Furthermore, the L-shaped conformers of Laurdan, which are suggested to be highly representative in liquid crystalline bilayers, are found to keep their broad naphthalene side perpendicular to the bilayer normal, rather than parallel to it as is the case of the short-tail homologues. This orientational behaviour is generally ignored in the literature, probably for the lack of knowledge, but it might influence the spectroscopic response of the probes. Especially intriguing appears the prediction of a perpendicular orientation, with respect to acyl chains, of

the naphthalene moiety of Laurdan, which contrasts the parallel orientation customarily assumed in the literature, where conformational effects are ignored. Since the transition dipole of the chromophore is roughly parallel to its long axis, this orientation can be probed by suitable techniques, like two-photon excitation fluorescence microscopy[43]. The absence of photoselection for Laurdan in vesicles in the liquid crystalline phase appears compatible with our prediction. On the contrary, the photoselection effect observed in the gel phase can be explained by a predominant orientation of naphthalene parallel to the acyl chains which, in the light of our results, could be a consequence of the stabilization of the most elongated conformers in the tightly packed gel phase.

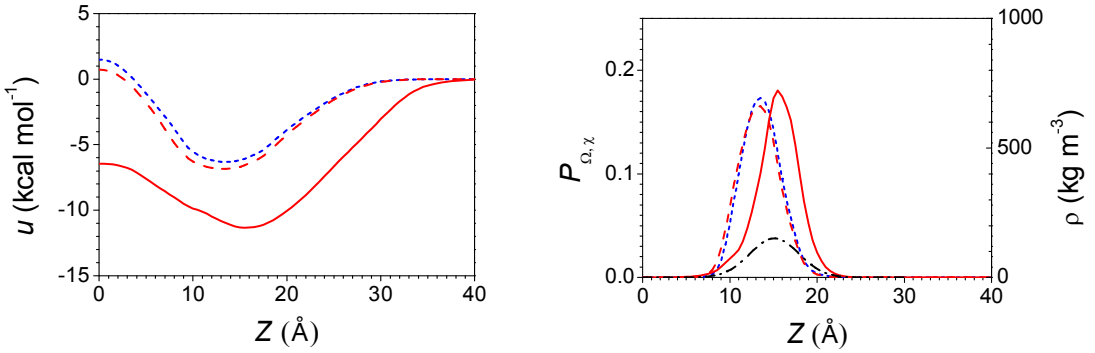

Figure 11: Transfer free energy $u(Z)$ (left) and position distribution function $P_{\Omega,\chi}(Z)$ (right) calculated for Acdan (dotted line), Prodan (dashed line) and Laurdan (solid line), as a function of the position of the center of the molecular frame across the lipid bilayer. The density profile of the glycerol moiety of DPPC[44] is shown for comparison (dash-dotted line). The coordinate Z=0 corresponds to the bilayer midplane. Given the symmetry of the system, only one half of the bilayer is shown.

The spectral behavior of the fluorescent probes under investigation is often described in terms of probe configurations more or less accessible to water. Solutes embedded in the interior of the bilayer would be responsible for emission at about 440 nm, close to that observed for the same probes in apolar isotropic solvents[8-10]. Emission would be shifted at longer wavelengths for probes in a polar environment. QM calculations showed that hydrogen bonds at the carbonyl oxygen of the dyes are needed to yield the large Stokes shifts which would place the emission band at about 490 nm.[45] So, to discuss the fluorescence behaviour of the three dyes it may be convenient to look at the location of their carbonyl oxygen across the membrane. The calculated profiles are shown in Figure 12, together with the density profile of water[44]. A clearly bimodal distribution appears for the carbonyl oxygens of Acdan and Prodan, the two maxima corresponding to different orientations of the probes,

one with the carbonyl group, the other with the amino group directed towards water. As also shown by the negative $\langle P_1 \rangle$ values between 10Å and 18Å, in Figure 6, Acdan and Prodan overall have a preference for keeping their carbonyl end in the hydrophilic region of the bilayer, where water is abundant. However, a significant probability, higher for Prodan, is also predicted for carbonyls sitting deeper in the hydrophobic region of the bilayer, where the amount of water becomes negligible. We can see in Figure 12 that the maximum corresponding to this buried site is absent for Laurdan. For this probe, the broad distribution of carbonyl oxygen across the bilayer can be decomposed in different contributions: L-shaped conformers, with gauche bonds at the very beginning of their acyl chains, are the main responsible for the peak at about 17Å (odd gauche bonds) and for the small shoulder at about 14.5Å (even gauche bonds), whereas the shoulder at about 12Å and the distribution tail at Z<10Å are mainly due to more extended conformers.

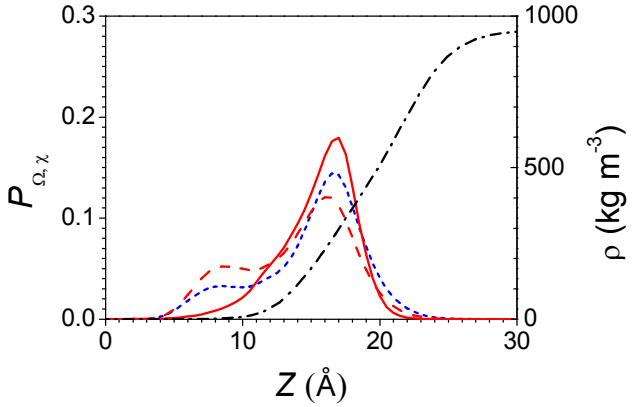

Figure 12: Position distribution function calculated for the carbonylic oxygen atom of conformers I and II of Acdan (dotted lines), Prodan (dashed lines) and Laurdan (solid line). The density profile of water across the bilayer[44] is shown for comparison (dash-dotted line). The coordinate Z=0 corresponds to the bilayer midplane. Given the symmetry of the system, only one half of the bilayer is shown.

The results of our calculations suggest a somewhat different origin of the features of the fluorescence spectra recorded in lipid membranes for Acdan and Prodan, on one side, and for Laurdan, on the other side. Assuming that hydrogen bonds are the major responsible for the large Stokes shifts, the emission bands of the short-tail homologues can be explained considering that, depending on the molecular location and orientation, the oxygen atom of the dyes will be more or less accessible to water (the outer and the inner peak in the distributions in Figure 12). The probes keeping their oxygen atom embedded in a region poor of water will emit at the blue edge of

the band, while the Stokes shift of the probes keeping their oxygen atom exposed to the contact with water and to hydrogen bonds will be larger. The relative weight of the long- and short- wavelength contributions to emission will be affected by the physical state and chemical composition of the bilayer, since temperature, pressure, nature of lipid headgroups and length/saturation of acyl chains, and presence of perturbing agents, affect both probe distribution and water penetration in the bilayer. In the case of Laurdan, the positional heterogeneity of carbonyl groups is coupled with the conformational distribution of the probe: the oxygen atom of bent conformers would be more or less exposed to water, and then more or less involved in hydrogen bonds, whereas elongated conformers would keep it buried in a region scarcely accessible to water. The stabilization of the latter in the gel phase, suggested by the two-photon excitation fluorescence microscopy experiments mentioned above[43], is in agreement with the dominating blue emission observed in lipid bilayers below their characteristic phase transition temperature[4]. Elongated conformers, which are more ordered and are likely to reorient more slowly than bent conformers, might be responsible for the significantly higher fluorescence anisotropy observed at 440 nm than at 490 nm, a result which was not explained[14]. Somehow surprisingly, the role of molecular flexibility has been disregarded when discussing the behaviour of Laurdan in lipid bilayers. The acyl chain conformation is expected to have a scarce influence on the electronic transitions of Laurdan, mainly involving the chromophore mojety. However, as shown by our results, it can affect the fluorescence response in an indirect way, by determining the location and orientation of the probe inside the bilayer.

Although, strictly speaking, our results refer to probes incorporated in a liquid crystalline DPPC bilayer, some conclusions, concerning the role of hydrogen bonds and the importance of the conformational and orientational distribution of the probes, are expected to be generally meaningful. However, due to the great sensitivity to the physical state and composition of the bilayer exhibited by the spectroscopic response, especially in the case of Prodan, the specific features of the lipid phase should be taken into account to get more accurate predictions and allow a closer comparison with experiments.

6.4 Conclusions

Environment sensitive fluorescence probes are an extremely useful tool for the investigation of lipid membranes; they have been shown to provide detailed information on the local structure, dynamics and interactions in lipid membranes. Several experimental techniques have been developed[26,46] and the design of fluorophores selective towards specific membrane properties has been devised as an important goal to increase the information content and spatial resolution of experiments[47]. At this stage the need of a better understanding of the spectroscopic response has been pointed out in several instances[33,47]: this implies the connection between the electronic states of the probe and how these are affected by the environment, on one side, and the probe distribution in the bilayer and the factors which determine its changes as a function of bilayer composition or external perturbations, on the other side. The theoretical and computational techniques nowadays available seem mature to address this topic.

Here we have used our implicit membrane methodology to investigate the distribution of the fluorescent probes Acdan, Prodan and Laurdan in a liquid-crystalline DPPC bilayer. On the basis of our results, and in the light of those of QM calculations of the spectroscopic properties of these molecules in different solvents, we have proposed an interpretation of experimental findings, which supports the hypothesis that the long wavelength emission (~ 490 nm) observed in the spectra of Prodan and Laurdan in liquid cristalline lipid bilayers must come from an H-bonded form of the probes[30].

Further detailed information were obtained on the distribution of the probes in membrane, which can be summarized as follows.

In agreement with the general belief[21], Prodan and Laurdan are predicted to locate the napthalene rings in the glycerol region of liquid crystalline lipid bilayers. However, according to our calculations Laurdan would not reside deeper than Prodan in the bilayer[27,31,32].

An important difference between the two probes, which was not sufficiently highlighted before, is their orientation in the bilayer. As usually assumed, Prodan is predicted to preferentially keep the naphthalene ring parallel to the lipid acyl chains, however a large probability, usually unexpected, is found for the ‘upside-down’

orientation with the carbonyl group closer to the headgroup region. On the contrary, the orientation of Laurdan would exhibit a strong dependence on the chain conformation, which was generally ignored in other studies: most conformers in the optimal orientation would have the naphthalene ring perpendicular to the acyl chains, so allowing the carbonyl group to reside in the proximity of the water/bilayer interface.

Another difference between Acdan and Prodan, on one side, and Laurdan, on the other side, is the higher stabilization of the latter in the bilayer, which is mainly due to its larger dispersion interactions with the lipid acyl chains. This is likely to be an important reason behind the weaker sensitivity of Laurdan to changes in the bilayer organization.

We can devise several developments of this work. Dealing with 6-acyl-2-dimethylaminonaphtahlene derivatives, an important step for a complete analysis of their behavior in lipid membranes is the extension of our study to bilayers differing from liquid crystalline DPPC for the physical state and composition. Moreover, the methodology can be applied to other fluorophores, and we expect that this investigation can provide novel insights into the effect of the chemical structure of probes on their spectroscopic response in lipid membranes.

Abbreviations

DPPC: 1,2-dipalmitoyl-sn-glycero-3-phosphocholine

MD: Molecular Dynamics

QM: Quantum Mechanics

SM: Statistical Mechanics

6.5 References

[1] Chong, P.L.-G. *Biochemistry* **1988**, *27*, 399-404.

[2] Chong, P.L.-G. *High Pressure Res.* **1990**, *5*, 761-763.

[3] Parasassi, T.; De Stasio, G.; d'Ubaldo, A.; Gratton, E. *Biophys. J.* **1990**, *60*, 1179-1186.

[4] Parasassi, T.; Krasnowska, E.K.; Bagatolli, L.; Gratton, E. *J. Fluoresc.* **1998**, *8*, 365-373.

[5] Sýkora, J.; Kapusta, P.; Fidler, V.; Hof, M. *Langmuir* **2002**, *18*, 571-574.

[6] Bagatolli, L.A. *Biochim. Biophys. Acta* **2006**, *1758*, 1541-1556.

[7] Lakowicz, J.R. Principles of Fluorescence Spectroscopy, 3rd Ed.; Springer: New York, 2006.

[8] Weber, G.; Farris, F.J. *Biochemistry* **1979**, *1*, 3075-3078.

[9] Catalan, J.; Perez, P.; Laynez, J.; Blanco, F.G. *J. Fluoresc.* **1991**, *1*, 215-223.

[10] Cerezo, F.M.; Rocafort, S.C.; Sierra, P.S.; Garcia-Blanco,F.; Oliva, C.D.; Sierra, J.C. *Helv. Chim. Acta* **2001**, *84*, 3306-3312.

[11] Rowe, B.A.; Roach, C.A.; Lin, J.; Asiago, V.; Dmitrenko, O.; Neal, S.L. *J. Phys. Chem. A* **2008**, *112*, 13402-13412.

[12] Massey, J.B.; She, H.S.; Pownall, H.J. *Biochemistry* **1985**, *24*, 6973-6978.

[13] Vequi-Suplicy, C.C.; Benatti, C.R.; Lamy, M.T. *J. Fluoresc.* **2006**, *16*, 431-439.

[14] Lúcio, A.D.; Vequi-Suplicy, C.C.; Fernandez, R.M.; Lamy, M.T. *J. Fluoresc.* **2010**, *20*, 473-482.

[15] Zeng, J.; Chong, P.L.-G. *Biophys. J.* **1995**, *68*, 567-573.

[16] Kusube, M.; Matsuki, H.; Kaneshina, S. *Colloids and Surf. B* **2005**, *42*, 79-88.

[17] Goto, M.; Sawaguchi, H.; Tamai, N.; Matsuki, H.; Kaneshina, S. *Langmuir* **2010**, *26*, 13377-13384.

[18] Zhang, Y.-L.; Frangos, J.H.; Chachisvilis, M. *Biochem. Biophys. Res. Commun.* **2006**, *347*, 838-841.

[19] Krasnowska, E.K.; Bagatolli, L.A.; Gratton, E.; Parasassi, T. *Biochim. Biophys. Acta* **2001**, *1511*, 330-340.

[20] Bondar, O.P.; Rowe, E.S. *Biophys. J.* **1999**, *76*, 956-962.

[21] Rottenberg, H. *Biochemistry* **1992**, *31*, 9473-9481.

[22] Parasassi, T.; Conti, F.; Gratton, E. *Cell. Mol. Biol.* **1986**, *32*, 99-102.

[23] Parasassi, T.; Conti, F.; Gratton, E. *Cell. Mol. Biol.* **1986**, *32*, 103-108.

[24] Sommer, A.; Paltauf, F.; Hermetter, A. *Biochemistry* **1990**, *29*, 11134-11140.

[25] Parasassi, T.; Gratton, E. *J. Fluoresc.* **1995**, *5*, 59-69.

[26] Sýkora, J.; Hutterer, R.; Hof, M. In Fluorescence Spectroscopy in Biology; Hof, M.; Hutterer, R.; Fidler, V. Eds.; Springer Verlag: Berlin, 2005, pp 71-78.

[27] Jurkiewicz, P.; Olżyńska, A.; Langner, M.; Hof, M. *Langmuir* **2006**, *22*, 8741-8749.

[28] Olżyńska, A.; Jurkiewicz, P.; Hof, M. *J. Fluoresc.* **2008**, *18*, 925-928.

[29] Samanta, A.; Fessenden, R.W. *J. Phys. Chem.* **2000**, *104*, 8972-8975.

[30] Klymchenko, A.S.; Duportail, G.; Demchenko, A.P.; Mély, Y. *Biophys. J.* **2004**, *86*, 2929-2941.

[31] Parasassi, T.; De Stasio, G.; Ravagnan, G.; Rusch, R.M.; Gratton, E. *Biophys. J.* **1991**, *60*, 179-189.

[32] Chong, P.L.-G.; Wong, P.T.T. *Biochim. Biophys. Acta* **1993**, *1149*, 260-266.

[33] Barucha-Kraszewska, J.; Kraszewski, S.; Jurkiewicz, P.; Ramseyer, C.; Hof, M. *Biochim. Biophys. Acta* **2010**, *1798*, 1724-1734.

[34] Bennett, W.F.D.; MacCallum, J.L.; Hinner, M.J.; Marrink, S.J.; Tieleman, D.P. *J. Am. Chem. Soc.* **2009**, *131*, 12714-12720.

[35] Mennucci, B.; Caricato, M.; Ingrosso, F.; Cappelli, C.; Cammi, R.; Tomasi, J.; Scalmani, G.; Frisch, M. J. *J. Phys Chem. B* **2008**, *112*, 414-423.

[36] Parisio, G.; Ferrarini, A. *J. Chem. Theory Comput.* **2010**, *6*, 2267-2280.

[37] Flory, P. J. Statistical Mechanics of Chain Molecules; Interscience: New York, 1969.

[38] Antollini, S.S.; Barrantes, F.J. *Biochemistry* **1998**, *37*, 16653-16662.

[39] Bernik, D.L.; Zubiri, D.; Tymczyszyn, E.; Disalvo, E.A. *Langmuir* **2001**, *17*, 6438-6442.

[40] Krasnowska, E.K.; Bagatolli, L.A.; Gratton, E.; Parasassi, T. *Biochim. Biophys. Acta* **2001**, *1511*, 330-340.

[41] Gliss, C.; Randel, O.; Casalta, H.; Sackmann, E.; Zorn, R.; Bayerl, T. *Biophys. J.* **1999**, *77*, 331-340.

[42] Harroun, T.A.; Katsaras, J.; Wassall, S.R. *Biochemistry* **2006**, *45*, 1227-1233.

[43] Bagatolli, L.A.; Gratton, E. *Biophys. J.* **2000**, *78*, 290-305.

[44] Kupiainen, M.; Falck, E.; Ollila, O.H.S.; Niemelä, P.; Gurtovenko, A. A. *J. Comp. Theory Nano* **2005**, *2*, 401-413.

[45] Marini, A. Mennucci, B. Preliminary communication.

[46] Bagatolli, L.A. In Fluorescence Spectroscopy in Biology, Hof, M.; Hutterer, R.; Fidler, V. Eds.; Springer Verlag: Berlin, 2005; pp 150-159.

[47] Demchenko, A.P.; Mély, Y.; Duportail, G.; Klymchenko, A.S. *Biophys. J.* **2009**, *96*, 3461-3470.

Chapter 7
Conclusions

7.1 Conclusions

Solute partitioning and permeation across lipid bilayers are important issues in biological and pharmaceutical fields dealing with the study of the structure and properties of membranes, drug-design and drug-delivery.

This work places in the field of implicit solvent models, where the problem of characterizing the behaviour of a solute in its environment is tackled focusing on the atomistic representation of the former, while neglecting the molecular discreteness of the latter, treating it as a continuum. We have developed an implicit membrane model for the description of the properties of solutes in lipid bilayers, concerning the way they distribute within a lipid membrane and their ability to cross it.

According to the implicit solvent approach, the average influence of the medium on the solute is taken into account introducing a mean field potential, which depends only on the coordinates describing the solute configuration. Few contributions to the mean field potential are considered representing different solute-solvent interactions. Short-range attractive and repulsive interactions and long-range electrostatic interactions are usually taken into account.

In existing implicit models for homogeneous isotropic solvents the mean field potential is decomposed into two non-polar and polar contributions.[1] The free energy changes due to dispersion (short-range attractive) and steric (short-range repulsive) interactions between the solute and the neighbouring solvent molecules, have an enthalpic molecular-surface-dependent and an entropic molecular-volume-dependent character, respectively[2]. In spite of this, these have been traditionally merged into one non-polar contribution, expressed in a phenomenological form where only an explicit dependence on the solvent-accessible-surface-area (SASA) of the solute appears.[3] On the contrary, a good level of accuracy has been reached in the evaluation of the polar contribution, given by the electrostatic free energy, through the expressions provided by generalized Born (GB) theories.[4]

Although the lack of an adequate representation of solute-solvent interactions has been recognized in these implicit solvent models, implicit membrane models have been developed as a simple extension of the GB/SASA approach to the case of a water/bilayer system[5], and one only attempt was done to accurately describe the internal heterogeneity of the bilayer environment[6]. There a rigorous GB formalism

for heterogeneous dielectric environments was proposed, while a MD simulation of O_2 in membrane, with explicit solvent, was employed to introduce a modulation of the SASA term reflecting the bilayer heterogeneity. However, while the dielectric properties of the hydrophilic and hydrophobic regions of a lipid bilayer, arising from the amphiphilic nature of the lipid molecules, are suitably represented by layered models, the structural properties of the bilayer interphase, its density and pressure gradients as well as molecular ordering, and their effects on non-polar solute-solvent interactions, are usually neglected[7].

In our implicit membrane[8] model we tried to improve the traditional description of solute-solvent interactions and of the non-uniform and ordered environment of a lipid bilayer. The mean field potential we defined, was decomposed into four contributions (I-IV). The GB model proposed in ref.[6] was adopted for the electrostatic contribution (I), while a generalized formalism based on the London expression[9] was extended to model the dispersion contribution (II) of short-range attractive solute-solvent interactions in the heterogeneous bilayer environment. The cavity contribution (III), related to short-range repulsive interactions, was given the form of the reversible volume work against an heterogeneous external pressure, required for the creation of a solute-shaped cavity in the bilayer interphase. An order contribution (IV) was introduced to represent the effect of anisotropic solute-solvent interactions in the ordered bilayer environment. In order to do this, an heterogeneous ordering potential was defined, adapting a theoretical model originally proposed for liquid crystals[10]. The dependence of each contribution to the mean field potential on the coordinates defining solute position and orientation within the bilayer, and the conformation of flexible solutes, was considered. Then from the mean field potential the coupled positional-orientational-conformational distribution and suitably averaged properties, depending on a reduced number of variables, were obtained within a statistical mechanical framework. (Chapter 2)

Our description of the solute-bilayer system relies on a limited number of molecular properties for the former and of phase properties for the latter. In particular calculations require information on solute geometry, charge distribution and polarizability which for drug-like molecules can be gained at the quantum mechanical level, and on dielectric permittivity, density, lateral pressure and order parameter profiles across the lipid bilayer, which specifically designed experiments

or a single atomic-level MD simulation of the pure bilayer can provide. A consistent formalism was achieved, wherein all the contributions to the mean field potential are modeled and parameterized in terms of the molecular surface of the solute, which was implemented in a software package, which will be made available to the scientific community. Given the molecular structure of a medium-sized solute, its free energy surface as a function of its position and orientation in the bilayer is obtained in a few minutes on a desktop PC. This combined atomistic/continuum representation has several advantages over existing implicit membrane models and MD approaches. *i*) It allows the accurate description of the solute-solvent interactions, sensitive to molecular details of the solute structure, and *ii*) the investigation of the solute behaviour everywhere across the bilayer, with a detailed analysis of orientational and conformational effects, even in almost unexplored solute configuration, *iii*) at a ridiculous computational cost; moreover *iv*) the possibility of isolating the effect of each contribution to the mean field potential allows the analysis of the role of different solute-solvent interactions in determining solute behaviour.

According to the solubility-diffusion approach, both the equilibrium distribution and diffusive behaviour of a solute determine its rate of translocation across a lipid membrane. In its traditional form, the main equation of the heterogeneous solubility-diffusion model relates the permeability coefficients of a solute to the profiles of its position-dependent partition and diffusion coefficients across the bilayer, while rotational and conformational degrees of freedom are implicitly averaged out.[11] In fact, however, depending on solute size, translational, rotational and conformational motions take place on different relative time scales, and, in general, the coupling of positional, orientational and conformational coordinates, introduced by the equilibrium distribution function, should not be neglected.

Starting from the stochastic description of roto-translational diffusion provided by the Fokker-Planck-Smoluchowski equation with explicit positional and orientational variables, we derived analytical expressions for the permeability coefficient in two limit cases. In the first case of much faster reorientational than translational motions, the traditional solubility-diffusion equation was actually recovered, where effective partition and diffusion coefficients were defined as orientational averages of the corresponding position- and orientation- dependent quantities; in the latter case of

much slower reorientational than translational motions, the overall permeability resulted from the independent contributions of solutes in all possible orientations. (Chapter 3)

Our implicit membrane model was applied for the calculation of the free energy profile and distribution of solutes with different polarity, size and shape, as a function of their position, orientation and conformation within a model lipid bilayer. In addition it was integrated into the solubility-diffusion model for the calculation of the permeability coefficients of solutes allowing also in this case the investigation of polarity and size effects. In view of the dominant role of partition properties in determining the location of a confined barrier region limiting the permeation rate, the diffusion coefficients of the solutes under investigation could be evaluated only in the regions of interest by hydrodynamic calculations.

Some general conclusions can be drawn on the role of the contributions to the mean field potential we included in our implicit membrane model for solute partitioning. As expected electrostatic interactions (I) drive the partitioning of polar compounds in the hydrophilic region of the lipid headgroups, near the bilayer surfaces, where also the polar substituents of mostly hydrophobic compounds are found to reside. Quite counterintuitive is the effect of dispersive interactions (II), far from favoring the distribution of apolar solutes in the lowest-dielectric region near the bilayer centre, are responsible for the confinement of most compounds in the region of highest tail packing, and hence highest polarizability density, around 1 nm away from the middle of the bilayer. The stabilization of solutes occupying the hydrophobic/hydrophilic interface is produced by the cavity contribution (III): it is an effect of the narrow deep well in the lateral pressure profile indicating the prevalence of attractive over repulsive interactions in this region, where the presence of solute molecules satisfies the local tendency to fill the voids among lipid molecules. For analogous reasons, elongated solute molecules partitioning in this region are found to preferentially lye with their long axis perpendicular to the bilayer normal. Higher effects on solute orientation rather than on solute position are generated by the order contribution (IV). Indeed, while favorable anisotropic interactions, taking place also between the ordered lipid tails and nearly spherical solute molecules, are optimized in the most ordered region of the bilayer just below the hydrophobic/hydrophilic interface, they are responsible for the preferential alignment of elongated molecules with their long

axis parallel to the bilayer normal. A broadening of the positional distribution of solutes is observed when these anisotropic effects are in action.

Experimental techniques can rarely provide detailed information on the distribution of solute configurations in lipid bilayers. In fact, with few exceptions, as in the case of neutron diffraction measurement, only average properties of solutes are experimentally accessible. Limited spatial and temporal resolution, or the use of oversimplified interpretative models, often reduce the possibility of asserting the location of membrane probes, of distinguishing their orientation, or the ability to identify the contributions of different probe populations. In particular, orientational and conformational effects, which can be directly measured as average order parameters by fluorescence anisotropy, NMR or EPR experiments, may also affect the response of polarity sensitive fluorescent probes in membranes. On the other hand, the characterization of the structure of a lipid bilayer requires the precise knowledge of the depths at which different order sensitive probes reside. This is due to the intrinsic positional-orientational-conformational coupling determining the distribution of solutes in the highly heterogeneous and ordered environment of a lipid bilayer.

Further less information are provided by experiments on the details of the permeation process of solutes crossing the lipid bilayer by passive non-mediated transport. In fact, since only the measurement of the overall permeability coefficient is allowed, the separated partition and diffusion contribution can not be evaluated.

MD simulations are, in principle, the right tool to achieve a detailed insight into the behaviour of solutes in membranes. In practice, however, the high computational cost, accompanying the explicit representation of the lipid molecules constituting the bilayer, poses severe limitations. During feasible simulation times, of the order of few tens of nanoseconds, solutes moving freely within the bilayer can hardly explore the space of available configurations. This reduces the amount of information which can be gained, since only frequently sampled configurations can be studied through a meaningful statistical approach. Constrained particle methods allow to follow the trajectories of solute molecules placed at fixed depths arbitrarily chosen across the whole bilayer thickness. In this way, however, only position-dependent properties, averaged over the solute orientations and conformations explored, can be obtained.

Time scale limitations also determine the impossibility of following the complete permeation of a solute across a lipid bilayer directly by a MD simulation. Despite this, the position-dependent profiles of solute partition and diffusion coefficients, entering the solubility-diffusion equation for solute permeability, can be obtained by constrained particle methods. However, our stochastic treatment of the permeation process, based on the Fokker-Planck-Smoluchowski description of roto-translational diffusion, showed that only under the assumption of much faster reorientational than translational motions, the constrained MD approach holds. Then, while this can be safely applied to small drug-like molecules, a different method is required in the case of large nano-scaled solute particles.

In this context our implicit membrane model proved to represent a valuable resource, since all the desired information on the properties of solutes in lipid bilayers can be extracted from the coupled positional-orientational-conformational distribution we defined from our mean field potential.

The comparison of our predictions with available literature data on the preferred location and orientation of solutes of interest revealed in general a good agreement between our results and corresponding quantities obtained from experiments or MD calculations, and confirmed the reliability of our description of the main effects of solute-bilayer interactions.

The distinguishing features of the distribution of cholesterol, and of the fluorescent probes of membrane structure DPH and pyrene, either deduced from experiments or calculated by MD simulations, were successfully reproduced. In particular, a bimodal distribution was predicted for DPH, with two distinct probe populations residing at different depths with different orientations, in line with what is suggested by neutron diffraction[12] and time-resolved fluorescence decay[13] and fluorescence anisotropy experiment[14,15]. Moreover, the average order parameters calculated for the C-H bonds along the flexible tail of cholesterol, as well as for the rigid pyrene molecule, were found to be very close to those determined by ^{2}N-NMR experiments[16,17]. (Chapters 2 and 5)

On the basis of the results of our calculations on fullerene C_{60}-derivatives (*i*) and on the fluorescent membrane probes Prodan and Laurdan (*ii*), we were able to propose an explanation of experimental findings, whose interpretation was not straighforward.

i) EPR experiments in oriented bicelles were performed on C_{60} (1) and on a diamagnetic fulleropyrrolidine (2) in spin labelled lipid bilayers, and on a paramagnetic fulleropyrrolidine nitroxide (3) in unlabelled bilayers: 1 and 2 were found to perturb the EPR spectra of spin labels covalently bound near the beginning of the lipid tails, while not affecting the spectra of spin labels near the end of the lipid tails; the response of 3 was found to differ in the liquid crystalline bilayer of bicelles from that shown in the liquid crystal mixture E7. The analysis of the distributions calculated for the solutes suggested that all the fullerenes under investigation preferentially reside in a quite narrow region just below the hydrophobic/hydrophilic interface. This may explain the absence of perturbation due to 1 and 2 in the deep core of the bilayer, and would locate the nitroxide group of 3 in a more polar environment than E7. This polarity effect together with the lower orientational order calculated for 3 in membrane than in E7, would account for the measured hyperfine splitting constants. (Chapter 4)

ii) The fluorescence emission spectra of Prodan and Laurdan in lipid bilayers show two distinct contributions, at 440 nm and 490 nm, whose origin is not established[18]. The calculated orientational-conformational distribution of Prodan and Laurdan individuated a bimodal distribution of the carbonyl groups of the two fluorophores, partly residing in the hydrophilic region of the bilayer, partly in the hydrophobic one. A different ability to form H-bonds with water distributed in the hydrophilic region of the membrane was recognized for the two different populations of the probes, due to the different expositions of their H-bond acceptor groups to water. Quantum Mechanical calculations demonstrated the fundamental effect of H-bond on the red shift of the fluorescence emission spectrum of these probes[19]. The short- and long-wavelength emission bands of Prodan and Laurdan in lipid bilayers were thus attributed to probes with carbonyl groups residing in the water-poor and water-rich region of the bilayer respectively. (Chapter 6)

A good predictive capability of our model emerged from the results of permeability calculations. Four derivatives of the *p*-toluic acid were considered, differing in the polarity of their *p*-substituent, whose measured permeability coefficients differed of up to five orders of magnitude, showing a striking substituent effect[20]. Experimental permeability coefficients were reproduced by calculations with good accuracy,

providing evidence of the sensitivity of our implicit membrane model to the molecular structure of solutes. (Chapter 3)

Less straightforward was the comparison between our results and those obtained from different MD simulations, sometimes showing significant discrepancies. The case of C_{60} showed to be quite troublesome in this regard, due to the absence of experimental data which would have been useful for ascertaining the reliability of the different approaches. Suffice it to say that stabilization free energies ranging form 8 to 48 kcal mol^{-1} have been reported for fullerene in lipid bilayers, and that the only two estimates of its permeability coefficient differ of four orders of magnitude[21]. (Chapter 4)

The investigation of both hydrophilic (*p*-toluic acids) and hydrophobic (benzene and C_{60}) compounds has highlighted the polarity effect on permeability. Calculated permeation rates, in fact, are mainly determined by the crossing of solutes through those regions, within the bilayers, where their partitioning is unfavoured. Then, while the barrier region to the permeation of hydrophilic solutes is located in the bilayer core, partitioning at the water/bilayer interfaces opposes the permeation of hydrophobic solutes. It is in the case of water-insoluble compounds that the definition of an intrinsic membrane permeability becomes critical for calculations. Disruption and formation of aggregates upon changes in the solute environment (from water to membrane and *vice versa*) may represent the rate-limiting step in the whole permeation process, moreover, the specification of water/bilayer boundaries is required for the application of the solubility-diffusion model[22]. According to the procedure we proposed in order to give an unambiguous definition of them, the bilayer limits enclose the whole region where the properties of the solute are perturbed by the presence of the bilayer, and hence deviate from those predicted for the solute in bulk water. (Chapters 3 and 4)

In the light of the encouraging results obtained, further improvements and applications could be thought of for the implicit membrane model we have developed.

In general, solute-solute interactions driving aggregation and disaggregation, as well as specific solute-solvent interactions such as H-bonding, could heavily affect the behaviour of solutes and should be included in a more accurate description of the solute-bilayer system. Non-negligible effects could also arise from the elastic

perturbation of the bilayer structure induced by large or concentrated solutes. The inclusion of electric field and ion effects would be fundamental when dealing with charged solutes.

The modulation of solute properties produced by the bilayer phase and composition represents a topic of great interest in biomembrane research, as well as the investigation of the behaviour of solutes such as peptides or photo-isomerizable compounds for biomedical applications.

7.2 References

[1] Roux, B.; Simonson, T. *Biophys. Chem.* **1999**, *78*, 1-20.

[2] Graziano, G. *J. Chem. Soc. Faraday Trans.* **1998**, *94*, 3345-3352.

[3] Still, W.C.; Tempczyk, A.; Hawley, R.C.; Hendrickson, T. *J. Am. Chem. Soc.* **1990**, *112*, 6127-6129.

[4] Feig, M.; Im, W.; Brooks C. L. III *J. Chem. Phys*. **2004**, *120*, 903-911.

[5] Spassov, V.Z.; Yan, L.; Szalma, S. *J. Phys. Chem. B* **2002**, *106*, 8726-8738.

[6] Tanizaki, S.; Feig, M. *J. Chem. Phys*. **2005**, *122*, 124706.

[7] Grossfield, A. *Curr. Top. Membr.* **2008**, *60*, 131-157.

[8] Parisio, G.; Ferrarini, A. *J. Chem. Theory Comput.* **2010**, *6* , 2267-2280.

[9] Gallicchio, E.; Levy, R.M. *J. Comp. Chem.* **2003**, *25*, 479-499.

[10] Ferrarini, A.; Moro, G. J.; Nordio, P. L.; Luckhurst, G. R. *Mol. Phys.* **1992**, *77*, 1-15.

[11] Diamond, J.M.; Katz, Y. *J. Membr. Biol.* **1974**, *17*, 121-154.

[12] Pebay-Peroula, E.; Dufourc, E.J.; Szabo, A.G. *Biophys. Chem.* **1994**, *53*, 45-46.

[13] Konopasek, I.; Kvasnicka, P.; Herman, P.; Linnertz, H.; Obsil, T.; Vecer, J.; Svobodova, J.; Strzalka, K.; Mazzanti, L.; Amler, E. *Chem. Phys. Lett.* **1998**, *293*, 429-435.

[14] Ameloot, M.; Hendrickx, H.; Herreman, W.; Pottel, H.; van Cauwelaert, F.; van der Meer, W. *Biophys. J.* **1984**, *46*, 525-539.

[15] Straume, M.; Litman, B.J. *Biochemistry* **1987**, *26*, 5113-5120.

[16] Dufourc, E. J.; Parish, E. J.; Chitrakorn, S.; Smith, I.C.P. *Biochemistry* **1984**, *23*, 6062-6071.

[17] Hoff B.; Strandberg, E.; Ulrich, A.S.; Tieleman, D.P.; Posten, C. *Biophys. J.* **2005**, *88*, 1818-1827.

[18] Massey, J.B.; She, H.S.; Pownall, H.J. *Biochemistry* **1985**, *24*, 6973-6978. Chong, P.L.-G. *Biochemistry* **1988**, *27*, 399-404. Vequi-Suplicy, C.C.; Benatti, C.R.; Lamy, M.T. *J. Fluoresc.* **2006**, *16*, 431-439. Lúcio, A.D.; Vequi-Suplicy, C.C.; Fernandez, R.M.; Lamy, M.T. *J. Fluoresc.* **2010**, *20*, 473-482.

[19] Marini, A.; Mennucci, B. Preliminary communication.

[20] Xiang, T.-X.; Anderson, B.D. *J. Pharm. Sci.* **1994**, *83*, 1511-1518.

[21] Qiao, R.; Roberts, A.P.; Mount, A.S.; Klaine, S.J.; Ke, P.C. *Nanolett*. **2007**, *7*, 614-619. Bedrov, D.; Smith, G.D.; Davande, H.; Li, L.W. *J. Phys. Chem. B* **2008**, *112*, 2078-2084. Wong-Ekkabut, J.; Baoukina, S.; Triampo, W.; Tang, I.M.; Tieleman, D.P.; Monticelli, L. *Nat. Nanotech*. **2008**, *3*, 363-368. D'Rozario, R.S.G.; Wee, C.L.; Wallace, E.J.; Sansom, M.S.P. *Nanotechnol*. **2009**, *20*, 115102. Redmill, P.S.; McCabe, C. *J. Phys. Chem. B* **2010**, *114*, 9165-9172. Fiedler, S.L.; DeVane, R.; Jusufi, A.; Shinoda, W.; Chiu, C.; Nielsen, S.O.; Moore, P.B.; Klein, M.L. *J. Phys. Chem. B* **2010**, *114*, 16364-16372.

[22] Fiedler, S.L.; Violi, A. *Biophys. J.* **2010**, *99*, 144-152.

Appendix A

SUPPORTING INFORMATION

1a. Derivation of average methylene positions across the bilayer from S_{CD} order parameters

Once fixed the average position $\langle Z_1 \rangle$ of the C_1 acyl chain atom (carbonyl carbon), for example from a density profile, the average positions of the other chain carbons, $\langle Z_i \rangle$, can be determined using the recursive relation:

$$\begin{cases} \langle Z_i \rangle = \langle Z_{i-2} \rangle - l \langle \cos \beta_{i-1} \rangle & i \geq 3 \\ \langle Z_2 \rangle \approx \dfrac{\langle Z_1 \rangle + \langle Z_3 \rangle}{2} \end{cases} \tag{S1}$$

where β_{i-1} is the angle between the C_{i-2}-C_i chord and the bilayer normal **N** (see Figure S1). The average value $\langle \cos \beta_{i-1} \rangle$ can be evaluated according to the following considerations.

Each methylene group is represented as a cylindrical unit; the *i*th unit is centred on the C_i atom and has its axis parallel to the C_{i-1}-C_{i+1} chord. The orientational distribution of each unit in the liquid crystalline bilayer has $C_{\infty v}$ symmetry and can be associated with a mean field potential, which is a function of the angle β_i between the cylinder axis and the bilayer normal. By truncating at the first term the expansion of this potential on a basis of Legendre polynomials $P_l(\cos \beta_i)$ [1], we can write:

$$U_i(\beta_i) \approx -c_1^i P_1(\cos \beta_i). \tag{S2}$$

where c_1^i is a positive constant (if in the preferred orientation the oriented segment $C_{i+1} \rightarrow C_{i-1}$ is parallel to **N**).

Then, the average value $\langle \cos\beta_i \rangle$ can be expressed as:

$$\langle \cos\beta_i \rangle = \frac{\int_{-1}^{1} \exp\left[c_1^i P_1(\cos\beta_i)/k_B T \right] \cos\beta_i \, d\cos\beta_i}{\int_{-1}^{1} \exp\left[c_1^i P_1(\cos\beta_i)/k_B T \right] d\cos\beta_i}. \tag{S3}$$

The coefficient c_1^i can be determined from the S_{CD}^i order parameter, which is defined as $S_{CD}^i = \left(3\left\langle \cos^2\theta_i \right\rangle - 1\right)/2$, where θ_i is the angle between normal **N** and the C_iH bond. This is related to the second rank order parameter of the C_{i-1}-C_{i+1} chord, $S_{CC}^i = \left(3\left\langle \cos^2\beta_i \right\rangle - 1\right)/2$ as: $S_{CC}^i \approx -2S_{CD}^i$ [2]. Thus c_1^i is obtained by solving the equation:

$$\left\langle \cos^2\beta_i \right\rangle = \frac{\int_{-1}^{1} \exp\left[c_1^i P_1(\cos\beta_i)/k_BT\right]\cos^2\beta_i \, d\cos\beta_i}{\int_{-1}^{1} \exp\left[c_1^i P_1(\cos\beta_i)/k_BT\right] d\cos\beta_i} = \frac{1-4S_{CD_i}}{3}. \qquad \text{(S4)}$$

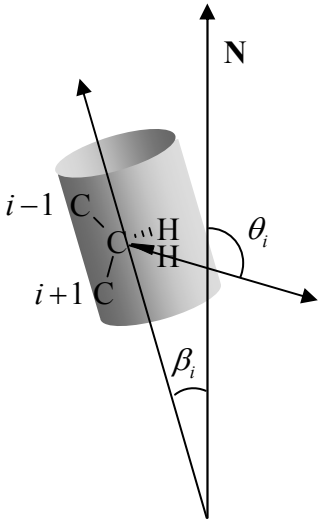

Figure S1: Definition of the cylindrical unit representing the *i*th methylene group in a phospholipid acyl chain. The vector **N** is parallel to the bilayer normal and points towards lipid headgroups, β_i is the angle between the normal and the C_{i-1}-C_{i+1} chord and θ_i the angle between the normal and the C_iH bond.

1b. Evaluation of the scaling factor between orienting strength ξ and S_{CD} order parameters

The bilayer environment is treated, at the local level, as a nematic of cylindrical units, each corresponding to a methylene group; the cylinder axis is parallel to the chord joining the two carbon atoms adjacent the CH_2 group (Figure S1). Then the *local* orienting strength at $\langle Z_i \rangle$, average position of the C_i chain atom, can be expressed as $\xi\left(\left\langle Z_i \right\rangle\right) = \left(\gamma^2 S_{cyl}/2v_{cyl}k_BT\right)S_{CC}^i$ [3,4], where S_{cyl} and v_{cyl} are the surface

area and volume of a cylindrical particle, whereas S^i_{CC} is the second rank order parameter for the C_{i-1}-C_{i+1} chord. Using the relation $S^i_{CC} \approx -2S^i_{CD}$ [2], we can write:

$$\xi\left(\langle Z_i \rangle\right) = -\left(A / k_B T\right) S^i_{CD} \quad \text{with} \quad A = \gamma^2 S_{cyl} / v_{cyl} \tag{S5}$$

To evaluate the constant *A*, we can consider an *apolar* probe with the centre of mass in $\langle Z_i \rangle$, which is assumed to be geometrically equivalent to a methylene unit, yet not inserted in an acyl chain. In the lipid environment the orientational distribution of the probe will be anisotropic, by virtue of nematic-like interactions with the ordered acyl chains. Expressing the mean field potential associated with this anisotropic distribution by the model presented in the main text, eq.9, we can write for the cylindrical probe: $U_{ord}(\beta) = -(1/2) k_B T \xi\left(\langle Z_i \rangle\right) S_{cyl} P_2(\cos\beta)$, where β is the angle between probe axis and bilayer normal. Then, using eq.S5 we obtain: $U_{ord}(\beta) = \left(A S_{cyl} / 2\right) S^i_{CD} P_2(\cos\beta)$. Under the assumption that the order parameter of the probe is identical to that of the surrounding acyl chain methylene groups, $\langle P_2 \rangle_{probe} = S^i_{CC} \approx -2S^i_{CD}$, the constant *A* can be determined by solving numerically the equation:

$$-2S^i_{CD}(Z) = -\frac{\int_{-1}^{1} \exp\left[-\left(A S_{cyl} / 2\right) S^i_{CD} P_2(\cos\beta)\right] P_2(\cos\beta)\, d\cos\beta}{\int_{-1}^{1} \exp\left[-\left(A S_{cyl} / 2\right) S^i_{CD} P_2(\cos\beta)\right] d\cos\beta}. \tag{S6}$$

We took as reference the S^3_{CD} order parameter of the sn_1 acyl chain, which belongs to the plateau region in the order parameter profile of DPPC, as reported in ref.[5] for the temperature *T*=323 K; assuming effective cylinder radius and height equal to 1.6 and 3.4 Å, respectively, the value $A = 0.33$ kcal mol^{-1} Å^{-2} was obtained.

Then the $\xi(\langle Z_i \rangle)$ values were calculated according to eq.S5 from the S^i_{CD} order parameters; the full $\xi(Z)$ profile was obtained by nonlinear fitting of the $\xi(\langle Z_i \rangle)$ data. A continuous function was used to interpolate the $\xi(\langle Z_i \rangle)$ profile in the hydrophobic region and to connect it to zero in the hydrophilic region.

2. Definition of polarizable units and corresponding mass density profiles

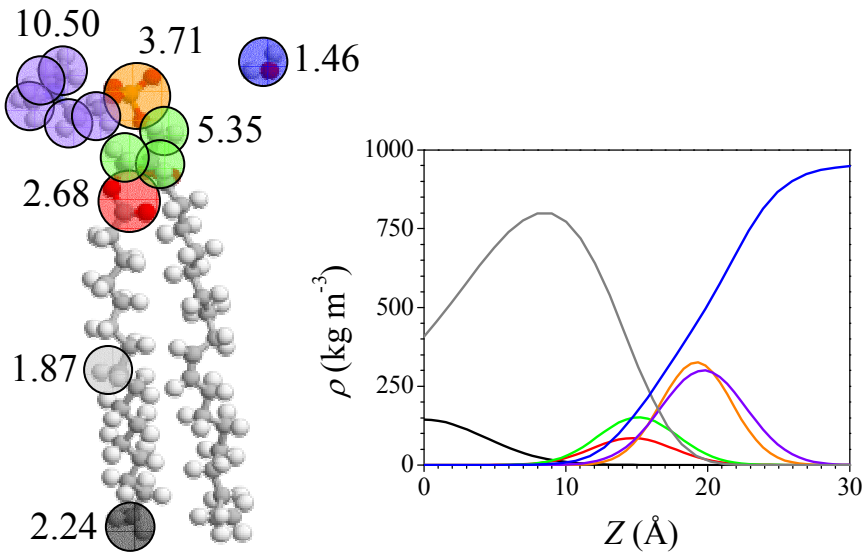

Figure S2: Ball and stick representation of a DPPC molecule with superimposed spheres, each corresponding to a polarizable unit. Total electronic polarizabilities (in units of $(4\pi\varepsilon_0)$ Å^3), as evaluated from single bond contributions [6] (left), and mass density profiles, as derived from the profiles shown in Figure 2B of ref.[7] (right), are reported for methyls (black) and methylenes (grey), for carbonyl groups (red), for glycerol backbone (green), phosphate (orange) and choline (purple) groups, and for water (blue). The contribution of the nitrogen atom in the choline group to polarizability was neglected. Each polarisable unit was given a van de Waals radius R_j^{vdW} equal to 2Å.

3. Evaluation of parameters in eqs.3,4 in main text

As in ref.[8], we used F=8 in eq.3 and obtained the empirical parameters in eq.4, C_0, C_1, D, E, by fitting the electrostatic solvation energies calculated for a test set of molecules according to eq.3 in the main text, to the corresponding quantities calculated by finite-difference solution of the Poisson equation. As in ref.[8], an isotropic liquid solvent was considered, and the values ε_{in}=1 and ε_{out}=80 were assumed. The Delphi software package [9] was used for the numerical solution of the Poisson equation. Being interested in the behavior of low molecular weight molecules in lipid bilayers, we took the test set shown in Figure S3. The values C_0=0.3028, C_1=1.009, D=0.00 Å^{-1}, E=-0.16 Å^{-1} were obtained.

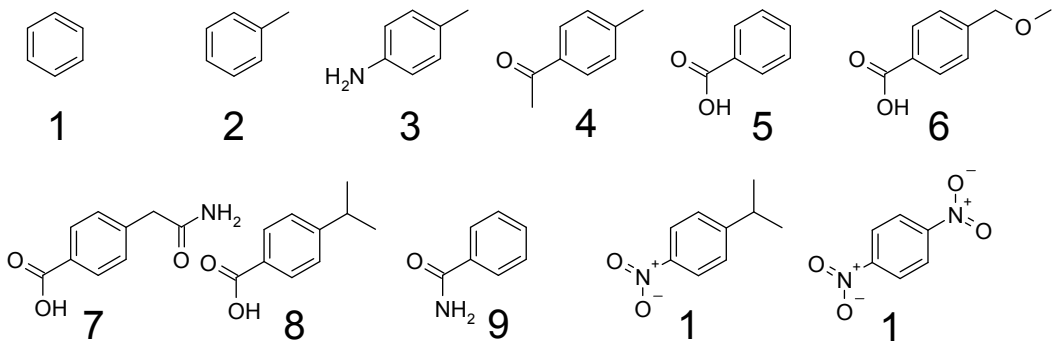

Figure S3. Test set for the parameterization of eqs.3,4 in the main text.

4. Evaluation of water / *n*-octanol transfer free energy

Water/*n*-octanol transfer free energies have been calculated for molecules 1-9 in Figure S3. Free energies in the isotropic environment were calculated on the basis of electrostatic and dispersion contributions, defined in eqs.3,6 in the main text, respectively. Values appropriate for temperature of 20°C and standard pressure were used: ε_{out}=10.3 and ρ= 0.827 g/cm^3 for *n*-octanol, ε_{out} =80.1 and ρ = 0.998 g/cm^3 for water [6]. For solutes, the parameters reported in Table 1 of the main text were used; the polarizability of a benzene C-C bond was taken equal to 1.07 (in $4\pi\varepsilon_0$Å^3 units) [6].

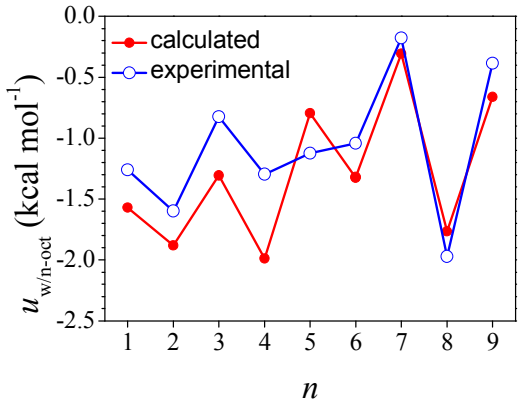

Figure S4: Water/*n*-octanol transfer free energy calculated for molecules 1-9 in Figure S3 (solid circles) compared with experimental values (open circles) [10]. Lines are drawn as a guide to eyes.

5. Structure and charges of cholesterol

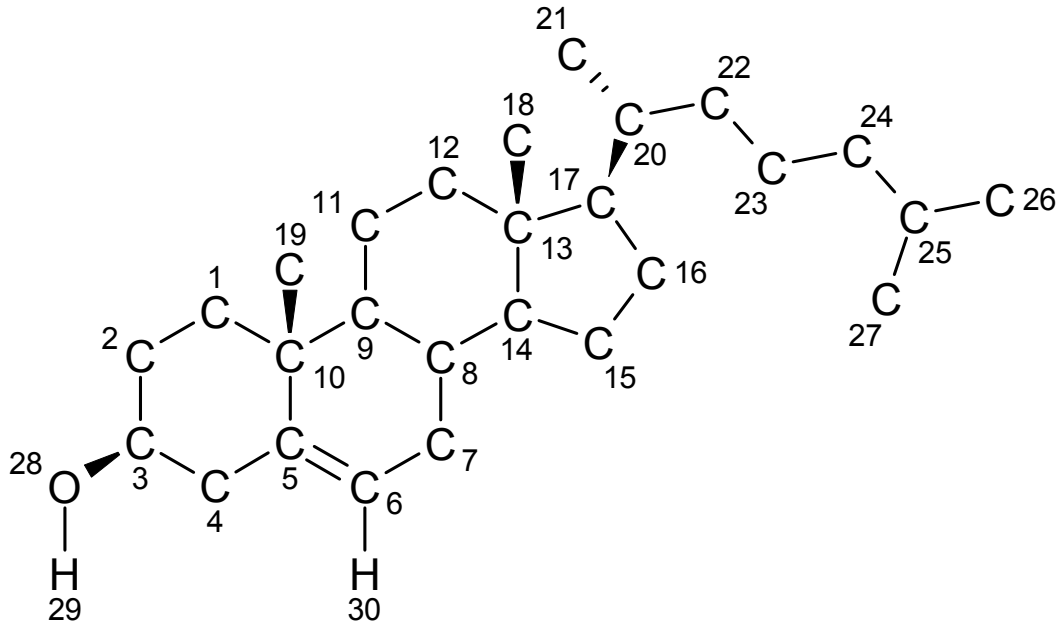

Figure S5. Molecular structure of cholesterol with atom numbering.

Table S1. OPLS [10] atomic charges for cholesterol (atom numbering as in Figure S2).

C_1	-0.120	C_{18}	-0.180
C_2	-0.120	C_{19}	-0.180
C_3	+0.205	C_{20}	-0.060
C_4	-0.120	C_{21}	-0.180
C_5	0.000	C_{22}	-0.120
C_6	-0.115	C_{23}	-0.120
C_7	-0.120	C_{24}	-0.120
C_8	-0.060	C_{25}	-0.060
C_9	-0.060	C_{26}	-0.180
C_{10}	0.000	C_{27}	-0.180
C_{11}	-0.120	O_{28}	-0.700
C_{12}	-0.120	H_{29}	+0.435
C_{13}	0.000	H_{30}	+0.115
C_{14}	-0.060	all other H	+0.060
C_{15}	-0.120		
C_{16}	-0.120		
C_{17}	-0.060		

6. Conformers of cholesterol

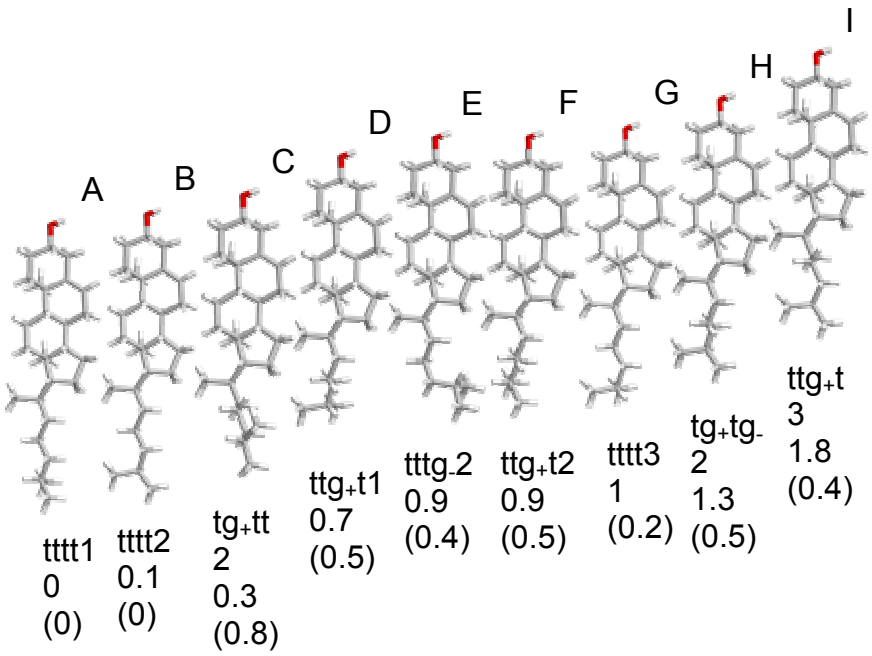

Figure S6. Geometry of the conformers of cholesterols, as obtained by DFT optimization in vacuum at the B3LYP/6-31g** level [11]; under each structure the corresponding potential energy, V_J is reported. In brackets we report the energy change for each conformer upon insertion in the bilayer, $\Delta V_J = V'_J - V_J$, calculated according to eq.28. Energy values are given in kcal mol^{-1} (with conformer A, the lowest in energy, taken as reference). The H–C_3–O–H dihedral is equal to 61°. Structures differ for the alkyl chain conformation; the string under each structure indicates the sequence of bond states, starting from the C_{17}-C_{20} bond (atom numbering as in Figure S2): labels g_+ (*gauche* +), t (*trans*), g_- (*gauche*-) are used up to the C_{23}–C_{24} bond; labels 1, 2, 3 correspond to C_{23}–C_{24}–C_{25}–C_{27} dihedral equal to 60°, 180° and 240°, respectively.

7. Conformer contributions to transfer free energy

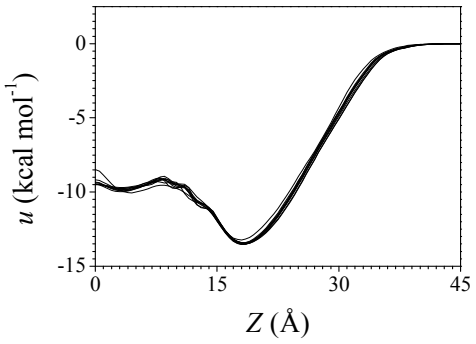

Figure S7. Transfer free energy profiles calculated for the individual conformers of cholesterol in shown in Figure S4, as a function of the distance of the oxygen atom from the bilayer midplane, at the temperature T=323K.

8. Shape and orientational axes of cholesterol

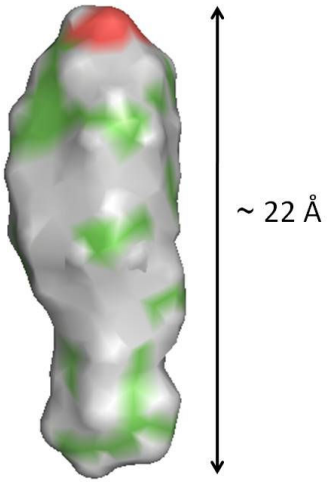

Figure S8. Molecular surface of the B conformer [13] with the molecular length [14].

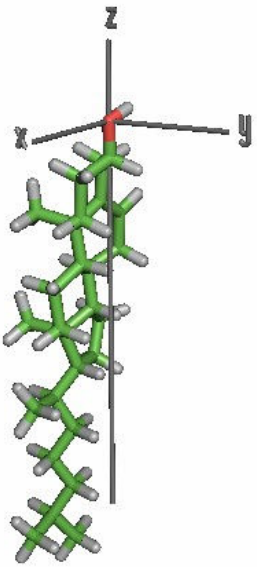

Figure S9. Principal axis system of the Saupe ordering tensor, calculated for cholesterol in DPPC at the temperature T=323 K (superimposed to the structure of the B conformer).

References

[1] Abramowitz, M.; Stegun, I.A. *Handbook of Mathematical Functions*; Dover: New York, 1972.

[2] Seelig, J. *Q. Rev. Biophys.* **1977**, *10*, 353-418.

[3] Ferrarini, A.; Moro, G.J.; Nordio, P.L.; Luckhurst, G.R. *Mol. Phys.* **1992**, *77*, 1-15.

[4] Ferrarini, A.; Luckhurst, G.R.; Nordio, P.L.; Roskilly, S.J. *J. Chem. Phys.* **1994**, *100*, 1460-1469.

[5] Falk, E.; Patra, M.; Karttunen, M.; Hyvönen, M.T.; Vattulainen, I. *Biophys. J.* **2004**, *87*, 1076-1091.

[6] *CRC Handbook of Chemistry and Physics*, 85th Edn.; Lide, D. R.; Ed.; CRC: Boca Raton, 2004.

[7] Kupiainen, M., Falck, E., Ollila, S., Niemelä, P., Gurtovenko, A. A. *J. Comp. Theor. Nano*, **2005**, *2*, 401-413.

[8] Feig, M., Im, W., Brooks III, C. L. *J. Chem. Phys*., **2004**, *120*, 903-911.

[9] Rocchia, W.; Alexov, E.; Honig, B. *J Phys. Chem. B*, **2001**, *105*, 6507-6514. Rocchia, W.; Sridharan, S.; Nicholls, A.; Alexov, E.; Chiabrera A.; Honig B. *J. Comp. Chem.*, **2002**, *23*, 128-137.

[10] BioByte Star List database (BioByte Corporation); Hansh, C.; Leo, A. J. *Substituent Constants for correlation Analysis in Chemistry and Biology*; Wiley: New York, 1979; Sangster, J. *J. Phys. Chem. Ref. Data*, **1989**, *18*, 1111-1229; Terada, H.; Kosuge, Y.; Murayama, W.; Nakaya, N.; Nunogaki, Y.; Nanogaki, K. I. *J. Chromatogr.*, **1987**, *400*, 343-351.

[11] Jorgensen, W. L., Maxwell, D. S., Tirado-Rives, J. *J. Am. Chem. Soc.*, **1996**, *118*, 11225-11236.

[12] Frisch, M. J. *et al.*, *Gaussian03*, Revision C.02; Gaussian, Inc.: Wallingford CT, 2004.

[13] Sanner, M.F.; Olson, A.; Spehner, J.-C. *Biopolymers* **1996**, *38*, 305-320.

[14] Craven, B. M. *Nature* **1976**, *260*, 727–729.

Appendix B

EXPERIMENTAL SECTION

1. Materials

1,2-Dihexanoyl-sn-Glycero-3-Phosphocholine (DHPC), 1,2-Dimyristoyl-sn-Glycero-3-Phosphocholine (DMPC), 1-palmitoyl-2-stearoyl-(5-doxyl)-sn-glycero-3-phosphocholine (5DPC), and 1-palmitoyl-2-stearoyl-(10-doxyl)-sn-glycero-3-phosphocholine (10DPC) were purchased from Avanti Polar Lipids (Alabaster, AL, USA) as chloroform solutions.

HEPES buffer and the lanthanide salts $TmCl_3 \cdot 6H_2O$ and $DyCl_3$ were purchased from Sigma-Aldrich. For the bicelle preparation, and the lanthanide salts stock solutions, a 100 mM, pH 7.0, HEPES buffer was prepared.

C_{60} (**1**) and the two fullerene derivatives **2** and **3** (Figure 1 in the main text) were kindly provided by Prof. Maggini from the Department of Chemical Sciences of the University of Padua.

2. Bicelle stock preparation

The chloroform solutions of the different phospholipids and, where present, the fullerene powder (~25 μg, about 30 nmol), were all added together to a single glass test tube. The experiments were performed with different amounts of the fullerenes to test the effect of concentration. For each sample the solution was composed of 2.3 mL of DMPC (34 μmol), 427 μL of DHPC (9.4 μmol), and, where present, 13 μL of spin label (5DPC or 10DPC, ~75 nmol). The final q= DMPC/DHPC of the samples was therefore q ~3.5, and the spin label amounted to ~0.2% of the lipid molecules. A thick lipid film was produced by evaporation of the chloroform under a stream of dry nitrogen gas; the film was then stored under vacuum overnight. The following day the dried lipid film was scratched off the glass tube and placed into an Eppendorf tube, 100 μL of buffer were added, and the film was suspended by vortexing the tube. The tube was then placed in a bath sonicator filled with an ice/water mix and sonicated for 30 minutes. Finally, the solution was subjected to four cycles of thermal shock: 30 minutes in a 328 K water bath were followed by a quick freeze in

liquid nitorgen; vortexing of the sample at each step was performed to insure perfect homogeneity. The final bicelle stock solution consisted of a 25% (w/w) phospholipid to solution ratio. The fullerene:lipid molar ratio in the samples was approximately 1:1500. More samples were prepared with increasing the fullerene:lipid molar ratio up to 1:500.

3. EPR sample preparation

For each sample 15 μL of bicelle stock were added to 10 μL of buffer (for non-oriented samples), or, for oriented samples, to 10 μL of buffered lanthanide solution of Tm^{3+} or Dy^{3+} (corresponding to a final lanthanide:DHPC molar ratio of 0.9:1). Each EPR sample had a total volume of 25 μL, corresponding to 17% (w/w) phospholipid to solution ratio. The resulting solution was transferred to a 1 mm inner diameter EPR quartz tube.

3. EPR experiments

Experiments on samples aligned by the magnetic field followed the procedure explained in [1]: the samples are placed at room temperature in the spectrometer with the magnetic field set at $\mathbf{B_0}$ = 800 mT, then the temperature is slowly raised up to 318 K and finally lowered to the temperature of choice, 308 K (35˚C). The spectra are then recorded at the usual magnetic field value of about $\mathbf{B_0}$ = 350 mT. At this temperature bicelle samples are highly viscous and the realignment at this magnetic field strength is slow, therefore, we were able to record spectra in two orientations of the sample tube with respect to the magnetic field: in the original orientation and after a rotation of 90˚ of the sample tube. As a control that no realignment has occurred, spectra were recorded after rotating the sample back to its original position obtaining the original spectral lineshape (data not shown).

EPR spectra were performed using a Bruker ER 200D at X-band (9.4 GHz), equipped with a rectangular cavity ER4102ST and the relative cryostat, and a variable-temperature controller Bruker ER 4111 VT, the frequency was measured by a microwave frequency counter HP 5342A. All spectra were obtained using the following parameters: microwave power 2.1 mW; modulation amplitude 0.5 mT;

modulation frequency 100 kHz; time constant 41 ms; conversion time 82 ms; scan width 15 mT; 1024 points; temperature 308 K.

4. Simulation of EPR lineshapes

The spectra of the fullerene derivative **3** in the liquid crystal E7 were simulated using a program that computes the spectra of a nitroxide in slow, axial motion under an orientation potential, adopting the Liouville formalism [2].

Table 1: EPR parameters for the simulation of the spectra of 3 in E7.

g tensor	**A** (^{14}N) tensor (mT)	Diffusion tensor* (R=logD)	Potential
$g_{xx} = 2.0094$	$A_{xx} = 0.565$	$R_{\perp} = 8.23$	$C_{20} = 2.07$
$g_{yy} = 2.0066$	$A_{yy} = 0.593$	$R_{\parallel} = 8.56$	
$g_{zz} = 2.0026$	$A_{zz} = 3.321$		

*The direction corresponding to R|| coincides with the *z* molecular axis (Figure 1 in the main text) forming an angle of 22° with the x principal axis of the magnetic tensors **g** and **A**, which is parallel to the N–O bond (Figures 1 and 5 in the main text).

References

[1] Cardon, T.B.; Tiburu, E.K.; Lorigan, G.A. *J. Magn. Res.* **2003**, *161*, 77-90.

[2] Schneider, D.J.; Freed, J.H. In Biological Magnetic Resonance, Vol.8; Berliner, L.J.; Reuben, J. Eds.; Plenum Press: New York, 1989. Budil, D.E., Lee, S.; Saxena, S.; Freed, J.H. *J. Magn. Reson.* **1996**, *120*, 155-189.

List of Publications related to this thesis work

Solute partitioning into lipid bilayers: an implicit model for nonuniform and ordered environmen. *J. Chem. Theory Comput.* **2010**, *6*, 2267-2280. (with A. Ferrarini)

Fluorescent probes Prodan and Laurdan in lipid bilayers: a QM/SM/Continuum approach to connect spectral observables to the polatity, anisotropy and heterogeneity of the environment. Manuscript in preparation. (with A. Ferrarini, A. Marini, B. Mennucci)

Penetration of monomeric [60]Fullerenes into lipid membranes: effects of molecular shape and polarity. Manuscript in preparation. (with A. Ferrarini, M. Bortolus, M. Maggini, A.L. Maniero)

Solute permeation across lipid bilayers: a generalized inhomogeneous solubility-diffusion model. Manuscript in preparation. (with A. Ferrarini, M. Stocchero)

Acknowledgements

I am grateful to Dr. Matteo Stocchero for stimulating discussions and insightful comments during the course of this work. I thank Dr. Marco Bortolus and Prof. Anna Lisa Maniero for their collaboration on the EPR study of fullerenes, Dr. Alberto Marini and Prof. Benedetta Mennucci for that on the theoretical investigation of fluorescent probes. I acknowledge Prof. Sergio Aragon for giving me the BEST Software.